THE UNIVERSITY OF CALGARY

BUCKLING STUDY OF AN ELASTIC RING CONFINED WITHIN A RIGID BOUNDARY

BY

CHENGXIAN SUN

A DISSERTATION

SUBMITTED TO THE FACULTY OF GRADUATE STUDIES

IN PARTIAL FULFILMENT OF THE REQUIREMENTS

FOR THE DEGREE OF DOCTOR OF PHILOSOPHY

DEPARTMENT OF MECHANICAL ENGINEERING

CALGARY, ALBERTA

May, 1994

ISBN 0-315-99498-3

Name CHENGXIAN SUN

Dissertation Abstracts International is arranged by broad, general subject categories. Please select the one subject which most nearly describes the content of your dissertation. Enter the corresponding four-digit code in the spaces provided.

Engineering — Mechanical | 0548 | U·M·I

SUBJECT TERM | SUBJECT CODE

Subject Categories

THE HUMANITIES AND SOCIAL SCIENCES

COMMUNICATIONS AND THE ARTS
Architecture 0729
Art History 0377
Cinema 0900
Dance 0378
Fine Arts 0357
Information Science 0723
Journalism 0391
Library Science 0399
Mass Communications 0708
Music 0413
Speech Communication 0459
Theater 0465

EDUCATION
General 0515
Administration 0514
Adult and Continuing 0516
Agricultural 0517
Art 0273
Bilingual and Multicultural 0282
Business 0688
Community College 0275
Curriculum and Instruction 0727
Early Childhood 0518
Elementary 0524
Finance 0277
Guidance and Counseling 0519
Health 0680
Higher 0745
History of 0520
Home Economics 0278
Industrial 0521
Language and Literature 0279
Mathematics 0280
Music 0522
Philosophy of 0998
Physical 0523
Psychology 0525
Reading 0535
Religious 0527
Sciences 0714
Secondary 0533
Social Sciences 0534
Sociology of 0340
Special 0529
Teacher Training 0530
Technology 0710
Tests and Measurements 0288
Vocational 0747

LANGUAGE, LITERATURE AND LINGUISTICS
Language
- General 0679
- Ancient 0289
- Linguistics 0290
- Modern 0291

Literature
- General 0401
- Classical 0294
- Comparative 0295
- Medieval 0297
- Modern 0298
- African 0316
- American 0591
- Asian 0305
- Canadian (English) 0352
- Canadian (French) 0355
- English 0593
- Germanic 0311
- Latin American 0312
- Middle Eastern 0315
- Romance 0313
- Slavic and East European 0314

PHILOSOPHY, RELIGION AND THEOLOGY
Philosophy 0422
Religion
- General 0318
- Biblical Studies 0321
- Clergy 0319
- History of 0320
- Philosophy of 0322

Theology 0469

SOCIAL SCIENCES
American Studies 0323
Anthropology
- Archaeology 0324
- Cultural 0326
- Physical 0327

Business Administration
- General 0310
- Accounting 0272
- Banking 0770
- Management 0454
- Marketing 0338

Canadian Studies 0385
Economics
- General 0501
- Agricultural 0503
- Commerce-Business 0505
- Finance 0508
- History 0509
- Labor 0510
- Theory 0511

Folklore 0358
Geography 0366
Gerontology 0351
History
- General 0578
- Ancient 0579
- Medieval 0581
- Modern 0582
- Black 0328
- African 0331
- Asia, Australia and Oceania 0332
- Canadian 0334
- European 0335
- Latin American 0336
- Middle Eastern 0333
- United States 0337

History of Science 0585
Law 0398
Political Science
- General 0615
- International Law and Relations 0616
- Public Administration 0617

Recreation 0814
Social Work 0452
Sociology
- General 0626
- Criminology and Penology 0627
- Demography 0938
- Ethnic and Racial Studies 0631
- Individual and Family Studies 0628
- Industrial and Labor Relations 0629
- Public and Social Welfare 0630
- Social Structure and Development 0700
- Theory and Methods 0344

Transportation 0709
Urban and Regional Planning 0999
Women's Studies 0453

THE SCIENCES AND ENGINEERING

BIOLOGICAL SCIENCES
Agriculture
- General 0473
- Agronomy 0285
- Animal Culture and Nutrition 0475
- Animal Pathology 0476
- Food Science and Technology 0359
- Forestry and Wildlife 0478
- Plant Culture 0479
- Plant Pathology 0480
- Plant Physiology 0817
- Range Management 0777
- Wood Technology 0746

Biology
- General 0306
- Anatomy 0287
- Biostatistics 0308
- Botany 0309
- Cell 0379
- Ecology 0329
- Entomology 0353
- Genetics 0369
- Limnology 0793
- Microbiology 0410
- Molecular 0307
- Neuroscience 0317
- Oceanography 0416
- Physiology 0433
- Radiation 0821
- Veterinary Science 0778
- Zoology 0472

Biophysics
- General 0786
- Medical 0760

EARTH SCIENCES
Biogeochemistry 0425
Geochemistry 0996
Geodesy 0370
Geology 0372
Geophysics 0373
Hydrology 0388
Mineralogy 0411
Paleobotany 0345
Paleoecology 0426
Paleontology 0418
Paleozoology 0985
Palynology 0427
Physical Geography 0368
Physical Oceanography 0415

HEALTH AND ENVIRONMENTAL SCIENCES
Environmental Sciences 0768
Health Sciences
- General 0566
- Audiology 0300
- Chemotherapy 0992
- Dentistry 0567
- Education 0350
- Hospital Management 0769
- Human Development 0758
- Immunology 0982
- Medicine and Surgery 0564
- Mental Health 0347
- Nursing 0569
- Nutrition 0570
- Obstetrics and Gynecology 0380
- Occupational Health and Therapy 0354
- Ophthalmology 0381
- Pathology 0571
- Pharmacology 0419
- Pharmacy 0572
- Physical Therapy 0382
- Public Health 0573
- Radiology 0574
- Recreation 0575
- Speech Pathology 0460
- Toxicology 0383

Home Economics 0386

PHYSICAL SCIENCES
Pure Sciences

Chemistry
- General 0485
- Agricultural 0749
- Analytical 0486
- Biochemistry 0487
- Inorganic 0488
- Nuclear 0738
- Organic 0490
- Pharmaceutical 0491
- Physical 0494
- Polymer 0495
- Radiation 0754

Mathematics 0405
Physics
- General 0605
- Acoustics 0986
- Astronomy and Astrophysics 0606
- Atmospheric Science 0608
- Atomic 0748
- Electronics and Electricity 0607
- Elementary Particles and High Energy 0798
- Fluid and Plasma 0759
- Molecular 0609
- Nuclear 0610
- Optics 0752
- Radiation 0756
- Solid State 0611

Statistics 0463

Applied Sciences

Applied Mechanics 0346
Computer Science 0984
Engineering
- General 0537
- Aerospace 0538
- Agricultural 0539
- Automotive 0540
- Biomedical 0541
- Chemical 0542
- Civil 0543
- Electronics and Electrical 0544
- Heat and Thermodynamics 0348
- Hydraulic 0545
- Industrial 0546
- Marine 0547
- Materials Science 0794
- Mechanical 0548
- Metallurgy 0743
- Mining 0551
- Nuclear 0552
- Packaging 0549
- Petroleum 0765
- Sanitary and Municipal 0554
- System Science 0790

Geotechnology 0428
Operations Research 0796
Plastics Technology 0795
Textile Technology 0994

PSYCHOLOGY
General 0621
Behavioral 0384
Clinical 0622
Developmental 0620
Experimental 0623
Industrial 0624
Personality 0625
Physiological 0989
Psychobiology 0349
Psychometrics 0632
Social 0451

Nom ________________________________

Dissertation Abstracts International est organisé en catégories de sujets. Veuillez s.v.p. choisir le sujet qui décrit le mieux votre thèse et inscrivez le code numérique approprié dans l'espace réservé ci-dessous.

________________________________ SUJET

☐☐☐☐ CODE DE SUJET

U·M·I

Catégories par sujets

HUMANITÉS ET SCIENCES SOCIALES

COMMUNICATIONS ET LES ARTS
- Architecture 0729
- Beaux-arts 0357
- Bibliothéconomie 0399
- Cinéma 0900
- Communication verbale 0459
- Communications 0708
- Danse 0378
- Histoire de l'art 0377
- Journalisme 0391
- Musique 0413
- Sciences de l'information 0723
- Théâtre 0465

ÉDUCATION
- Généralités 515
- Administration 0514
- Art 0273
- Collèges communautaires 0275
- Commerce 0688
- Économie domestique 0278
- Éducation permanente 0516
- Éducation préscolaire 0518
- Éducation sanitaire 0680
- Enseignement agricole 0517
- Enseignement bilingue et multiculturel 0282
- Enseignement industriel 0521
- Enseignement primaire. 0524
- Enseignement professionnel 0747
- Enseignement religieux 0527
- Enseignement secondaire 0533
- Enseignement spécial 0529
- Enseignement supérieur 0745
- Évaluation 0288
- Finances 0277
- Formation des enseignants 0530
- Histoire de l'éducation 0520
- Langues et littérature 0279
- Lecture 0535
- Mathématiques 0280
- Musique 0522
- Orientation et consultation 0519
- Philosophie de l'éducation 0998
- Physique 0523
- Programmes d'études et enseignement 0727
- Psychologie 0525
- Sciences 0714
- Sciences sociales 0534
- Sociologie de l'éducation 0340
- Technologie 0710

LANGUE, LITTÉRATURE ET LINGUISTIQUE
- Langues
  - Généralités 0679
  - Anciennes 0289
  - Linguistique 0290
  - Modernes 0291
- Littérature
  - Généralités 0401
  - Anciennes 0294
  - Comparée 0295
  - Mediévale 0297
  - Moderne 0298
  - Africaine 0316
  - Américaine 0591
  - Anglaise 0593
  - Asiatique 0305
  - Canadienne (Anglaise) 0352
  - Canadienne (Française) 0355
  - Germanique 0311
  - Latino-américaine 0312
  - Moyen-orientale 0315
  - Romane 0313
  - Slave et est-européenne 0314

PHILOSOPHIE, RELIGION ET THEOLOGIE
- Philosophie 0422
- Religion
  - Généralités 0318
  - Clergé 0319
  - Études bibliques 0321
  - Histoire des religions 0320
  - Philosophie de la religion 0322
- Théologie 0469

SCIENCES SOCIALES
- Anthropologie
  - Archéologie 0324
  - Culturelle 0326
  - Physique 0327
- Droit 0398
- Économie
  - Généralités 0501
  - Commerce-Affaires 0505
  - Économie agricole 0503
  - Économie du travail 0510
  - Finances 0508
  - Histoire 0509
  - Théorie 0511
- Études américaines 0323
- Études canadiennes 0385
- Études féministes 0453
- Folklore 0358
- Géographie 0366
- Gérontologie 0351
- Gestion des affaires
  - Généralités 0310
  - Administration 0454
  - Banques 0770
  - Comptabilité 0272
  - Marketing 0338
- Histoire
  - Histoire générale 0578
  - Ancienne 0579
  - Médiévale 0581
  - Moderne 0582
  - Histoire des noirs 0328
  - Africaine 0331
  - Canadienne 0334
  - États-Unis 0337
  - Européenne 0335
  - Moyen-orientale 0333
  - Latino-américaine 0336
  - Asie, Australie et Océanie 0332
- Histoire des sciences 0585
- Loisirs 0814
- Planification urbaine et régionale 0999
- Science politique
  - Généralités 0615
  - Administration publique 0617
  - Droit et relations internationales 0616
- Sociologie
  - Généralités 0626
  - Aide et bien-àtre social 0630
  - Criminologie et établissements pénitentiaires 0627
  - Démographie 0938
  - Études de l' individu et de la famille 0628
  - Études des relations interethniques et des relations raciales 0631
  - Structure et développement social 0700
  - Théorie et méthodes. 0344
  - Travail et relations industrielles 0629
- Transports 0709
- Travail social 0452

SCIENCES ET INGÉNIERIE

SCIENCES BIOLOGIQUES
- Agriculture
  - Généralités 0473
  - Agronomie. 0285
  - Alimentation et technologie alimentaire 0359
  - Culture 0479
  - Élevage et alimentation 0475
  - Exploitation des péturages 0777
  - Pathologie animale 0476
  - Pathologie végétale 0480
  - Physiologie végétale 0817
  - Sylviculture et faune 0478
  - Technologie du bois 0746
- Biologie
  - Généralités 0306
  - Anatomie 0287
  - Biologie (Statistiques) 0308
  - Biologie moléculaire 0307
  - Botanique 0309
  - Cellule 0379
  - Écologie 0329
  - Entomologie 0353
  - Génétique 0369
  - Limnologie 0793
  - Microbiologie 0410
  - Neurologie 0317
  - Océanographie 0416
  - Physiologie 0433
  - Radiation 0821
  - Science vétérinaire 0778
  - Zoologie 0472
- Biophysique
  - Généralités 0786
  - Medicale 0760

SCIENCES DE LA TERRE
- Biogéochimie 0425
- Géochimie 0996
- Géodésie 0370
- Géographie physique 0368
- Géologie 0372
- Géophysique 0373
- Hydrologie 0388
- Minéralogie 0411
- Océanographie physique 0415
- Paléobotanique 0345
- Paléoécologie 0426
- Paléontologie 0418
- Paléozoologie 0985
- Palynologie 0427

SCIENCES DE LA SANTÉ ET DE L'ENVIRONNEMENT
- Économie domestique 0386
- Sciences de l'environnement 0768
- Sciences de la santé
  - Généralités 0566
  - Administration des hipitaux 0769
  - Alimentation et nutrition 0570
  - Audiologie 0300
  - Chimiothérapie 0992
  - Dentisterie 0567
  - Développement humain 0758
  - Enseignement 0350
  - Immunologie 0982
  - Loisirs 0575
  - Médecine du travail et thérapie 0354
  - Médecine et chirurgie 0564
  - Obstétrique et gynécologie 0380
  - Ophtalmologie 0381
  - Orthophonie 0460
  - Pathologie 0571
  - Pharmacie 0572
  - Pharmacologie 0419
  - Physiothérapie 0382
  - Radiologie 0574
  - Santé mentale 0347
  - Santé publique 0573
  - Soins infirmiers 0569
  - Toxicologie 0383

SCIENCES PHYSIQUES

Sciences Pures
- Chimie
  - Genéralités 0485
  - Biochimie 487
  - Chimie agricole 0749
  - Chimie analytique 0486
  - Chimie minérale 0488
  - Chimie nucléaire 0738
  - Chimie organique 0490
  - Chimie pharmaceutique 0491
  - Physique 0494
  - PolymÇres 0495
  - Radiation 0754
- Mathématiques 0405
- Physique
  - Généralités 0605
  - Acoustique 0986
  - Astronomie et astrophysique 0606
  - Electronique et électricité 0607
  - Fluides et plasma 0759
  - Météorologie 0608
  - Optique 0752
  - Particules (Physique nucléaire) 0798
  - Physique atomique 0748
  - Physique de l'état solide 0611
  - Physique moléculaire 0609
  - Physique nucléaire 0610
  - Radiation 0756
- Statistiques 0463

Sciences Appliqués Et Technologie
- Informatique 0984
- Ingénierie
  - Généralités 0537
  - Agricole 0539
  - Automobile 0540
  - Biomédicale 0541
  - Chaleur et ther modynamique 0348
  - Conditionnement (Emballage) 0549
  - Génie aérospatial 0538
  - Génie chimique 0542
  - Génie civil 0543
  - Génie électronique et électrique 0544
  - Génie industriel 0546
  - Génie mécanique 0548
  - Génie nucléaire 0552
  - Ingénierie des systämes 0790
  - Mécanique navale 0547
  - Métallurgie 0743
  - Science des matériaux 0794
  - Technique du pétrole 0765
  - Technique minière 0551
  - Techniques sanitaires et municipales 0554
  - Technologie hydraulique 0545
- Mécanique appliquée 0346
- Géotechnologie 0428
- Matières plastiques (Technologie) 0795
- Recherche opérationnelle 0796
- Textiles et tissus (Technologie) 0794

PSYCHOLOGIE
- Généralités 0621
- Personnalité 0625
- Psychobiologie 0349
- Psychologie clinique 0622
- Psychologie du comportement 0384
- Psychologie du développement 0620
- Psychologie expérimentale 0623
- Psychologie industrielle 0624
- Psychologie physiologique 0989
- Psychologie sociale 0451
- Psychométrie 0632

THE UNIVERSITY OF CALGARY

FACULTY OF GRADUATE STUDIES

The undersigned certify that they have read, and recommended to the Faculty of Graduate Studies for acceptance, a thesis entitled "Buckling Study of an Elastic Ring Confined Within a Rigid Boundary" submitted by Chengxian Sun in partial fulfilment of the requirements for the degree of Doctor of Philosophy.

Dr. W.J.D. Shaw, Supervisor
Dept. of Mechanical Engg.

Dr. S. Lukasiewicz
Dept. of Mechanical Engg.

Dr. E. Mikulcik
Prof. Emeritus, Dept. of Mechanical Engg.

Prof. B.W. Langan
Civil Engg.

Dr. R. Seshadri, External Examiner
Memorial University, Newfoundland

ABSTRACT

Local buckling behaviour of an elastic ring confined within a rigid boundary was investigated both theoretically and experimentally. The study involved considerations of material properties, dimensions, geometric imperfection, and the friction effect at the interface.

The study started by using the dimensional analysis method to develop a fundamental relationship of the critical buckling compression stress with the elastic modulus, dimensions and the initial deflection. Then two discrete models were developed. One model was developed under the frictionless assumption and another was developed by taking the friction into consideration. Following this, an experimental apparatus was developed and a large scale tests were carried out. Finally, a finite element model was established and ANSYS 4.4 was used to carry out the calculations.

The results indicated:

(1) The Critical buckling load is proportional to the elastic modulus of materials.

(2) The initial deflection δ, which may be caused by geometric imperfection of the boundary, or external disturbance, or combination of geometric imperfection and external disturbance, makes the ring buckle. When $\delta=0$, there is no critical load in the elastic region.

(3) Friction at the interface increases the stability of the ring. The larger the friction, the larger the critical load. The larger the friction, the more difficult for the ring to slide along the boundary.

(4) Local plastic deformation which occurs in the lift out region of the ring has a

negative effect on the critical buckling load. The larger the local plastic deformation, the lower the critical buckling load becomes.

(5) In the elastic region, the critical load is proportional to the two dimensional variables: the ratio of the thickness of the ring to the radius of the rigid boundary, $(\frac{t}{r})$ and the ratio of the thickness of the ring to the height of a point imperfection on the rigid boundary, $(\frac{t}{\delta})$.

ACKNOWLEDGEMENT

The Author wishes to express sincere gratitude to his supervisors, Dr. W.J.D. Shaw and Dr. A.M. Vinogradov, for their guidance, support and encouragement throughout this program.

Sincere thanks goes to A. Moehrle for his technical assistance and N. Vogt for his excellent drafting work.

Special thanks are due to the staff of the Mechanical Engineering Workshop, especially R. Bechtold and M. Johnson for their technical assistance.

Finally, the author acknowledges the financial support of the Department of Mechanical Engineering and the Natural Science and Engineering Research Council of Canada.

DEDICATION

To my wife, Xinxin Wu and my daughter, Zhifang Sun with love and appreciation.

献给：

爱妻 吴昕昕

爱女 孙志方

TABLE OF CONTENTS

LIST OF TABLES

LIST OF FIGURES

NOMENCLATURE

A	cross-section area of a ring
B	width of a ring
C	coefficient of the buckling function
C_{α}	coefficient of frictionless discrete element model
C_f	friction effect coefficient
D	diameter if a ring
E	elastic modulus of material
F_f	friction resistance force
H	height for friction measurement
I	moment of cross-section inertia of a ring
L	length for friction measurement
L_1, L_2	total specimen length for modulus measurement
M	bending moment
P	compression force
P_{cr}	critical compression force
R	reaction force
U	energy
W	weight
b, d	undetermined exponents of buckling function
k	spring constant
l	specimen gauge length for modulus measurement or link length

q	compression pressure
q_c	critical compression pressure
r	radius of a ring or a boundary
s	acre length
t	thickness of a ring
α	half center angle of lifted portion of a ring
δ	initial deflection or height of imperfection
μ	friction coefficient
ϕ	friction angle
σ	axial stress
σ_{cr}	critical axial stress

Chapter 1

INTRODUCTION

1.1 Problem

A common type of design used in many mechanical applications is that of sleeving the inside of cylinders, pumps, or other types of pressure components or storage containers. The application may be in order to improve acoustic, electrical or thermal insulation, to prevent leakage, corrosion or mechanical damage. In addition, the installation of a liner is often used for repairing components. The process involves machining a thin cylindrical shell and forcing it to contract by the use of cold temperature application and inserting the contracted shell into a pre-machined cylinder or casing. Once the two components have equalized in temperature a presure is set up at the interface due to the designed mismatch. This combined with the effect of friction, mechanically fixes the sleeve to the outer support cylinder.

In practice, failure of interference fits often occurs as a result of local buckling and separation of the cylinders in contact. This problem has become of increasing concern in view of its safety and economic implications. For some pressure components where these interference shrink liners are utilized, equipment costs can be in excess of one million dollars. Therefore the repair of a unit using a liner becomes extremely significant in terms of economic considerations. However, despite the fact that the stresses generated by various interference fits can be accurately determined by calculations, to date,

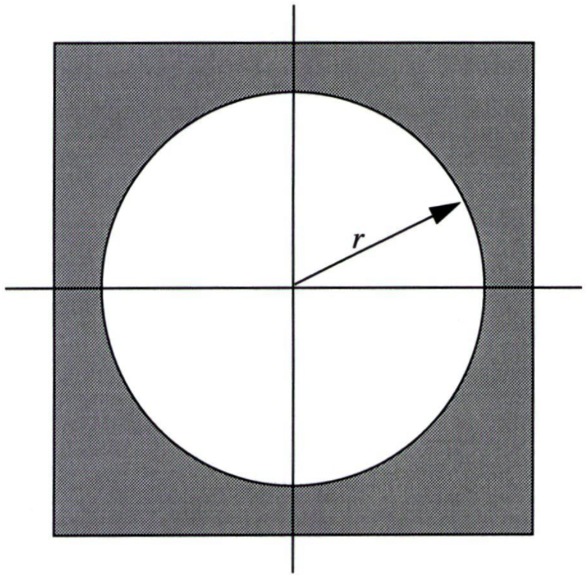

(a) Before buckling

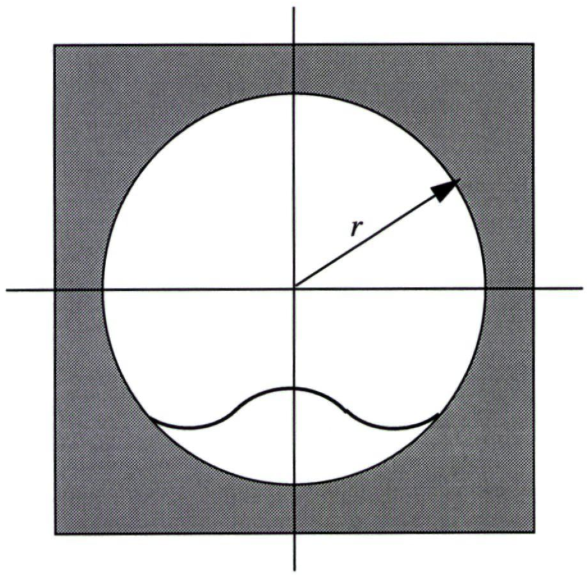

(b) After buckling

Figure 1.1 A Ring Confined within a Rigid Boundary little information is available that can be used to predict the critical buckling conditions of interference fits. The design procedures currently employed by manufacturers such as Peacock Inc. and Fluor Canada rely on the experience accumulated from various trial and error experiments which can not provide a general solution especially when new materials or different dimensions are considered in the design.

This problem can simplified as a ring surrounded by a rigid circular surface as shown in Figure 1.1. A hoop compression stress of the ring is created by themal expansion, shrink-fitting, etc. When the value of the compression hoop stress reaches some critical point, the ring will suddenly lift off the rigid boundary and buckle inward as shown in Figure 1.1 (b). This problem has some characteristics which differ from ordinary buckling problems in that, (1) it is an one-way buckling problem since the rigid boundary prevents outward displacement of the ring; (2) before and after buckling, the load conditions are largely different from each other. Before buckling occurs, there is a constant pressure at the interface between the ring and the rigid boundary. But after buckling occurs, a portion of the ring lifts off the rigid boundary and the pressure between the ring and the rigid boundary at this portion will vanish.

1.2 Existing Industrial Rules of Thumb for Critical Buckling Pressure

Although the analytical solution for buckling of thin rings due to an externally applied pressure does exist, there is not an analytical solution for buckling of thin rings shrunk in the inside of tubes. However, industrial rules of thumb are available. These rules are based on trial and error results from shop work, and have evolved into an accepted industry practice. A calculation using buckling versus non-buckling conditions from industrial experience shows that buckling occurs at a factor of 3.5 times that predicted from external pressure on thin rings, while no buckling condition occurs at a factor of 3.0 [56]. This means when $q \le 3.0 \times q_c$ the inner ring will not buckle and when $q \ge 3.5 \times q_c$ the inner ring will likely buckle, where q is a radial compression pressure for the shrunk ring and q_c is the critical radial compression pressure for the free ring.

1.3 Objective and Outline of This Work

The purpose of this study is to develop a general relationship that describes the critical buckling conditions for various materials, dimensions, degrees of interference fits and imperfections or external disturbance. Meeting this objective should allow designers of these components to accurately predict the conditions at which buckling or instability occurs.

In this study the literature review was first conducted to become familiar with the current research situation on this problem. Then an initial experiment was carried out to obtain some first hand information. Upon this information, an experimental apparatus was designed and manufactured. By use of the principles of the dimensional analysis method, an approximate relationship between the critical buckling force and the geometric parameters and material properties was derived with some undetermined coefficients. Under the guidelines of this fundamental relationship, a large scale test was conducted and the undetermined coefficients were derived by experimental data fitting. Thereafter, two discrete element models were established. One is the frictionless model and another is the friction model. Finally a finite-element model was established and a finite-element software package, ANSYS 4.4 was used to carry out the calculations.

1.4 Major Contributions of the Study

(1) Successfully introduce the dimensional analysis method to establish the fundamental relationship between the geometric parameters and material properties.

(2) Design and conduct large scale experiments on various of materials and dimensions.

(3) Take the friction factor into consideration quantitatively in this problem.

(4) Discrete models simplify the analysis.

(5) Finite-element model makes simulation on various and real situations possible and provides verification of other results.

Chapter 2

LITERATURE REVIEW

2.1 Introduction

It is well known that thin-wall shells exhibit very favorable strength to weight ratios. Thus it is not surprising that they play an important role in modern engineering design, especially when it comes to weight sensitive applications, such as in the aerospace and related fields. However, thin shell structures are often prone to buckling instabilities. In the last few decades, due to the rapid development in many fields in which light structures and new materials have been utilized, numerous technical papers and books dealing with the subject of shell stability have been published. Good reviews on the subject can be found in [1-3, 44-46].

At the beginning of the 1960's, another kind of shell stability problem came to the attention of scientists and engineers. This problem was concerned with the buckling behaviour of a cylindrical shell confined in a rigid or elastic circumferential boundary. In many applications a protective lining or coating is inserted into the interior of a cavity or cylindrical structure. Such a situation may occur, for instance, in pipes, vessels, tunnels, etc. For a long cylindrical shell with free end boundary conditions, this problem can be simplified as a thin elastic ring confined within a rigid boundary. Because the rigid boundary prevents outward displacement, this problem is also known as a "one-way" buckling problem. A number of investigations were carried out to study the buckling of a cylindrical shell or circular ring with one-side connection with a surrounding elastic or absolutely rigid outside boundary. Experimental works were also conducted by some investigators. The following is a brief review of theoretical analysis and experimental results for one way buckling which appear in the literature.

2.2 Theoretical Analysis

A solution to the problem of buckling of a ring within a rigid surrounding was first proposed by Lo, Bogdanoff, Goldberg and Crawford in 1962 [4]. They considered a complete circular ring surrounded by a rigid circular surface which prevented any outward radial displacements. When the ring is subjected to a temperature increase or an end compression load, the induced hoop stress may cause the ring to buckle inward in a snap-through process.

In order to conduct a theoretical analysis for the problem, there are some basic assumptions: (1) The buckled configuration is single-wave as shown in Figure 2.1. That is the configuration consists of two regions, the detached region, where the ring separates from the boundary wall; the attached region, where the ring keeps contact with the outside wall and has a constant curvature. (2) Buckled configuration is symmetric to one diameter of the ring. (3) The ring remains elastic and obeys Hooke's law all through the buckling process, which means that non-linearity of the stress-strain curve of the materials and possible plastic deformation in buckling process are not considered in the theoretical studies. (4) There is no friction resistance at the interface of the ring and the rigid boundary.

The solution to this reference [4] is as follows. In order to obtain the buckled configuration of the ring, the post-buckling analysis was conducted. As shown in Figure 2.1, in its equilibrium configuration, the buckled ring may be separated into two parts: the buckled part *C'D'* and the unbuckled *A'C'* and *B'D'*. The buckled part of the ring is free of the support except at the two end points *C'* and *D'*. At these end points, the ring is tangent to the circular surface and has the same curvature ($1/r$) as the circular surface. Since there is no vertical load, equilibrium of the buckled portion *C'D'* is maintained by two horizontal forces N as shown in Figure 2.2.

To determine the buckled shape of part *C'D'*, a coordinate system O_1XY is chosen as shown in Figure 2.2. The arc length s along the buckled part of the ring is measured from the point O_2. The angle θ is defined by the following relations:

$$\begin{aligned} \frac{dx}{ds} &= \cos\theta \\ \frac{dy}{ds} &= \sin\theta \end{aligned} \tag{2.1}$$

The equation of bending is

$$EI\left(\frac{d\theta}{ds} - \frac{1}{r}\right) = Ny \tag{2.2}$$

where E is the Young's modulus and I is the moment of inertia of cross section of the ring.

The boundary conditions are

$$\text{at } O_2 \ \ s = 0 \text{ and } \theta = 0 \tag{2.3a}$$

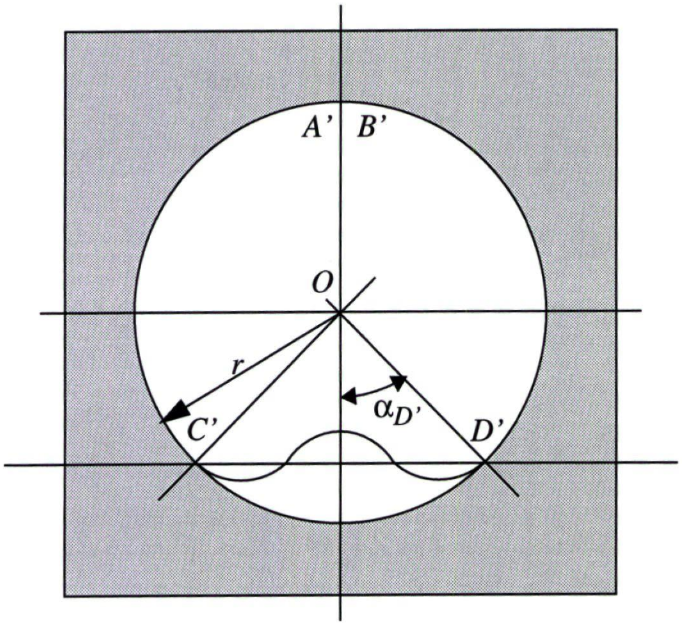

Figure 2.1 Buckled Configuration of a Ring
Confined within a Rigid Boundary

$$\text{at } D' \; s = s^* \text{ and } \theta = \theta_{D'} \tag{2.3b}$$

where 2s* is the total arc length of the buckled part *C'D'* of the ring.

After some mathematical manipulations, equations defining the shape of the buckled part *C'D'* of the ring are obtained as,

$$\frac{s^*}{r} = \frac{1}{\sqrt{\overline{N}}} F(\beta^*, k) \tag{2.4}$$

$$\frac{x}{r} = \frac{1}{\sqrt{\overline{N}}} [2E(\beta, k) - F(\beta, k)] \tag{2.5}$$

$$\frac{y}{r} = \frac{2k}{\sqrt{\overline{N}}} (\cos\beta - \cos\beta^*) \tag{2.6}$$

where *F(b,k)* and *E(b,k)* are the elliptic integrals of the first and second kind respectively

$$\sin\beta = -\frac{\sin(\theta/2)}{\sin(\theta_m/2)} \tag{2.7}$$

$$k = \sin(\theta_m/2) \tag{2.8}$$

$$\overline{N} = Nr^2/EI \tag{2.9}$$

Three constant parameters $\overline{N}$, k, and β^* are related to one another by the following conditions. The first condition is that the curvature of the buckled part of the ring should be equal to the curvature of the unbuckled part at the point *D'*. That is

$$\frac{1}{\sqrt{\overline{N}}} = -2k\cos\beta^* \tag{2.10}$$

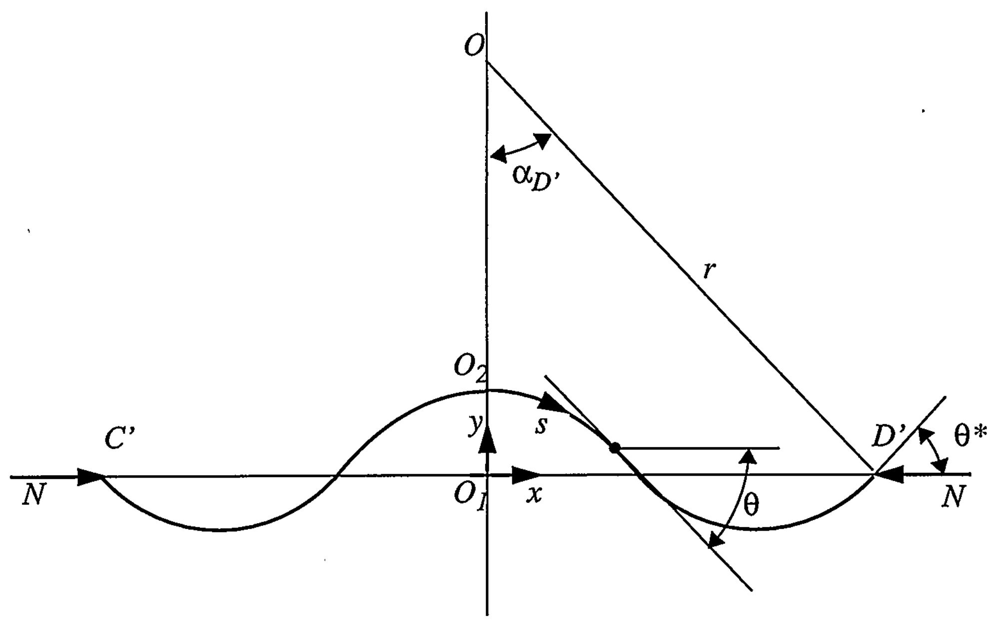

Figure 2.2 Coordinate system

The second condition is that the coordinate x of the buckled part of the ring should be equal to the coordinate x of the unbuckled part at point D'.

$$2E(\beta^*, k) - F(\beta^*, k) = \tan\beta^* \sqrt{1 - k^2 sin^2\beta^*} \qquad (2.11)$$

If one of the three parameters, $\bar{N}$, β^* and k, is given, the other two can be determined from Equations (2.10) and (2.11), and then the buckled shape is completely defined by Equations (2.5) and (2.6).

To determine the critical end compression load P_{cr} or the critical temperature increment $(\Delta T)_{cr}$ which causes the ring to buckle, Lo, et al. assumed that there is no energy transfer to or from the environment during the snap-through process. Thus, the total energy U^- just before the snap-through is equal to the total energy U^+ just after.

$$U^- = U^+ \qquad (2.12)$$

From Equation (2.12) the critical end compression load or the critical temperature increment can be obtained. Unfortunately this energy criterion is not suitable for this particular situation and the critical end compression loads obtained from this energy criterion are not confirmed by experimental results [6,7].

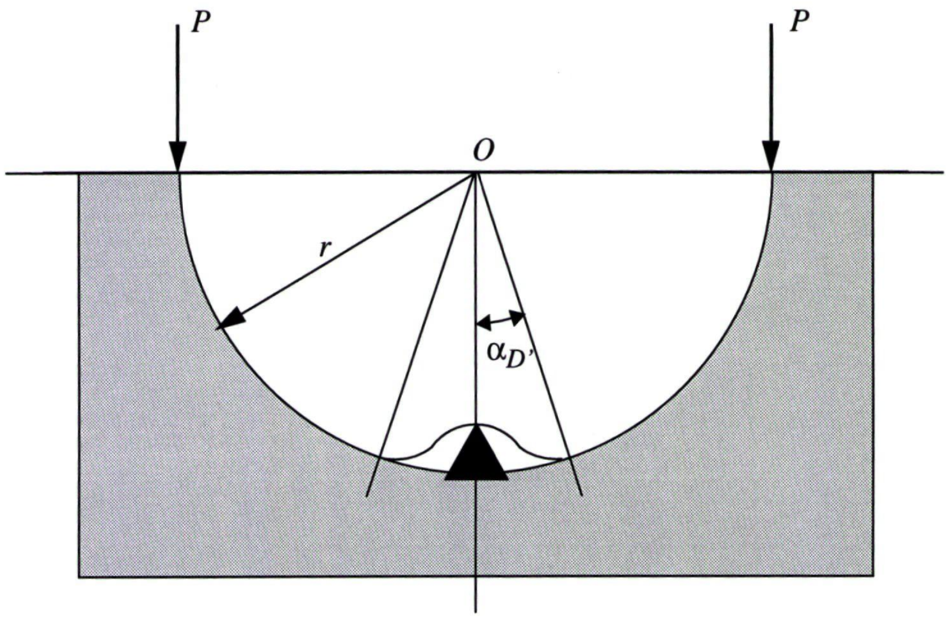

Figure 2.3 A Ring under End Compression Load with

a Point Obstacle on the Boundary

Hsu, Elkon and Pian [5] re-studied this problem by considering the effect of a point obstacle located at a point on the circular boundary, as shown in Figure 2.3. They were able to determine the critical compression load as a function of the height of the point obstacle. Their results also show that when the height of a point obstacle decreases to zero the critical end compression load goes to infinity. This means that if the system is geometrically perfect there is no limit point or critical end compression load as that found in a classical stability problem.

Chan and McMinn [6,7] conducted an analysis similar to [4] and [5] when they studied the buckling of thin steel linings inside prestressed concrete cylinders. Their analysis indicated that there was no critical load as defined by classical theory, but that there was a state of unstable equilibrium which can be reached by small displacements only from the unbuckled position and a state of stable equilibrium which necessitated large displacements. Work must always be done to displace the ring from the unbuckled state, but this was reduced as the uniform compression was increased. By investigating the effect of the imperfections, they concluded that errors in the curvature of the ring have no effect, but errors in curvature of the rigid support change the equilibrium states. The ring would buckle at the point where the radius of curvature is largest and would behave as though it had this radius throughout the whole ring.

Later on, Bucciarelli and Pian [8] studied the effect of three types of initial geometric imperfections on the buckling behavior by employing shallow arch approximations. Figure 2.4 describes three types of initial imperfections for the ring. To conform with the shallow-beam approximation, the undeformed configurations are described by z(s), where the origin of the z-axis is so located that the boundary of the imperfect region is at s=L, z=0. The three types of initial imperfections are as follows.

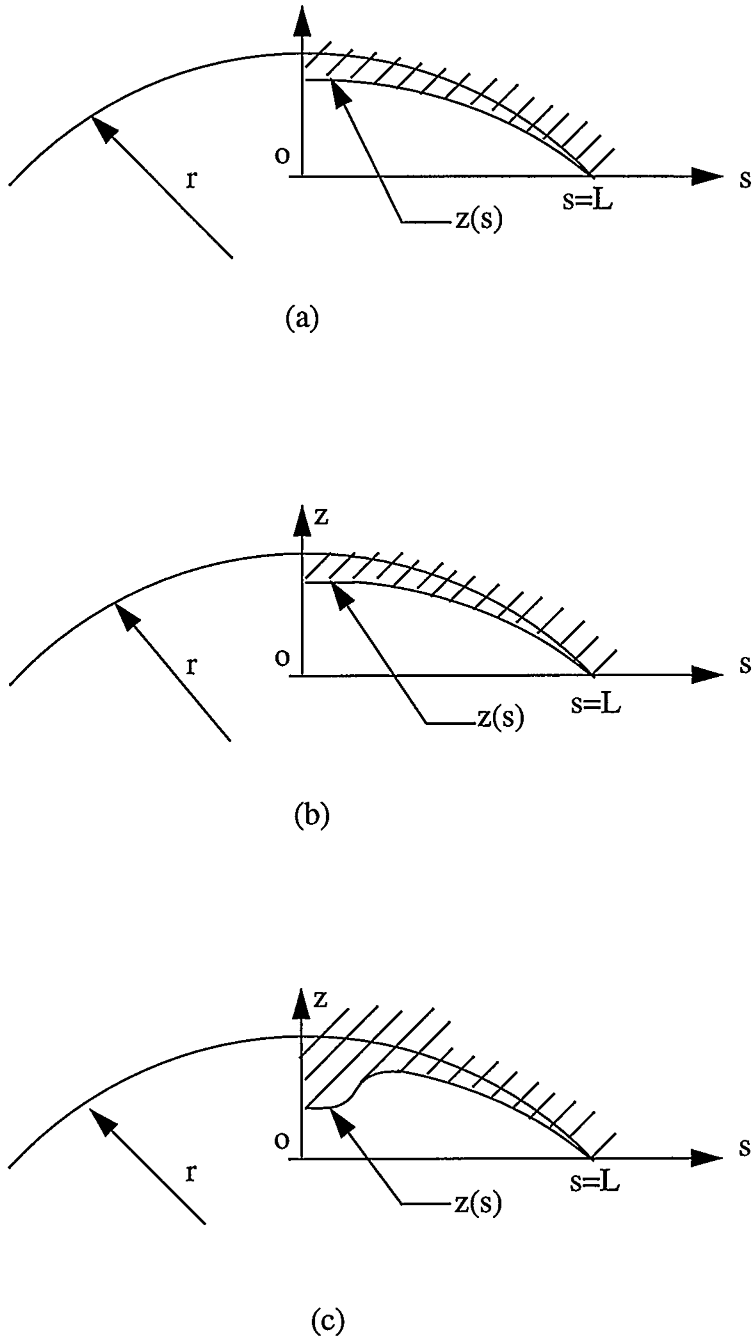

Figure 2.4 Three Forms of Geometric Imperfections

Case (a). The curvature of z(s) is everywhere negative as depicted in Figure 2.4 (a).

Case (b). The slope and curvature are identically zero over a finite portion, while the curvature of the remaining portion is negative, as shown in Figure 2.4 (b).

Case (c). The curvature of z(s) changes from positive to negative within this region of imperfection, as shown in Figure 2.4 (c).

Their analysis yielded that in case (a), no bifurcation or limit point exists at finite load level; in case (b), bifurcation and snap buckling may occur; in case (c), the system admits of a limit point.

Pian and Bucciarelli [9] and Zagustin and Herrmann [10,11] studied the stability of an elastic ring constrained in a rigid cavity and subjected to a uniformly distributed parallel loading per unit length of the ring in its plane. The buckling behavior of a ring under this load condition is different from the ring under end compression load.

El-Bayoumy [12] analyzed the problem of a circular elastic ring confined to a uniformly contracting circular boundary by the variational method. He assumed that the detached (buckled) region of ring covered only a small portion of the circumference, thus the shallow-beam approximation could be employed. He treated the problem as a variational problem with variable end points (the points of separation). The advantage of the variational formulation was that all the differential equations of equilibrium and the associated boundary conditions, including transversality conditions, followed automatically as a consequence of applying the fundamental principles of the calculus of variations. Their study found that the constrained ring has three equilibrium branches I, II, and III which correspond to the unbuckled uniformly contracted state, the buckled "small" deformation state and the buckled "large" deformation state. The total potential energy along the three branches is plotted in Figure 2.5, in which Π is the total potential energy and ΔD is the contraction parameter of the boundary. The figure shows that branch II (small deformation state) corresponds to higher energy than the other two branches. This means that equilibrium states along this branch are unstable. As the ring starts to contract, its equilibrium state moves along branch I which has the smallest energy up to point M at which branch I and branch III intersect. Beyond point M, the potential energy is lowest along branch III. It seems that the ring would buckle as soon as D_M is reached. However, in order for ring to buckle at point M to the large deformation state, it must go through the small deformation state first. But the total potential energy along branch II is always higher than the total potential energy along branch I. Therefore an energy barrier given by the difference between the energies along branches I and II must be overcome in order for the ring to buckle. This difference in energy may be supplied by an external disturbance. That branches I and II did not intersect suggests that the circular ring, in the absence of geometric imperfections and external disturbances, will not snap through to the buckled state.

Liszka and Trojnacki [13] considered the problem of two thin elastic rings of different stiffness (due to different materials or different thickness), one which has been forced into the other. Again, post buckling analysis was performed in order to determine the possible equilibrium states. In the deformed configuration, in which the rings have changed their initially circular shape so that an unknown separation region appears. For simplicity of analysis an equivalent system of three slender bars was analyzed, the continuity conditions must be satisfied at the point of connections. Their solution of the problem was also in implicit form in terms of elliptic functions but much more complicated than Lo's solution [4].

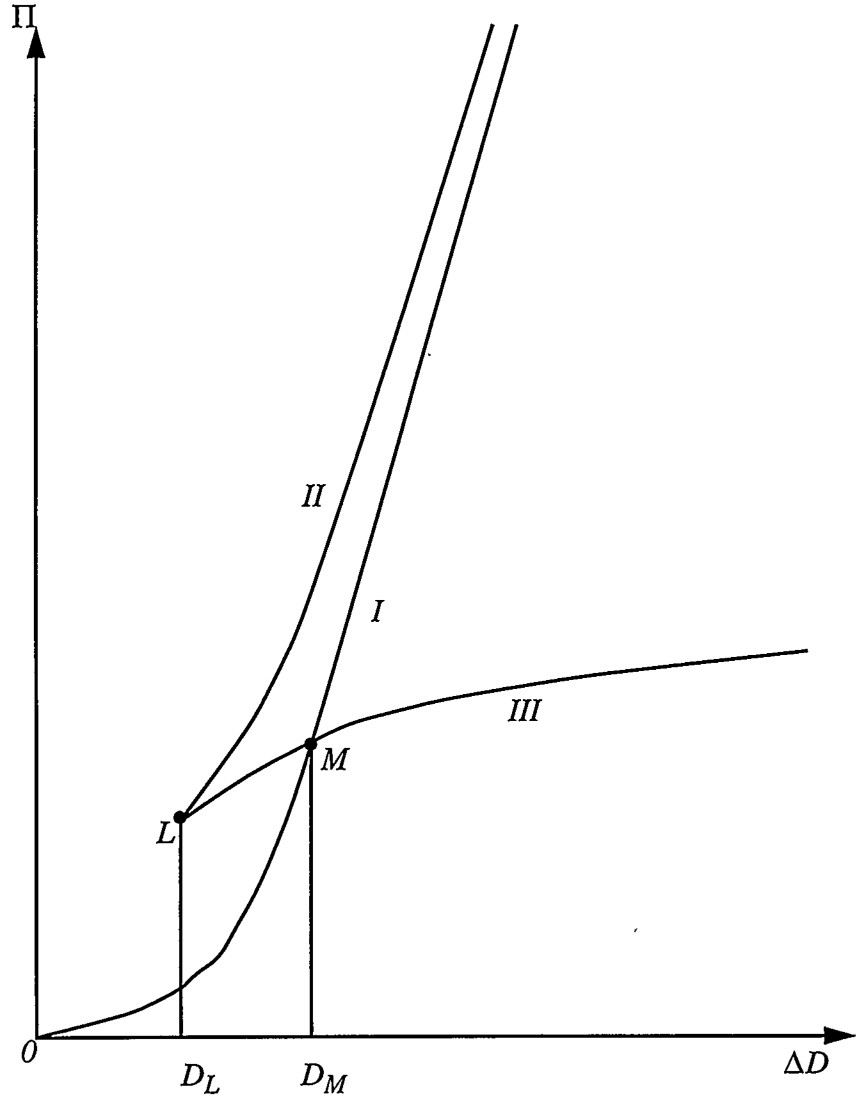

Figure 2.5 Potential Energy along Equilibrium Branches

Chicurel [14] was the first to study the problem by taking into account the friction between the ring and the external wall. When buckling occurs, part of the compressive strain is removed to make up for the slight difference in chordal lengths. This release of compressive strain would be confined to the buckled part of the ring if friction outside of the buckled region is sufficient to inhibit slip (non-slip case). On the other hand, if some slip takes place, then the buckled part must absorb a greater amount of released compressive strain, and the extreme case would occur when the friction coefficient is zero (non-friction case). Based on the non-slip assumption and the non-friction assumption, two expressions of critical diametric interference were developed. For non-slip case

$$P_{01} = 2.487\frac{E}{r}\sqrt{AI} \tag{2.13}$$

For non-friction case

$$P_{02} = 2.67AE\left(\frac{I}{Ar^2}\right)^{3/5} \tag{2.14}$$

By comparison of the two results, it was found that the non-friction case was always more conservative.

Burgess [15,16]developed a general discrete variational method for one way structural system and later on used this method to investigated the buckling behavior of a radially constrained imperfect ring. It was found that when the initial imperfection on a ring is very small, initial loading tends to suppress the imperfection and the ring is locked on the boundary. So only when the initial imperfection on the ring reaches a relatively large magnitude, does the buckling occur for the ring.

Soong and Choi [17] carried out the more general analysis of buckling of a complete, thin ring confined in a non-circular hole subjected to hoop stress and studied an elliptical ring in detail. Their analysis included both the non-friction buckling case and the non-slip buckling case.Their study indicated that the ellipticity reduced the buckling load, because buckling occurred at the flatter part of the ring. The numerical results were obtained by an exact analysis in which the curvature change due to slipping was included. However, if the curvature change due to slipping in the contact zone was neglected, the error was relatively insignificant. For the case they studied, the difference in buckling load was found to be less than one percent.

Various other aspects of the problem of an elastic ring contained within a smooth rigid cavity were considered by several workers. These included a radially directed point load [18] and external and internal pressure[19-27]. The problems of a ring or a tube contained within a soil boundary or a elastic boundary were also explored [28 - 34]. Another kind of one-way buckling problem associated with a sheet or a beam on a flat foundation were also studied in [35-43].

2.3 Experimental Results

Hsu, Elkon and Pian [5] conducted experimental investigations into this problem with controlled initial boundary imperfections. Snap-buckling behavior was in qualitative agreement with the analytical results. However, because of friction between the ring and the rigid boundary and the development of plastic hinges, quantitative agreement was difficult to obtain. For specimens with very small initial boundary imperfections, yielding of the material was observed prior to local buckling of the circular ring. The experimental data was not provided in the paper.

Chan's experimental work [7] revealed two things. First, none of the observed buckling loads agreed with Lo's predictions, and second, the actual buckling loads of apparently identical rings varied enormously. They attributed the first discrepancy to the use of the equal energy criterion, which was not suitable for this particular situation. But they did not give any reasons for the second phenomenon.

2.4 Summary

From the preceding review it can be seen that there is no bifurcation or limit point for the geometrically perfect system and buckling occurs at a limit load only when geometric imperfections or external disturbances provided energy to overcome the energy barrier. For the majority of the theoretical works, the interface condition of the ring and the ring boundary was simplified as the frictionless situation. This simplification made the analysis relatively simpler but experimental verification very difficult. For those who did take the friction into consideration [14,17], they only considered two extreme situations: non-slip case and non-friction case. Furthermore, their results were contradictory to each other. In [14], the critical load ratio of non-slip case to non-friction case is $0.932\left(\frac{Ar^2}{I}\right)^{0.1}$. If $\left(\frac{Ar^2}{I}\right) = 10^6$, the critical load ratio is 3.71. But in [17], the difference between two cases is only about 8 percent. This indicates that the friction effect on the buckling behaviour of the ring has to be considered in more detail before getting a more realistic result.

Although there are many papers carry the theoretical analysis of buckling of an elastic ring constrained by a rigid boundary, the experimental works are relatively limited and the results reported in the literature are rare. Agreement between theoretical and experimental results to date is very poor.

Chapter 3

PRELIMINARY EXPERIMENTS

3.1 Objective of the Experiments

The buckling of interference fits is an important application problem in the industrial field in view of its safety and economic implications. It is also a very complicated and difficult problem to be solved due to the following factors:

a). large deformations of the cylinder in contact;

b). influence of initial imperfections;

c). interaction conditions at the interface surfaces;

To solve this problem, both the analytical approach and the experimental approach are necessary. As pointed out in Chapter 2, although there are a number of researchers dealing with the problem by various of theoretical analysis methods, the experimental works are relatively rare. In addition large discrepancies exist between the experiments and the analytical solutions. Therefore it is necessary to conduct a preliminary experiment and obtain some first hand information.

3.2 Background Information

In order to design the experiment, some background information is first introduced here.

3.2.1 Critical Buckling Pressure of a Free Circular Cylindrical Shell

For a better understanding of this problem and design of the experiment, a free circular ring subjected to a constant external compression pressure is first discussed. For a ring submitted to a uniform external pressure shown in Figure 3.1, the critical value of the compression force P_c is [44]

$$P_c = \frac{3EI}{r^2} \tag{3.1}$$

where E is the Young's modulus and I is the moment of inertia of the cross section of the ring. The critical external pressure q_c is

$$q_c = \frac{3EI}{r^3} \tag{3.2}$$

Equation (3.1) can also be applied in the case of cylindrical shells with free edges subjected to a uniform lateral pressure. In this case as shown in Figure 3.2, an elemental ring of unit width is taken into consideration and the critical value of the compression force P_c in such a ring can be obtained by using $\frac{E}{(1-\nu^2)}$ to substitute for E and by taking $I = \frac{t^3}{12}$, where ν is Poisson's ratio and t is the thickness of the circular cylinder; then from Equation (3.2)

$$P_c = \frac{Et^3}{4(1-\nu^2)r^2} \tag{3.3}$$

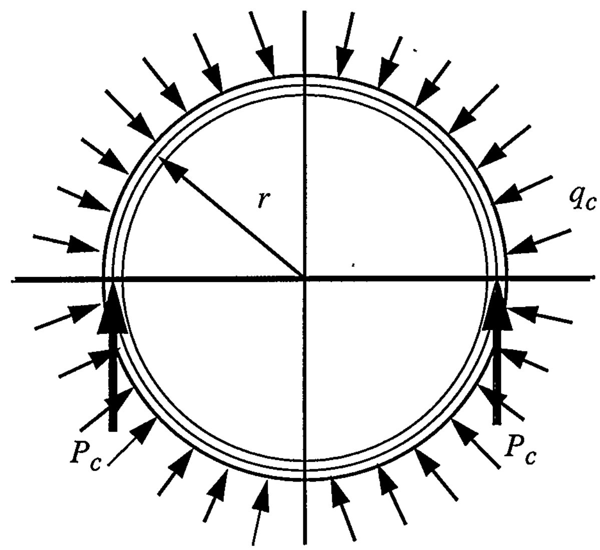

Figure 3.1 A Ring Subjected to the External Compression Force

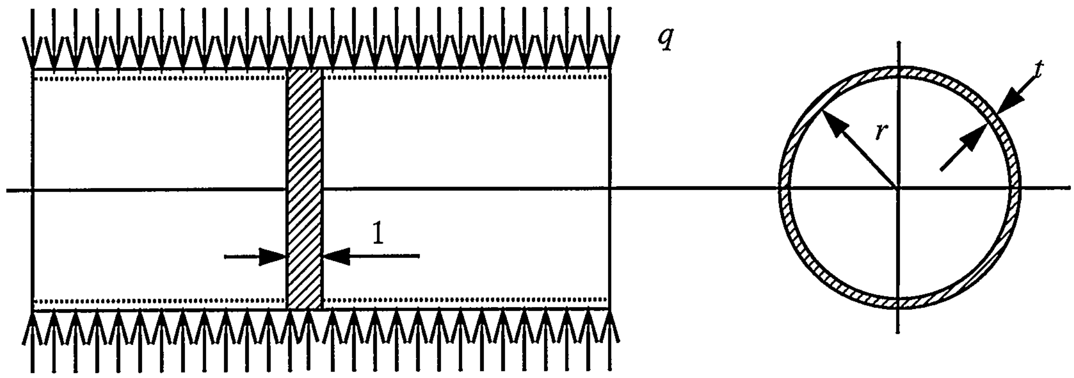

Figure 3.2 A Circular Cylinder Subjected to a Uniform External Pressure

Observing that the compression force P in the elemental ring of unit width is equal to qr where q is the uniform pressure, from Equation (3.3) the critical value of the external pressure for an edge free circular cylinder is

$$q_c = \frac{E}{4(1-\nu^2)}\left(\frac{t}{r}\right)^3 \tag{3.4}$$

Equations (3.3) and (3.4) can also be applied in the case of a shell with some constraint at the edges if the length of the shell is so long that the stiffening effect of any constraint at the edges can be neglected.

3.2.2 The Relationship of Interference and Interface-Pressure for Two Layer Cylinders

For a long circular cylinder subjected to internal pressure, q_1 and external pressure, q_2, as shown in Figure 3.3, the displacement in the radial direction is [47]

$$u_r = \frac{1-\nu}{E}\left(\frac{q_1r_1^2 - q_2r_2^2}{r_2^2 - r_1^2}\right)r + \frac{1+\nu}{E}\left(\frac{(q_1-q_2)\,r_1^2r_2^2}{r_2^2 - r_1^2}\right)\frac{1}{r} \tag{3.5-a}$$

If there is only external pressure, i.e., q_1=0, the equation (3.5-a) becomes

$$u_{r1} = -\frac{1-\nu}{E}\left(\frac{q_2r_2^2}{r_2^2 - r_1^2}\right)r - \frac{1+\nu}{E}\left(\frac{q_2r_1^2r_2^2}{r_2^2 - r_1^2}\right)\frac{1}{r} \tag{3.5-b}$$

If there is only internal pressure, i.e, q_2=0, the equation (3.5-a) becomes

$$u_{r2} = \frac{1-\nu}{E}\left(\frac{q_1r_1^2}{r_2^2 - r_1^2}\right)r + \frac{1+\nu}{E}\left(\frac{q_1r_1^2r_2^2}{r_2^2 - r_1^2}\right)\frac{1}{r} \tag{3.5-c}$$

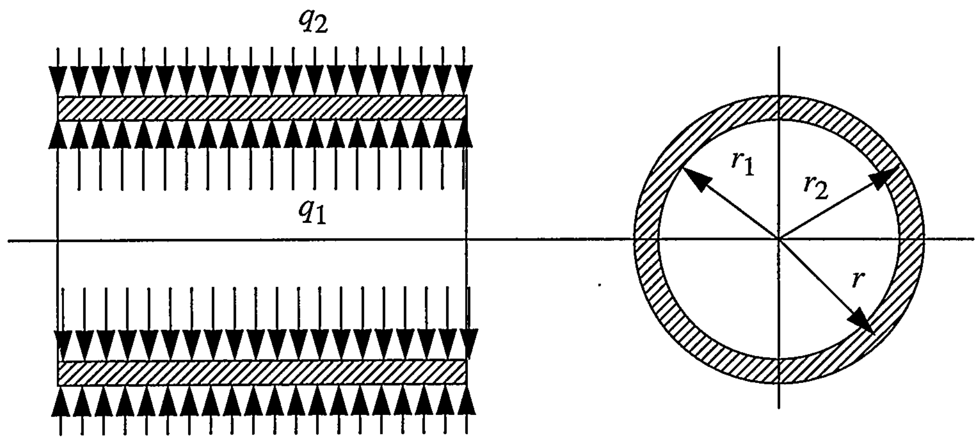

Figure 3.3 A Cylinder Subjected to Internal and External Pressures

For the interference fitted two layer circular cylinders, if the pressure q between the interference surface is given, then we can get the changes in diameters of the inner cylinder and the outer cylinder at the interference surface respectively. For the inner cylinder, we have

$$\Delta D_1 = 2\left[-\frac{1-\nu_1}{E_1}\left(\frac{qr_2^2}{r_2^2-r_1^2}\right)r_2 - \frac{1+\nu_1}{E_1}\left(\frac{qr_1^2r_2^2}{r_2^2-r_1^2}\right)\frac{1}{r_2}\right] \qquad (3.6\text{-a})$$

Similarly for the outer cylinder, we have

$$\Delta D_2 = 2\left[\frac{1-\nu_2}{E_2}\left(\frac{qr_2^2}{r_3^2-r_2^2}\right)r_2 + \frac{1+\nu_2}{E_2}\left(\frac{qr_2^2r_3^2}{r_3^2-r_2^2}\right)\frac{1}{r_2}\right] \qquad (3.6\text{-b})$$

From equations (3.6-a) and (3.6-b), we obtain the interference allowance ΔD for the given interference pressure q.

$$\Delta D = \Delta D_2 - \Delta D_1 = 2r_2q\left[\frac{r_3^2+r_2^2}{E_2(r_3^2-r_2^2)} + \frac{r_2^2+r_1^2}{E_1(r_2^2-r_1^2)} + \frac{\nu_2}{E_2} - \frac{\nu_1}{E_1}\right] \qquad (3.7)$$

where ν_1, ν_2 and E_1, E_2 are Poisson's ratios and Young's moduli of inner layer and outer layer respectively, and as shown in Figure 3.4, r_1 is inner layer's inside radius, r_3 is outer layer's outside radius and r_2 is the interference surface radius, and ΔD is the interference allowance. If the interference allowance ΔD is given based on the end use of the component, the pressure q in the interference surface also can be obtained from Equation (3.7)

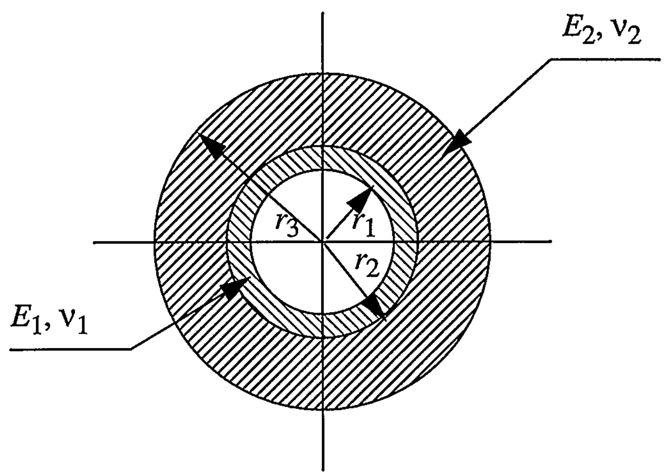

Figure 3.4 An Inner Ring Shrunk in an Outside Ring

$$q = \frac{\Delta D}{2r_2}\frac{1}{\frac{r_3^2+r_2^2}{E_2(r_3^2-r_3^2)}+\frac{r_2^2+r_1^2}{E_1(r_2^2-r_1^2)}+\frac{\nu_2}{E_2}-\frac{\nu_1}{E_1}} \tag{3.8}$$

For a thin elastic ring confined within a rigid boundary, the relationship between the interference allowance and the interface-pressure *(q)* at the interference surface can be obtained from Equation (3.7) and Equation (3.8) directly.

$$\Delta D = \frac{2qr^2}{Et} \tag{3.9}$$

and

$$q = \frac{\Delta DEt}{2r^2} \tag{3.10}$$

where *t* is the thickness of the ring and *r* is the middle radius of the ring.

3.3 Specimens and Dimensions

The material of the specimens was C-4161 steel tube, and the properties of the material are as following [48]:

$E = 200$ GPa, $\nu = 0.3$, $\sigma_y = 1700$ MPa, $\sigma_u = 1900$ MPa

The configuration of the specimens is shown in Figure 3.5, where D_{11} is the inside diameter of the inner tube, D_{12} is the outside diameter of the inner tube, D_{21} is the inside diameter of the outside tube, and D_{22} is the outside diameter of the outer tube, L is the length of the tubes.

From Figure 3.5, the interference allowance ΔD is

$$\Delta D = D_{12} - D_{21} \tag{3.11}$$

From Equation (3.4), the critical buckling pressure of the inner tube in the free boundary conditions is

$$q = \frac{E}{4(1-\nu^2)} \left(\frac{D_{12} - D_{11}}{D_{21}}\right)^3 \tag{3.12}$$

According to [56], if the buckling factor f is selected, the interface-pressure between the two tubes is

$$q_c = \mathrm{f}q \tag{3.13}$$

By using Equation (3.7), we can calculate the interference allowance ΔD for the correspondent pressure q.

$$\Delta D = \frac{D_{21} q_c}{E} \left[\frac{D_{22}^2 + D_{21}^2}{D_{22}^2 - D_{21}^2} - \frac{D_{21}^2 + D_{11}^2}{D_{21}^2 - D_{11}^2}\right] \tag{3.14}$$

The first experiment is designed to check the buckling data provided by industrial experience [56]. The inner tube's dimensions are

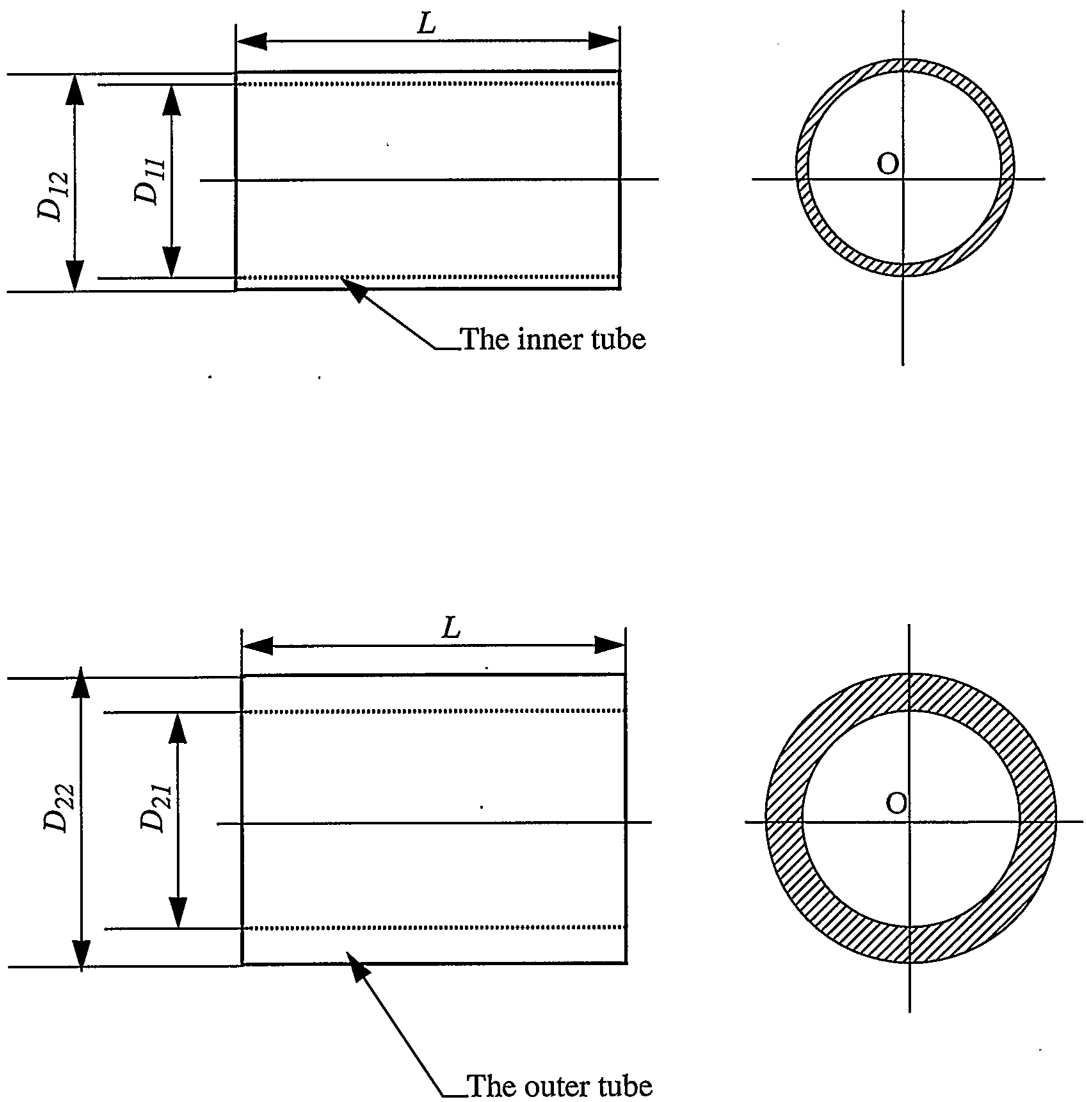

Figure 3.5 Specimen Configuration

$$D_{12} = 95\text{mm} \qquad D_{11} = 92.5\text{mm}$$

In free boundary conditions, from Equation (3.12) the critical buckling external pressure is

$$q = 0.76\text{MPa}$$

The industrial rule of thumb states that buckling occurs at a factor of 3.5 times that predicted from external pressure on thin ring and no buckling condition occurs at a factor of 3.0 [56]. In order to observe the buckling behaviour of the inner tube, the buckling factor f = 3.65 was selected and the corresponding interface-pressure q_c is

$$q_c = fq = 2.8\text{MPa}$$

Using equation (3.14) and taking D_{12} approximately equal to D_{21}, we obtain the interference allowance ΔD for the correspondent pressure q_c

$$\Delta D = 0.062\text{mm}$$

Then from Equation (3.11), we can determine the D_{12}

$$D_{12} = D_{21} - \Delta D = 95 - 0.062 = 94.938\text{mm}$$

In order to machine the specimens, the reasonable tolerance in dimensions should be defined. In consideration of practical usage and the machining ability in the workshop, the final dimensions of the specimens are defined as following:

$$D_{12} = 95^{+0.089}_{+0.068}\,\text{mm} \qquad D_{11} = 92.5^{+0.017}_{-0.017}\,\text{mm}$$

$$D_{21} = 95^{+0.034}_{-0.000}\,\text{mm} \qquad D_{22} = 115.0\text{mm}$$

According to above dimensions, the average, maximum and minimum interference allowance are

$$\Delta D_{\text{m}} = 0.0615\text{mm} \qquad \Delta D_{\max} = 0.089\text{mm} \qquad \Delta D_{min} = 0.034\text{mm}$$

respectively.

In order to investigate the effect in longitudinal direction, two different lengths of tube are designed, they are

$$L_1 = 25\text{mm} \qquad L_2 = 50\text{mm}$$

3.4 Experimental procedure

In assembling the two tubes together, the inner tube is contracted by sub-zero cooling to permit insertion into the outer tube and a tight fit is obtained as the temperature rises and the inner tube expands. In order to obtain the sub-zero temperature, liquid nitrogen was used, which has a temperature of about -196 °C. During a temperature reduction from 24 °C to -196 °C, the shrinkage per millimetre of diameter varies from about 0.002 to 0.003 millimetre for steel [48]. For the inner tube specimen, the shrinkage by using liquid nitrogen can reduce the outside diameter from D_{22} = 95 mm to 94.99-94.72 mm. This is enough for dropping the inner tube into the outer tube.

The experiment procedure includes following steps:

Step 1 Place the inner ring into a container and pour liquid nitrogen into the container. Ensure that the whole inner tube is immersed in the liquid nitrogen for about 10-20 seconds.

Step 2 Pick up the inner ring and drop it into the outer tube quickly. This step should be completed in about 3-5 seconds.

Step 3 Observe the inner tube's behaviour during the process in which the temperatures of inner and outer rings become equal.

3.5 Results and Discussion

The inner tube did not buckle even after the temperatures of the two tubes became equal. In order to investigate the buckling conditions, the assembly was mounted on the lathe and was cut little by little from inside. The cutting increment was 0.125 mm each time. When the thickness of the inner tube was reduced to 0.28 mm, it became loose along the interference surface but it still did not buckle.

When the inner tube was loose, the ratio of the pressure at the interface surface, q_c, to the free tube buckling critical pressure, q, is

$$f = \frac{q_c}{q} = 66$$

which is much larger than the rules of industrial thumb.

The preliminary experimental result shows that the rules of industrial thumb are too conservative and a more accurate method should be established to predict the buckling conditions for a ring confined within a rigid boundary.

Chapter 4

DIMENSIONAL ANALYSIS METHOD

4.1 Introduction

Many problems in engineering and particularly in fluid mechanics are successfully resolved by an experimental analysis based on tests of appropriately established models using the dimensional analysis method. This method is particularly useful in the solution of complex problems in which prototype systems can be simulated by adequate models which can be easily built and tested. The feasibility of this analysis is usually limited by the material and other properties of the models. In experimental fluid mechanics a general methodology based on the dimensional analysis of models is well established. In the field of elastic stability, however, theoretical methods dominated the area and experiments are used just as a verification on theoretical work. But a practical structural system may become extremely complex and a theoretical solution of the problem is very difficult or even impossible. Sometimes in a simplified and idealized situation, a theoretical solution may be obtained but it can only be used as a guide to the practical behaviour. Although no general experimental discipline based on the dimensional analysis of model structures has yet emerged in problems of structural stability, a basis for an analysis of buckling problems is the same as for experimental fluid mechanics.

4.2 Dimensional Analysis

The dimensional analysis method is based on two axioms [49] which are inherent in our methods of measurement and evaluation of quantities.

1. Absolute numerical equality of quantities may exist only when the quantities are similar qualitatively. That is, a general relationship may be established between two quantities only when the two quantities have the same dimensions.

2. The ratio of the magnitude of two like quantities is independent of the units used in their measurement, provided that the same units are used for evaluating each.

Dimensional analysis, developed from these two axioms, differs from other methods of analysis in that it is based solely on the relationships that must exist among the pertinent variables because of their dimensions, instead of being based on other so-called natural laws, such as Newton's Laws of Motion for example. In itself, dimensional analysis gives qualitative rather than quantitative relationships, but when combined with experimental procedures it often results in quantitative relationships and accurate prediction equations.

If a certain number of dimensional variables are involved in a problem these variables can be combined in a definite number of dimensionless products. These products are usually denoted by the letter Π. A theorem due to Buckingham[49], also known as the Pi theorem, states that the number of such independent products is equal to the difference of the number m of the dimensional variables in the problem and the minimum number n of dimensions, in terms of how these variables can be described. Then, a homogeneous function F of the dimensionless products exists, such that

$$F(\Pi_1, \Pi_2, ..., \Pi_{m-n}) = 0 \tag{4.1}$$

From this relation any one of the products, say Π_1, can be written as

$$\Pi_1 = f(\Pi_2, \Pi_3, ..., \Pi_{m-n}) \tag{4.2}$$

The key for the success of a dimensional analysis model is the choice of correct and suitable quantities for the functional Equation (4.2).

For example[50], a cable is stretched between two points a fixed distance apart at the same level. Find a relationship between the tension, P, and the sag, h, the length of the cable, l, and its weight, W. The problem is to express P as a function of W, h and l, or

$$P = f(W, h, l)$$

where $f(W, h, l)$ is an unknown function. Assuming that this function is in the form of a production of powers, we have

$$P = AW^a h^b l^c \tag{a}$$

where A, a, b and c are unknown numbers.

The dimensions of the quantities for the terms in Equation (a) are

$$
\begin{aligned}
[P] &= [MLT^{-2}] \\
[W] &= [MLT^{-2}] \\
[h] &= [L] \\
[l] &= [L]
\end{aligned}
\qquad \text{(b)}
$$

where [M] presents for the dimension of mass, [L] for dimension of length and [T] for dimension of time. Substituting (b) in (a) we have

$$[MLT^{-2}] = [MLT^{-2}]^{a}[L]^{b}[L]^{c} \qquad \text{(c)}$$

For dimensional homogeneity the powers of M, L and T must be the same on both sides of Equation (c).

M: $\quad 1 = a$

L: $\quad 1 = a + b + c$

T: $\quad -2 = -2a$

From which we have

$$
\begin{aligned}
a &= 1 \\
b &= -c
\end{aligned}
$$

Thus Equation (a) becomes

$$P = AWh^{-c}l^{c} = W\left[A\left(\frac{h}{l}\right)^{-c}\right] \tag{d}$$

In dimensionless form, this equation becomes

$$\frac{P}{W} = f\left(\frac{h}{l}\right) = A\left(\frac{h}{l}\right)^{-c} \tag{e}$$

Since neither A nor c is known, dimensional analysis has not provided a complete solution in this case. But it has indicated that P is directly proportional to W and that the ratio $\frac{h}{l}$ is a determining factor in the relationship rather than the separate quantities h and l.

Now consider the shrink buckling problem, as pointed out in Chapter 2, if both the ring and rigid confinement are perfect geometrically and there is no external disturbance, there will be no limit point or critical pressure. In other words, the ring will never buckle when both the ring and rigid confinement are perfect geometrically unless there is a large enough external disturbance to overcome the energy barrier [12]. The external disturbance is a random factor and is very difficult to be simulated and controlled. Therefore in the dimensional analysis model, the geometric imperfections of a ring and a rigid confinement should be taken into consideration. However, the influence of imperfections of the ring is not as large as the rigid confinement and can generally be ignored[6,7]. For simplification, only a point imperfection on the rigid confinement was taken into consideration. Nevertheless, this point imperfection can also be considered as a combination effect of the geometric imperfection and the external disturbance. It is assumed that a point imperfection on the rigid confinement has a height δ and as a result the ring has an initial deflection δ before buckling.

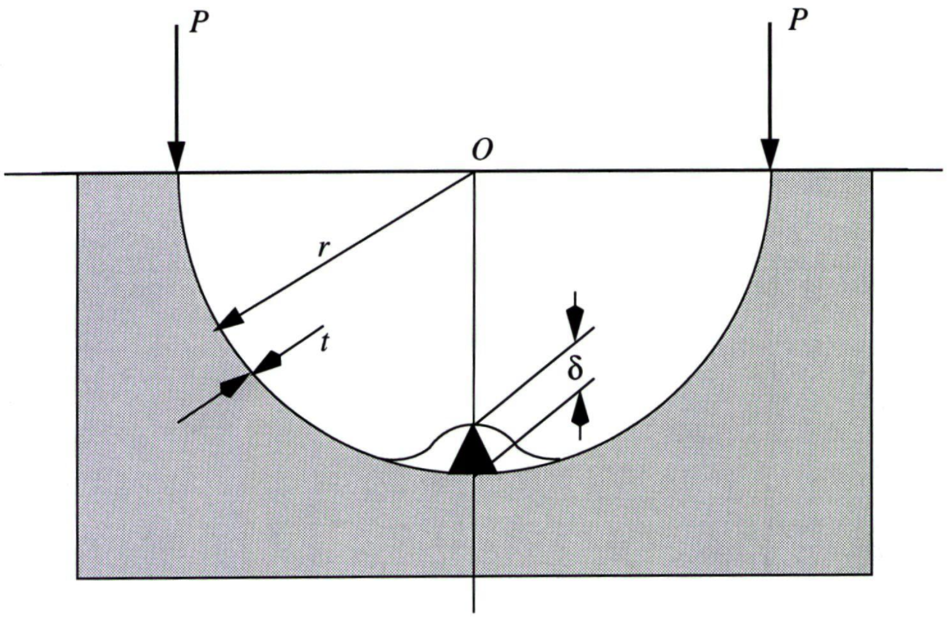

Figure 4.1 A Ring under Compression Load with
a Point Obstacle on the Boundary

In the following process some basic assumptions were used:

(1) The ring is made of a homogeneous, isotropic and linear elastic material.

(2) There is no friction on the interface between a ring and a rigid boundary.

(3) The unbuckled and the buckled configurations of the ring are both symmetrical to one of the diametral lines of the original ring.

Under the above assumptions it is evident that the axial compressive buckling force P_c is determined completely by the following parameters (see Figure 4.1):

E -- modulus of elasticity of the material of the ring.

r -- radius of the ring.

t -- thickness of the ring.

δ -- initial deflection of the ring due to the imperfection of the rigid confinement at the buckling location.

For a unit width ring it can be assume that

$$P_c = CE^a r^b t^c \delta^d \tag{4.3}$$

where P_c is the critical buckling compression force per unit width of a ring, C is an undetermined coefficient and a, b, c, and d are undetermined exponents. There are five dimensional quantities in Equation (4.3), which are P_c, E, r, t, and δ. And the minimum of dimensions are two in Equation (4.3), which are [F] (force) and [L] (length). According to Pi theorem, $m - n = 5 - 2 = 3$; that is, Equation (4.3) can be described by three dimensionless products. The dimensions of the quantities in Equation (4.3) are

$$
\begin{aligned}
[E] &= [\mathrm{FL}^{-2}] \\
[r] &= [\mathrm{L}] \\
[t] &= [\mathrm{L}] \\
[\delta] &= [\mathrm{L}] \\
[P_c] &= [\mathrm{FL}^{-1}]
\end{aligned}
\tag{4.4}
$$

Substituting Equation (4.4) into Equation (4.3), we have

$$[\mathrm{FL}^{-1}] = [\mathrm{FL}^{-2}]^{a}[\mathrm{L}]^{b}[\mathrm{L}]^{c}[\mathrm{L}]^{d} \tag{4.5}$$

According to Axiom 1 both sides of Equation (4.5) should have the same dimensions. That is the exponents of F(force) and L(length) must be the same on both sides of Equation (4.5) for dimensional homogeneity. Thus we obtain

$$\mathrm{F}: \qquad a = 1 \tag{4.6a}$$

$$\mathrm{L}: \qquad -2a+b+c+d = -1 \tag{4.6b}$$

Expressing a and c in terms of b and d in Equations (4.6), we obtain

$$
\begin{aligned}
a &= 1 \\
c &= 1-b-d
\end{aligned}
\tag{4.7}
$$

Substituting Equation (4.7) into Equation (4.3) yields

$$P_c = CEr^b t^{(1-b-d)} \delta^d$$
$$= CEt \left(\frac{r}{t}\right)^b \left(\frac{\delta}{t}\right)^d \tag{4.8}$$

Dividing two sides of Equation (4.8) by *Et*, we finally obtain

$$\frac{\sigma_c}{E} = f\left[\left(\frac{r}{t}\right), \left(\frac{\delta}{t}\right) \right] \tag{4.9}$$

where

$$f\left[\left(\frac{r}{t}\right), \left(\frac{\delta}{t}\right) \right] = C \left(\frac{r}{t}\right)^b \left(\frac{\delta}{t}\right)^d \tag{4.10}$$

$f\left[\left(\frac{r}{t}\right), \left(\frac{\delta}{t}\right) \right]$ is an unknown function with two non-dimensional variables $\left(\frac{r}{t}\right)$ and $\left(\frac{\delta}{t}\right)$, one undetermined coefficient C and two undetermined exponents b and d. This function is referred to as the buckling function hereafter.

4.3 Validation Test for the Buckling Function

From Equation (4.8) it can be seen that the critical buckling stress σ_c is proportional to elastic modulus, E, and the buckling function $f\left[\left(\frac{r}{t}\right), \left(\frac{\delta}{t}\right) \right]$ is independent of the material properties in the elastic region. Whether or not the buckling function $f\left[\left(\frac{r}{t}\right), \left(\frac{\delta}{t}\right) \right]$ is in the form of Equation (4.10) can be examined by an experimental method [49]. First, experiments can be carried out by varying $\left(\frac{r}{t}\right)$ and holding $\left(\frac{\delta}{t}\right)$

as a constant. From a plot of $\left(\frac{\sigma_c}{E}\right)$ against $(\frac{r}{t})$, the relationship

$$\left(\frac{\sigma_c}{E}\right)_1 = f_1\left[\,(\frac{r}{t}),\ (\frac{\bar{\delta}}{t})\right] \tag{4.11}$$

where the bar over $(\frac{\delta}{t})$ denotes constant values, could be established. From another set of experiments with $(\frac{r}{t})$ constant and $(\frac{\delta}{t})$ variable,

$$\left(\frac{\sigma_c}{E}\right)_2 = f_2\left[\,(\frac{\bar{r}}{t}),\ (\frac{\delta}{t})\right] \tag{4.12}$$

may be established. Equations such as equations (4.11) and (4.12), determined by holding all but one of the dimensionless variables in the function constant, will be called component equations.

Under certain conditions the component equations may be combined to form the general prediction equation by the multiplication of Equation (4.11) and Equation (4.12), i.e.,

$$\frac{\sigma_c}{E} = C\left(\frac{\sigma_c}{E}\right)_1\left(\frac{\sigma_c}{E}\right)_2 \tag{4.13}$$

To establish those conditions, the constant C in equation (4.13) can first be determined by assuming that the component equations are simply multiplied to form the general equation.

$$f\left[\,(\frac{r}{t}),\ (\frac{\delta}{t})\right] = f_1\left[\,(\frac{r}{t}),\ (\frac{\bar{\delta}}{t})\right]f_2\left[\,(\frac{\bar{r}}{t}),\ (\frac{\delta}{t})\right] \tag{4.14}$$

If this is true, the first set of tests, with $(\frac{\delta}{t})$ constant, will give

$$f\left[(\frac{r}{t}), (\frac{\bar{\delta}}{t})\right] = f_1\left[(\frac{r}{t}), (\frac{\bar{\delta}}{t})\right] f_2\left[(\frac{\bar{r}}{t}), (\frac{\bar{\delta}}{t})\right] \tag{4.15}$$

From which

$$f_1\left[(\frac{r}{t}), (\frac{\bar{\delta}}{t})\right] = \frac{f\left[(\frac{r}{t}), (\frac{\bar{\delta}}{t})\right]}{f_2\left[(\frac{\bar{r}}{t}), (\frac{\bar{\delta}}{t})\right]} \tag{4.16}$$

The second set of tests, with $(\frac{\delta}{t})$ constant, gives, from Equation (4.14)

$$f_2\left[(\frac{\bar{r}}{t}), (\frac{\delta}{t})\right] = \frac{f\left[(\frac{\bar{r}}{t}), (\frac{\delta}{t})\right]}{f_1\left[(\frac{\bar{r}}{t}), (\frac{\bar{\delta}}{t})\right]} \tag{4.17}$$

Values of $f_1\left[(\frac{r}{t}), (\frac{\bar{\delta}}{t})\right]$ and $f_2\left[(\frac{\bar{r}}{t}), (\frac{\delta}{t})\right]$ from Equations (4.16) and (4.17) are substituted into Equation (4.14) to give

$$f\left[(\frac{r}{t}), (\frac{\delta}{t})\right] = \frac{f\left[(\frac{r}{t}), (\frac{\bar{\delta}}{t})\right] f\left[(\frac{\bar{r}}{t}), (\frac{\delta}{t})\right]}{f_2\left[(\frac{\bar{r}}{t}), (\frac{\bar{\delta}}{t})\right] f_1\left[(\frac{\bar{r}}{t}), (\frac{\bar{\delta}}{t})\right]} \tag{4.18}$$

However, from Equation (4.14) it is found that

$$f\left[\left(\frac{\bar{r}}{t}\right), \left(\frac{\bar{\delta}}{t}\right)\right] = f_1\left[\left(\frac{\bar{r}}{t}\right), \left(\frac{\bar{\delta}}{t}\right)\right] f_2\left[\left(\frac{\bar{r}}{t}\right), \left(\frac{\bar{\delta}}{t}\right)\right] \tag{4.19}$$

Thus

$$f\left[\left(\frac{r}{t}\right), \left(\frac{\delta}{t}\right)\right] = \frac{f\left[\left(\frac{r}{t}\right), \left(\frac{\bar{\delta}}{t}\right)\right] f\left[\left(\frac{\bar{r}}{t}\right), \left(\frac{\delta}{t}\right)\right]}{f\left[\left(\frac{\bar{r}}{t}\right), \left(\frac{\bar{\delta}}{t}\right)\right]} \tag{4.20}$$

Comparing equation (4.13) with equation (4.20), it is found

$$C = \frac{1}{f\left[\left(\frac{\bar{r}}{t}\right), \left(\frac{\bar{\delta}}{t}\right)\right]} \tag{4.21}$$

and that the two component equations must have the same form.

A test for the validity of combining the component equations as a product may now be developed by assuming that a third component equation is determined from a third set of data in which one of the dimensionless variables is held constant at a different value than in the preceding set of data. For example, the general equation (4.20) was determined by holding the $\left(\frac{r}{t}\right)$ constant at a value of $\left(\frac{\bar{r}}{t}\right)$, but if valid, it could also have been determined from a set of data in which $\left(\frac{r}{t}\right) = \left(\frac{\bar{\bar{r}}}{t}\right)$. Then

$$f\left[\left(\frac{r}{t}\right), \left(\frac{\delta}{t}\right)\right] = \frac{f\left[\left(\frac{r}{t}\right), \left(\frac{\bar{\delta}}{t}\right)\right] f\left[\left(\frac{\bar{\bar{r}}}{t}\right), \left(\frac{\delta}{t}\right)\right]}{f\left[\left(\frac{\bar{\bar{r}}}{t}\right), \left(\frac{\bar{\delta}}{t}\right)\right]} \tag{4.22}$$

The right-hand side of equation (4.20) must equal the right-hand side of equation (4.22), hence,

$$\frac{f\left[\left(\frac{\bar{r}}{t}\right), \left(\frac{\delta}{t}\right)\right]}{f\left[\left(\frac{\bar{r}}{t}\right), \left(\frac{\bar{\delta}}{t}\right)\right]} = \frac{f\left[\left(\frac{\bar{\bar{r}}}{t}\right), \left(\frac{\delta}{t}\right)\right]}{f\left[\left(\frac{\bar{\bar{r}}}{t}\right), \left(\frac{\bar{\delta}}{t}\right)\right]} \tag{4.23}$$

Similarly, if $\left(\frac{\delta}{t}\right)$ had been held constant at a different value, $\left(\frac{\bar{\bar{\delta}}}{t}\right)$,

$$\frac{f\left[\left(\frac{r}{t}\right), \left(\frac{\bar{\delta}}{t}\right)\right]}{f\left[\left(\frac{\bar{r}}{t}\right), \left(\frac{\bar{\delta}}{t}\right)\right]} = \frac{f\left[\left(\frac{r}{t}\right), \left(\frac{\bar{\bar{\delta}}}{t}\right)\right]}{f\left[\left(\frac{\bar{r}}{t}\right), \left(\frac{\bar{\bar{\delta}}}{t}\right)\right]} \tag{4.24}$$

Equations (4.23) and (4.24) constitute a test for the validity of Equation (4.20). That is, if the supplementary sets of data satisfy either Equation (4.23) or Equation (4.24), the general equation may be formed by multiplying the component equations together and dividing by the constant, as indicated in Equation (4.20).

4.4 Summary

From the dimensional analysis we know:

1. The critical buckling compression stress of a ring confined within a rigid boundary is directly proportional to the elastic modulus of the material.

2. The buckling function $f\left[\left(\frac{r}{t}\right), \left(\frac{\delta}{t}\right)\right]$, is independent of material properties but

dependent on two dimensionless variables $(\frac{r}{t})$ and $(\frac{\delta}{t})$.

3. The buckling function has one undetermined coefficient C and two undetermined exponents b and d. These undetermined coefficient and exponents can be derived from experimental results.

All these conclusions are held only in elastic region.

Chapter 5

DISCRETIZATION OF PROBLEM: MODEL ONE

5.1 Introduction

In Chapter 4, a approximate relationship between the compressive buckling stress of a thin elastic ring confined within a rigid boundary was derived by use of the dimensional analysis. It was based upon the ring dimensions, material properties and the geometric imperfection of the rigid boundary. The geometric imperfection was treated as a point obstacle which results in creating an initial deflection in the ring prior to the buckling condition. This relationship (see Equations (4.9) and (4.10)) can be rewritten as one equation as follows:

$$\frac{\sigma}{E} = C\left(\frac{r}{t}\right)^{b}\left(\frac{\delta}{t}\right)^{d} \tag{5.1}$$

In this chapter, the problem will be approached in a totally different manner. First, a physical discrete model will be established by applying the discrete element method. A relationship of the compressive buckling stress σ with the radius of the boundary, r, the thickness of the ring, t, and the initial deflection, δ, will be derived from the equilibrium analysis to the model. Finally, a comparison of the results from this model with results from the dimensional analysis method and the experiment will be made.

5.2 Basic Assumptions

Before establishing the discrete model, some basic assumptions should be made as follows,

(1) The ring is inextensible, i.e., before and after buckling, the length of the ring is the same;

(2) The buckled configuration of the ring is symmetrical to one of the diameter lines of the boundary;

(3) The ring is made of a homogeneous, isotropic and linear elastic material;

(4) There is no friction in the interface between the ring and the rigid boundary.

5.3 Discrete Element Method

The discrete element method may be regarded as an elementary version of the finite element method [51]. The basic idea of the discrete element method can be illustrated by considering the elementary problem of finding the deflection of a simply supported beam such as that shown in Figure 5.1. The deflection curve will be approximated by two lines as shown in Figure 5.1(a). These straight lines of deflection correspond to a fictitious discrete system consisting of two rigid links connected at an elastic hinge (1) as shown in Figure 5.1 (b). The idea is equivalent to replacing the original continuous beam by a number of fictitious discrete links, and localizing the rotation at discrete nodal points which can be viewed as elastic hinges or frictionless hinges with linear elastic rotational springs. The main task is thus to find the elastic constants

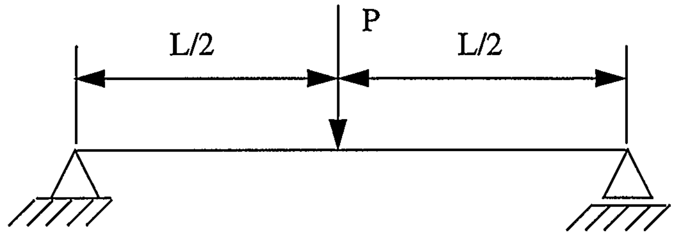

(a)

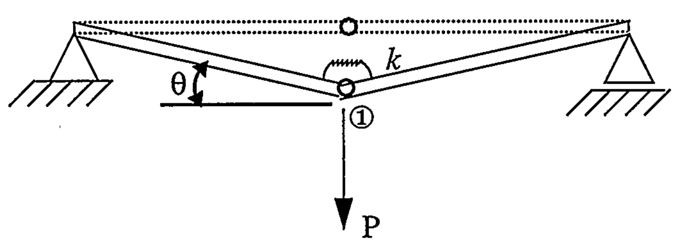

(b)

Figure 5.1 Basic Idea of the Discrete Element Method

k of these fictitious springs. To achieve this, we start from the well-known beam formula (see Figure 5.2):

$$M = EI\theta' \qquad \theta' = \frac{d\theta}{dx} \tag{5.2}$$

From this, we see that

$$\theta' = \frac{d\theta}{dx} = \frac{M}{EI} \tag{5.3}$$

which means

$$\lim_{\Delta x \to 0} \frac{\Delta\theta}{\Delta x} = \frac{M}{EI} \tag{5.4}$$

Discretilizing Equation (5.3), an approximate expression can be obtained as:

$$\frac{\Delta\theta}{\Delta x} \approx \frac{M}{EI} \qquad \text{or} \qquad M \approx \frac{\Delta\theta}{\Delta x} EI \tag{5.5}$$

which for small angles is nearly exact. On the other hand, the bending moment in the two-link discrete model is

$$M = k\Delta\theta \tag{5.6}$$

where $\Delta\theta$ is the change in the slope at the hinge. If the bending moment is to be the same in both the discrete and the continuous model, as it should be, then we would have

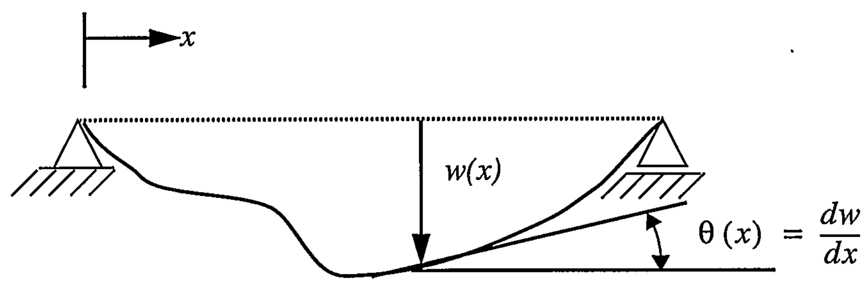

Figure 5.2 General Relationship of the Slope and the Bending Moment

$$M = EI\theta' \approx EI\frac{\Delta\theta}{\Delta x} = k\Delta\theta \tag{5.7}$$

from which we obtain

$$k = \frac{EI}{\Delta x} \tag{5.8}$$

Observing that the Δx is nothing but $\frac{L}{n}$, where n is the number of links, we immediately find the expression for the constants of the fictitious spring as

$$k = \frac{nEI}{L} \tag{5.9}$$

In our particular example, $k = \frac{2EI}{L}$. Finding the maximum deflection is now a trivial matter from a simple application of the equilibrium method. In Figure 5.3, we find from $\sum M_{(1)} = 0$ that

$$\frac{PL}{4} - k\Delta\theta = 0 \tag{5.10}$$

Since $k = \frac{2EI}{L}$ and $\Delta\theta = \frac{4\delta}{L}$, we obtain

$$\delta = \frac{PL^3}{32EI} = 0.03125\frac{PL^3}{EI} \tag{5.11}$$

The exact value is $\delta = 0.0208\frac{PL^3}{EI}$; the error is 33 per cent. In order to improve the result, we simply increase the number of links.

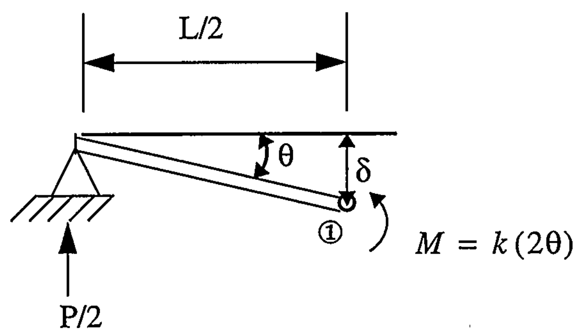

Figure 5.3 Discrete Beam Link

5.4 Model Description

According to the idea of the discrete element method and our basic assumptions, the ring will be replaced by the elastic chain shown in Figure 5.4, which consists of straight rigid links connected at frictionless hinges with elastic rotational springs whose spring constants are k. Therefore, the portion of buckled ring can be simplified as a model as shown in Figure 5.5 which consists of four rigid links with rotational springs at connect node 1,0 and 2. The node 0 lifts off from the rigid boundary because of an initial deflection which is caused by the imperfection at the point 0'. One half of the central angle subtended by the lifted portion 102 is α. The other nodes keep contact with the boundary.

The length of each link is

$$l = \alpha r \tag{5.12}$$

and considering Equation (5.8), the constant of the rotational spring is

$$k = \frac{EI}{l} = \frac{EI}{\alpha r} \tag{5.13}$$

Based on the inextensible assumption, node 1 and node 2 will not move when node 0 is lifted off the boundary by a point imperfection. Thus link chain $\overline{102}$ is symmetric about the x-axis with the original position $\overline{10'2}$. Then from Figure 5.5 we have

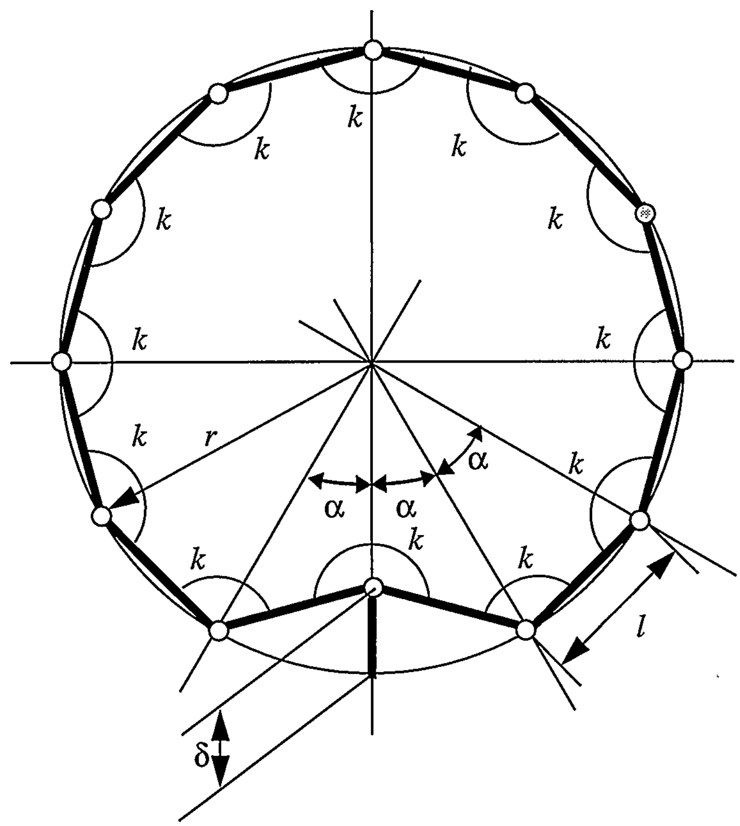

Figure 5.4 The Discrete Model of a Thin Ring with An Initial Deflection δ

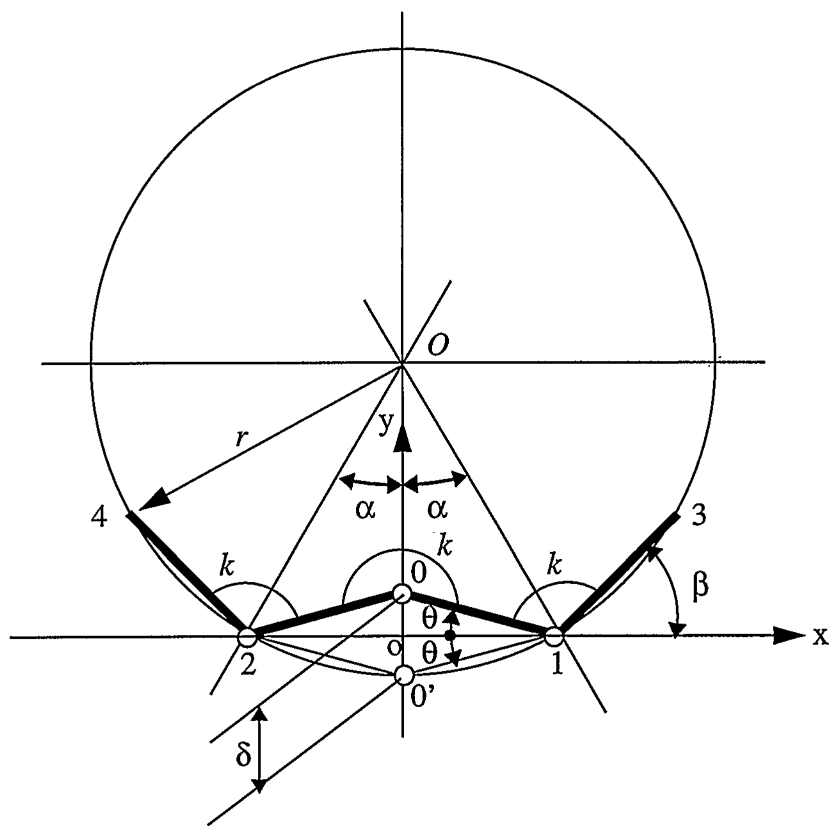

Figure 5.5 Geometric Parameters at the Location

of the Point Boundary Imperfection

$$\delta = 2r(1-\cos\alpha) \tag{5.14}$$

$$\theta = \frac{\alpha}{2} \tag{5.15}$$

$$\beta = \frac{3}{2}\alpha \tag{5.16}$$

From Equations (5.12)-(5.26) it can be seen that for a given ring radius, *r*, the number of rigid link is totally determined by the initial deflection, δ. For instance, if $r = 200mm$, when $\delta = 1mm$, the number of rigid link for a quarter of ring is about 22; when $\delta = 5mm$, the number of rigid link for a quarter ring is about 10.

5.5 Equilibrium Equation and Solution

Considering the free body diagram of link $\overline{01}$ as shown in Figure 5.6 and taking moments about point 1, we have

$$M_0 + M_1 - F\frac{\delta}{2} - \frac{R_0}{2}l\cos\theta = 0 \tag{5.17}$$

where M_0 and M_1 are reaction moments at node 0 and 1 caused by the changes of angle between two bars connected at these points, i.e.,

$$M_0 = 4k\theta \tag{5.18}$$

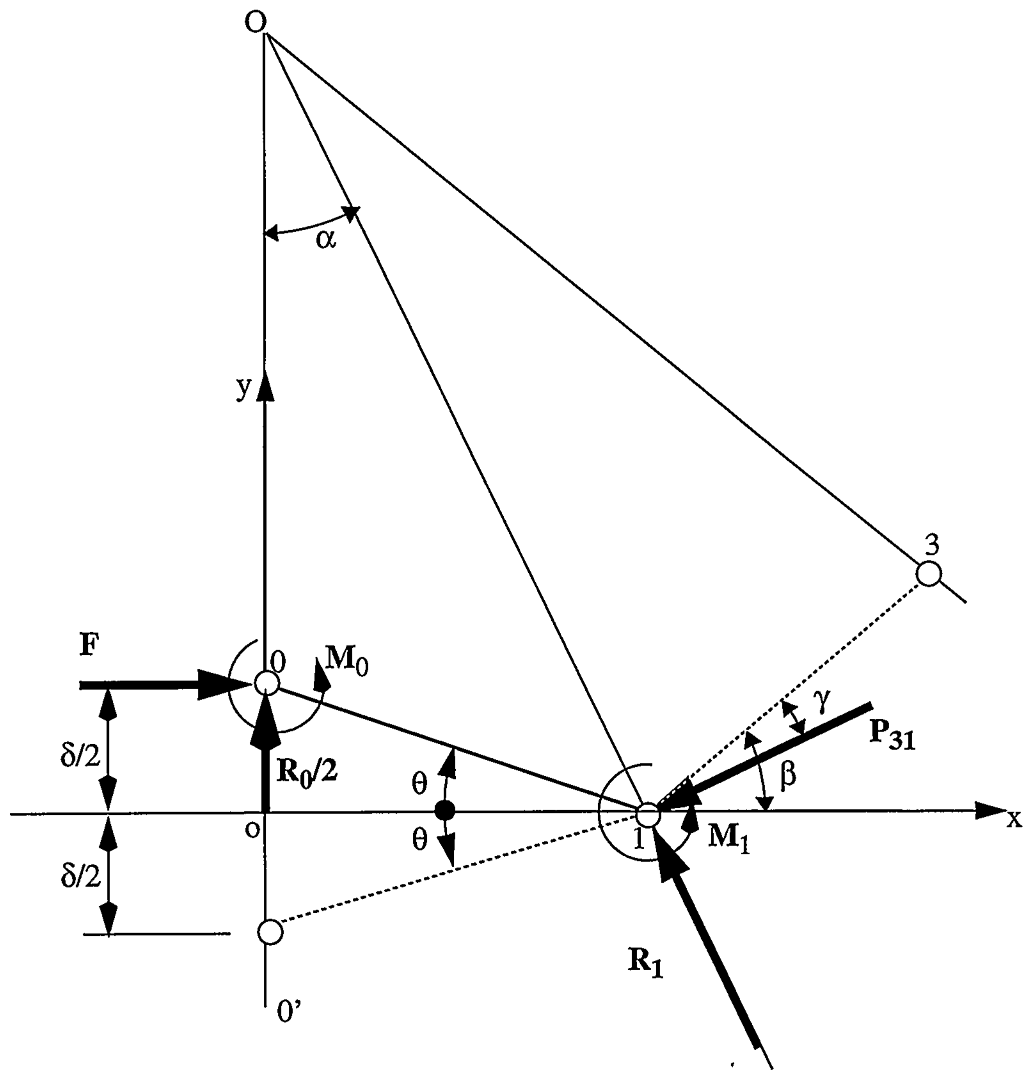

Figure 5.6 Free Body Diagram of Link $\overline{01}$

$$M_1 = 2k\theta \qquad (5.19)$$

R_0 is the reaction force of the point imperfection to the ring at point 0. There is only a horizontal reaction force F of link $\overline{02}$ to link $\overline{01}$ at point 0 because of the symmetric condition. When buckling occurs, the reaction force of the point imperfection on the rigid boundary to the point 0 of the ring will vanish, thus $R_0 = 0$. Then Equation (5.17) becomes

$$M_0 + M_1 - F\frac{\delta}{2} = 0 \qquad (5.20)$$

There are two forces at point 1, R_1 and P_{31}. $P_{31}$is the reaction force of link $\overline{13}$ to link $\overline{10}$ and R_1 is the reaction force of the rigid boundary toward point 1of the ring. From the equilibrium force equations in x and y directions, we have

$$F - [P_{31}\cos(\beta-\gamma) + R_1\sin\alpha] = 0 \qquad (5.21a)$$

$$R_1\cos\alpha - P_{31}\sin(\beta-\gamma) = 0 \qquad (5.21b)$$

Solving the above equations we obtain

$$F = P_{31}[\cos(\beta-\gamma) + \sin(\beta-\gamma)\tan\alpha] \qquad (5.22)$$

Bringing equations (5.18), (5.19) and (5.22) into equation (5.20) yields

$$2k\theta + 4k\theta - P_{31}\left[\cos(\beta-\gamma) + \sin(\beta-\gamma)\tan\alpha\right]\frac{\delta}{2} = 0 \tag{5.23}$$

then

$$P_{31} = \frac{12k\theta}{\delta}\frac{1}{\cos(\beta-\gamma) + \sin(\beta-\gamma)\tan\alpha} \tag{5.24}$$

Figure 5.7 is the free body diagram of link $\overline{13}$. Considering the moments about node 3 (Figure 5.7 (a)) we have

$$M_1 - P_{13}l\sin\gamma = 0 \tag{5.25}$$

Because P_{13}=P_{31} and M_1=$2k\theta$, we get

$$2k\theta - P_{31}l\sin\gamma = 0 \tag{5.26}$$

Bringing equation (5.24) into equation (5.26) yields

$$3\alpha\sin\gamma - (1-\cos\alpha)\left[\cos(\beta-\gamma) + \sin(\beta-\gamma)\tan\alpha\right] = 0 \tag{5.27}$$

From Figure 5.7 (b) we have

$$P = P_{31}\frac{\cos\left(\frac{\alpha}{2}+\gamma\right)}{\cos\frac{\alpha}{2}} \tag{5.28}$$

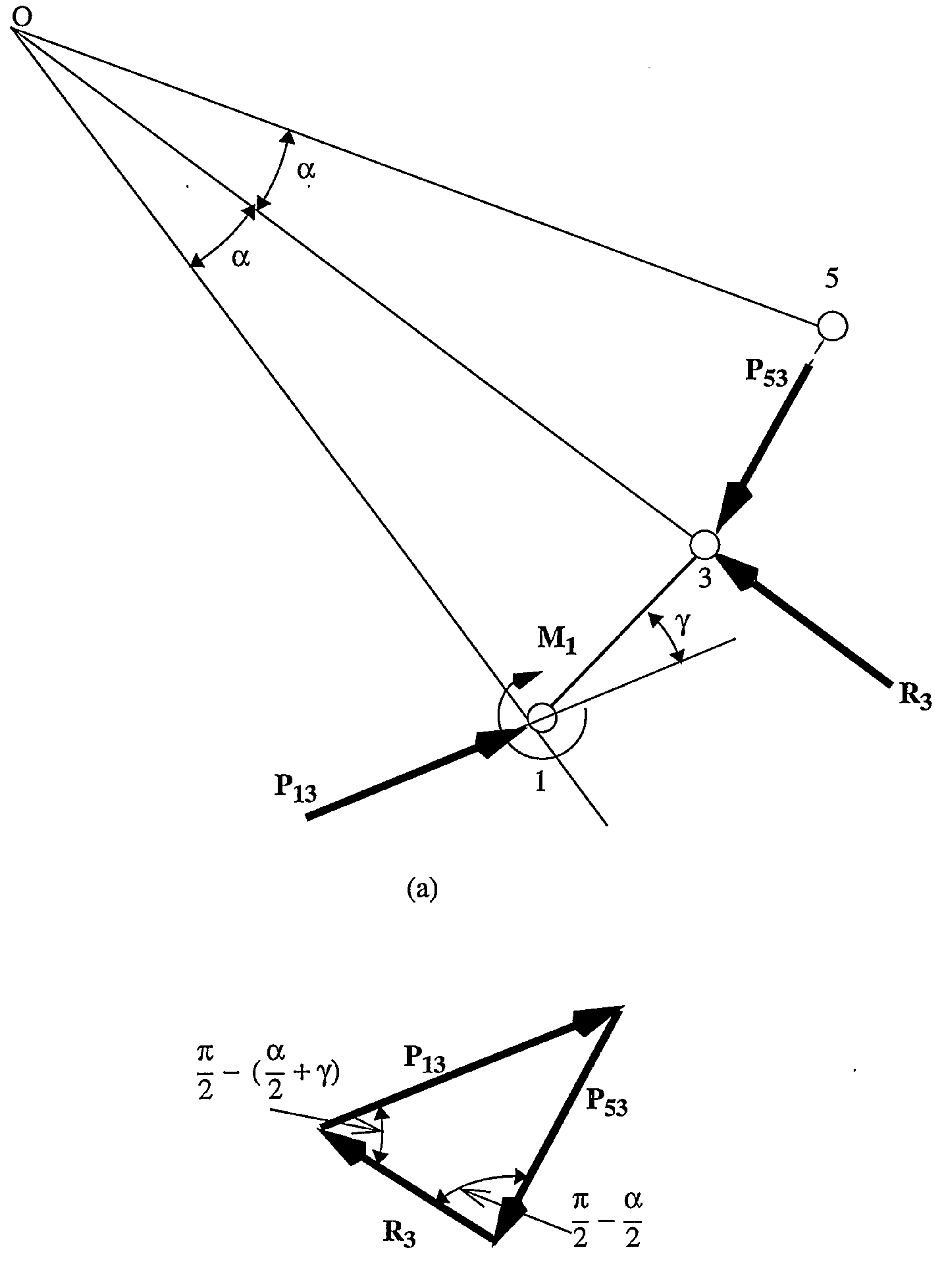

Figure 5.7 Free Body Diagram of Link $\overline{13}$

Substituting equation (5.24) into equation (5.28) we obtain

$$P = \frac{12k\theta}{\delta} \frac{\cos\left(\frac{\alpha}{2}+\gamma\right)}{\cos\frac{\alpha}{2}\left[\cos\left(\beta-\gamma\right)+\sin\left(\beta-\gamma\right)\tan\alpha\right]} \tag{5.29}$$

Substituting equations (5.13),(5.15) and (5.16) into equation (5.29), we obtain

$$P = \frac{6EI}{r\delta} \frac{\cos\left(\frac{\alpha}{2}+\gamma\right)}{\cos\frac{\alpha}{2}\left[\cos\left(\frac{3}{2}\alpha-\gamma\right)+\sin\left(\frac{3}{2}\alpha-\gamma\right)\tan\alpha\right]} \tag{5.30}$$

Considering

$$I = \frac{Bt^3}{12} \tag{5.31}$$

and letting

$$C_\alpha = \frac{\cos\left(\frac{\alpha}{2}+\gamma\right)}{\cos\frac{\alpha}{2}\left[\cos\left(\frac{3}{2}\alpha-\gamma\right)+\sin\left(\frac{3}{2}\alpha-\gamma\right)\tan\alpha\right]} \tag{5.32}$$

we finally obtain

$$\frac{\sigma}{E} = \frac{1}{2}\left(\frac{r}{t}\right)^{-1}\left(\frac{\delta}{t}\right)^{-1} C_\alpha \tag{5.33}$$

where $\sigma = \frac{P}{Bt}$ is the compression stress of the ring.

5.6 Comparison with the Results of the Dimensional Analysis Method

Up to now, we have obtained two formulations of the relationship between the critical buckling stress and the geometric factors of the structure from two totally different methods. Following the principles of the dimensional analysis, we derived Equation (5.1). By processing discrete model analysis, we obtained Equation (5.33). Comparing Equation (5.1) with Equation (5.33), it is obvious that the two equations have essentially the same relations. In Equation (5.1), there are three undetermined constants *C, b* and *d* which can be determined by experimental data analysis. While in Equation (5.33) the corresponding three constants are

$$C = \frac{1}{2}C_\alpha$$
$$b = -1$$
$$d = -1$$

But the coefficient C_α is not a constant. The coefficient C_α in Equation (5.33) is a function of the center angle α as shown in Equation (5.32). Studying Equation (5.32) in detail, it can be found that C_α has a little effect on the result for small α, which is always the case in real situations. Figure 5.8 is a diagram of C_α with α. It can be seen that C_α is very close to 1 in the range of α as shown in Figure 5.8. If we take C_α as 1, Equation (5.33) has a constant coefficient $C = \frac{1}{2}$. Overall the comparison indicates that the discrete model for the buckling of an elastic thin ring confined in a rigid boundary is reasonable and quite accurately describes the characteristics of the problem.

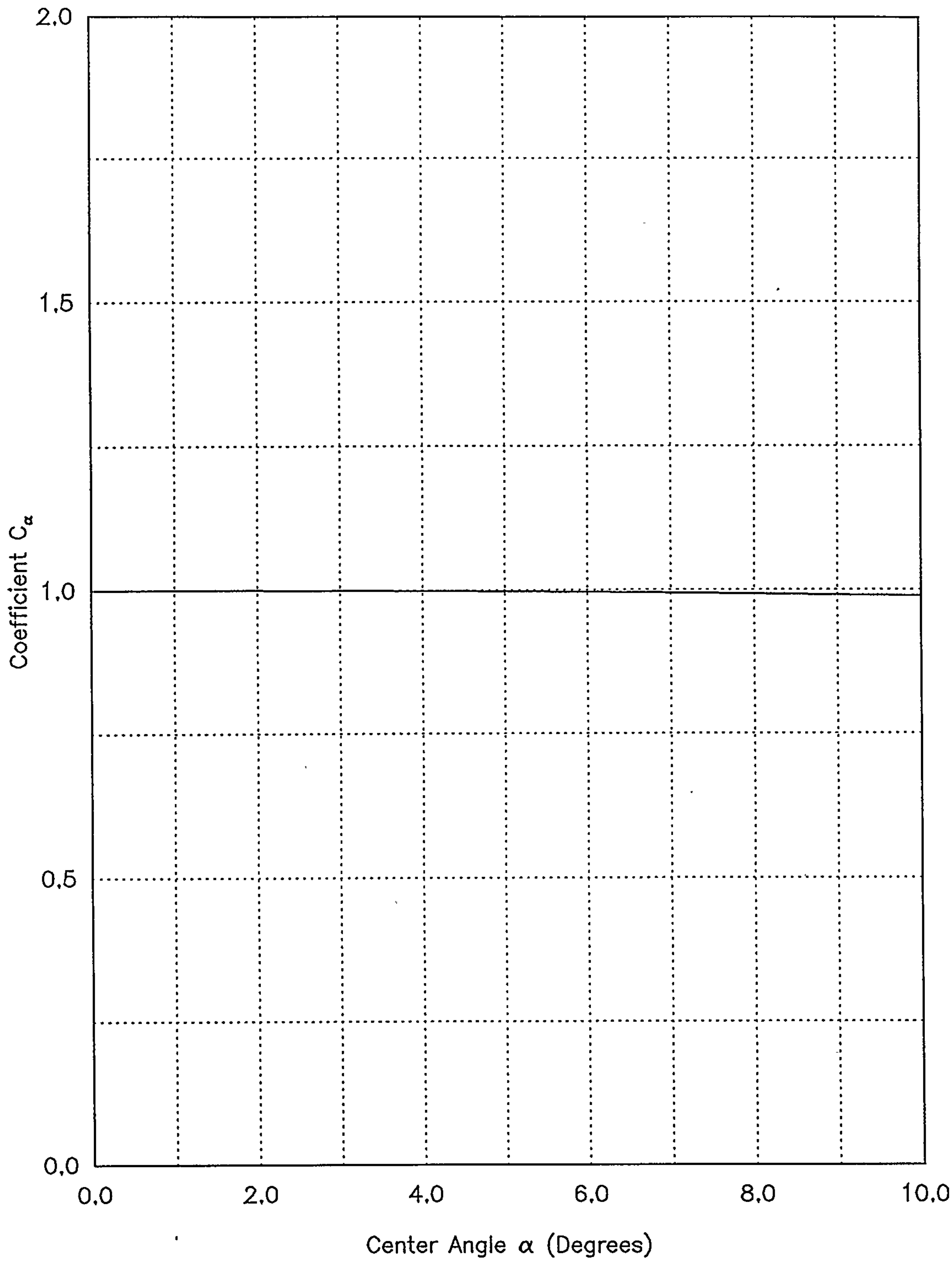

Figure 5.8 Relationship of Coefficient C_α with the Center Angle α

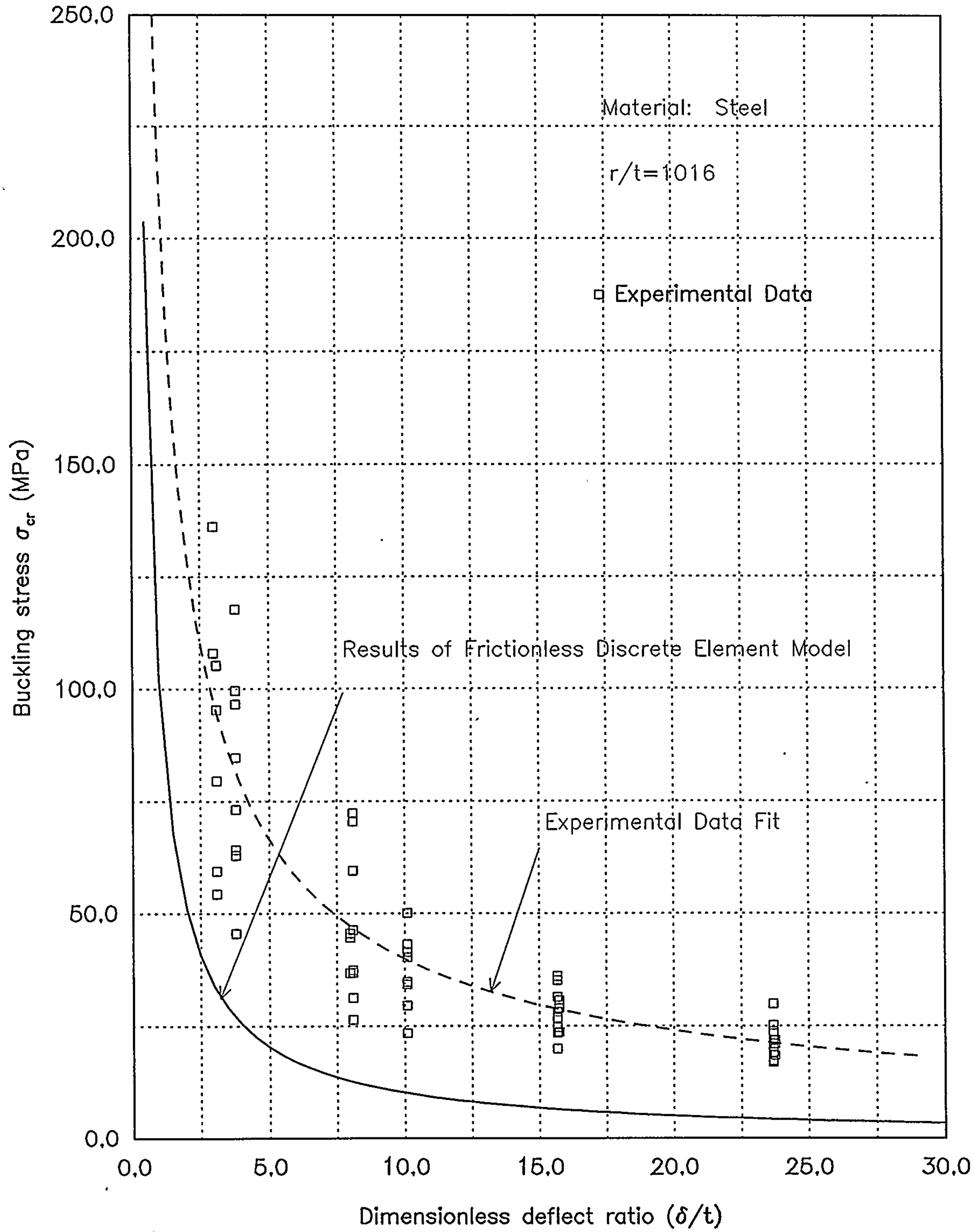

Figure 5.9 Comparison of Results from Discrete Model and Experiments for Steel

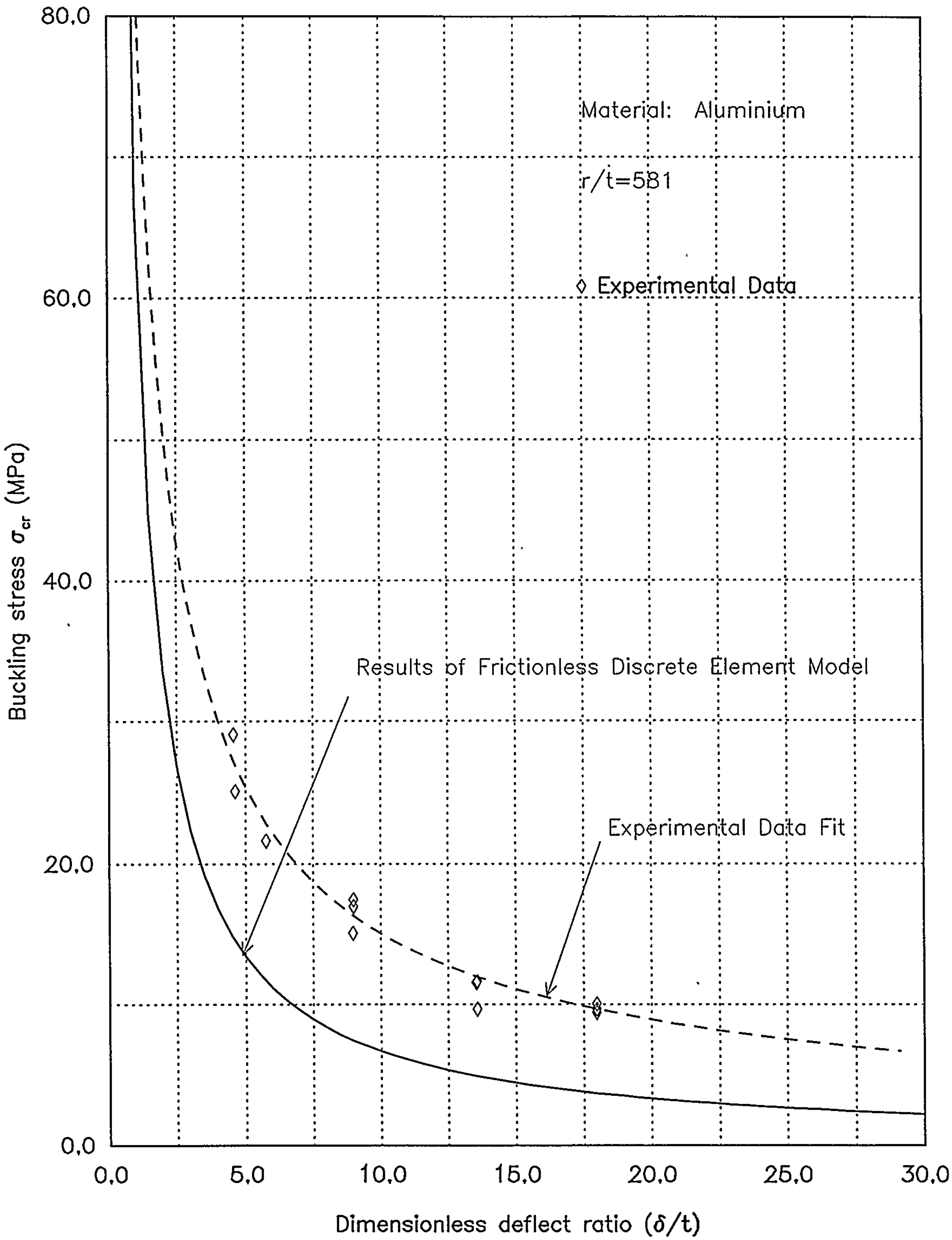

Figure 5.10 Comparison of Results from Discrete Model and Experiments for Aluminium

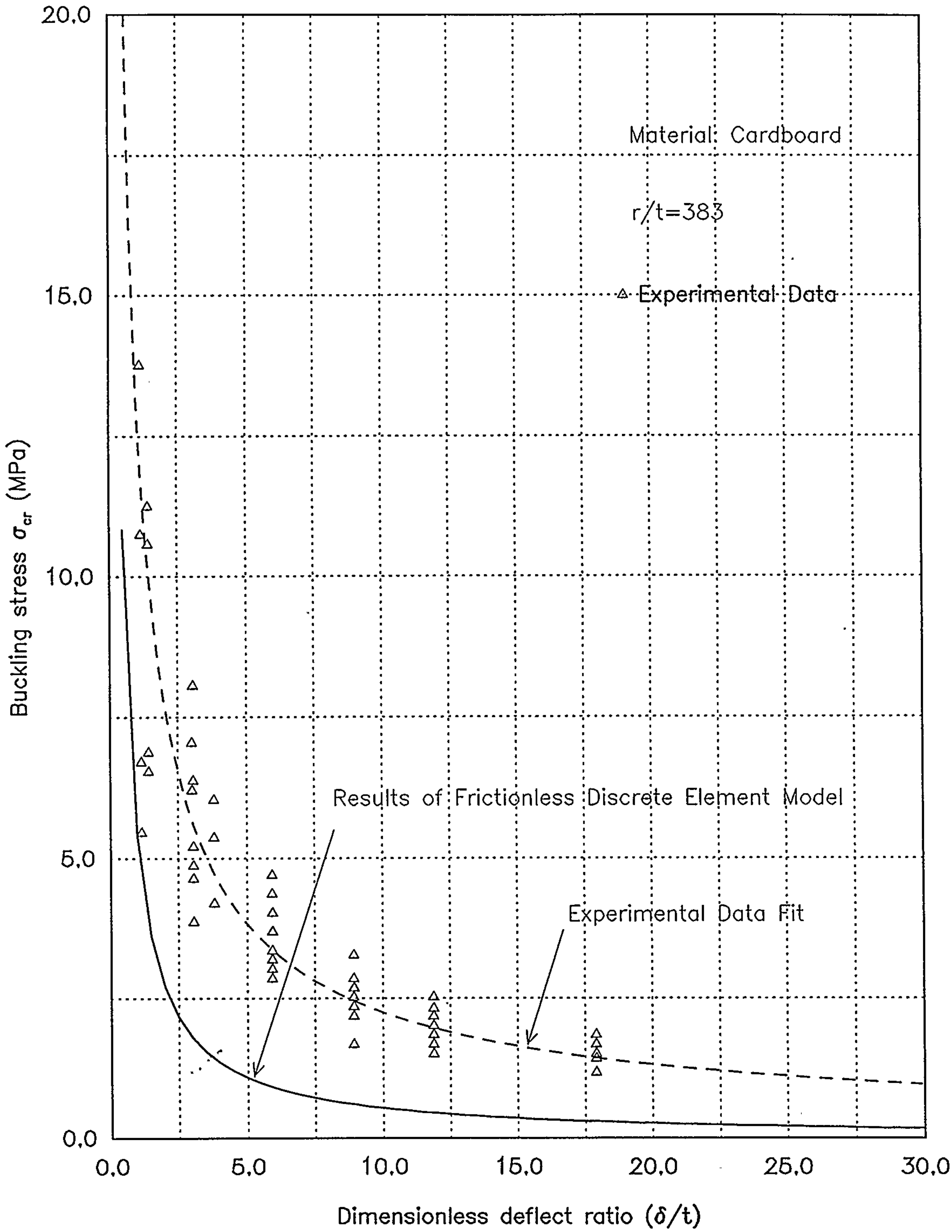

Figure 5.11 Comparison of Results from Discrete Model and Experiments for Cardboard

5.7 Comparison with the Results From Experiment

Figures 5.9-5.11 are comparisons of the experimental results (detail experimental procedure will be discussed in Chapter 7 and Chapter 8) and the discrete model result for three different materials. From these Figures we can see that the experimental data fitted curves are always above the curves of Equation (5.33). This may be due to two reasons. One is that the discrete element model is very accurate for small α but less accurate for large α. The other one is due to the frictionless assumption in the discrete element model. Because in reality we can not eliminate the friction at the interface of the ring and the rigid boundary no matter how carefully we conduct the experiment. Fortunately by neglecting the friction, the results of the discrete model are on the safe side which would be very conservative for design purposes.

5.8 Summary

From above discussions it can be seen that:

The discrete model can accurately describe the behaviour of the buckling of the ring confined in a rigid boundary and is a simple and good model for theoretical analysis. In addition the results from the dimensional analysis method and the discrete element method have the same pattern which demonstrates that these two methods are powerful tools for the structure stability analysis and helps to substantiate the methods.

The frictionless assumption results are on the safe side for a prediction of the critical buckling condition and are quite conservative for design purpose. This model is accurate for small α, and with α increasing, the error will increase. For more accurate analysis, the friction at the interface of the ring and the rigid boundary should be taken into consideration. In the next chapter, the model will be extended to account for friction.

Chapter 6

DISCRETIZATION OF PROBLEM: MODEL TWO

6.1 Introduction

In Chapter 5, a discrete model was developed. In establishing the discrete model, the frictionless assumption was used. In this chapter, the discrete model will be expanded and the friction at the interface of the ring and the rigid boundary will be taken into consideration.

6.2 Basic Assumptions

Similar to Chapter 5, the assumption (4) is changed as:

(4) The frictional resistance force between the ring and the rigid boundary obeys Amonton's Laws, which are summarized as following statements [52]: (a) For low pressures the frictional force is directly proportional to the normal pressure between the two surfaces. (b) The frictional force both in its total amount and its coefficient is independent of the areas in contact, providing the total pressure remains the same.

6.3 Model Descriptions

The model is established by the same discrete element method as described in Chapter

5. As shown in Figure 5.4 the continuous ring is replaced by a group of discrete rigid links which are connected at nodes by linear elastic rotational springs whose constant is k. The only difference is that there is frictional resistance force at each node which contacts with the rigid boundary.

6.4 Friction Consideration

According to Amonton's laws of friction, the frictional force F_f is proportional to the weight W of the object which is being moved as shown in Figure 6.1a.

$$F_f = \mu W \tag{6.1}$$

where μ is the coefficient of friction. In the frictionless situation, the reaction force R_n at the interface is in the direction of normal line n-n to the surface, while in the friction case, the total reaction force R is in the direction which has a angle ϕ with the surface normal line n-n due to the friction resistance force F_f. According to Figure 6.1b, we have

$$\tan\phi = \frac{F_f}{R_n} \tag{6.2}$$

But $R_n = W$, then

$$\tan\phi = \frac{F_f}{W} \qquad \text{and} \qquad F_f = \tan\phi W \tag{6.3}$$

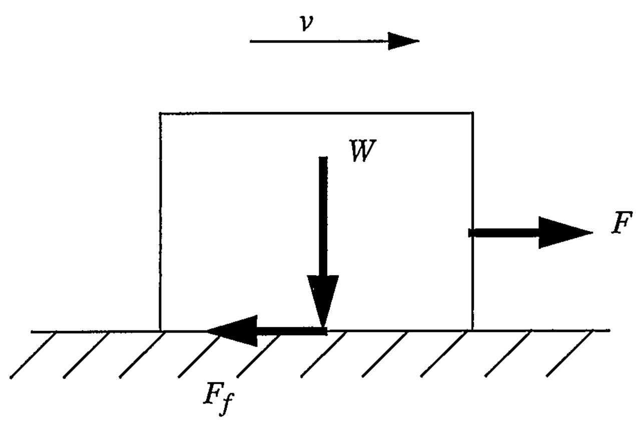

(a)

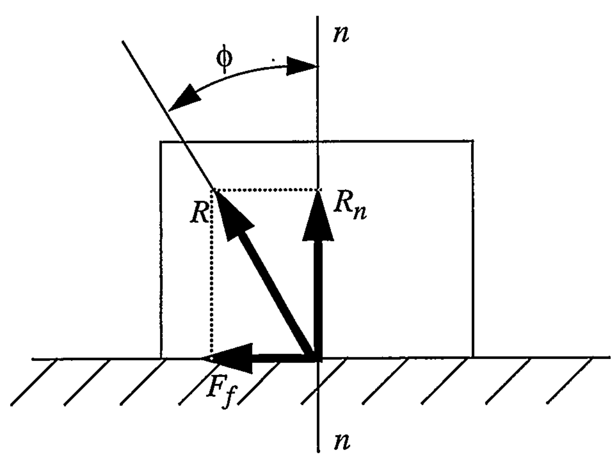

(b)

Figure 6.1 Friction Coefficient and Friction Angle

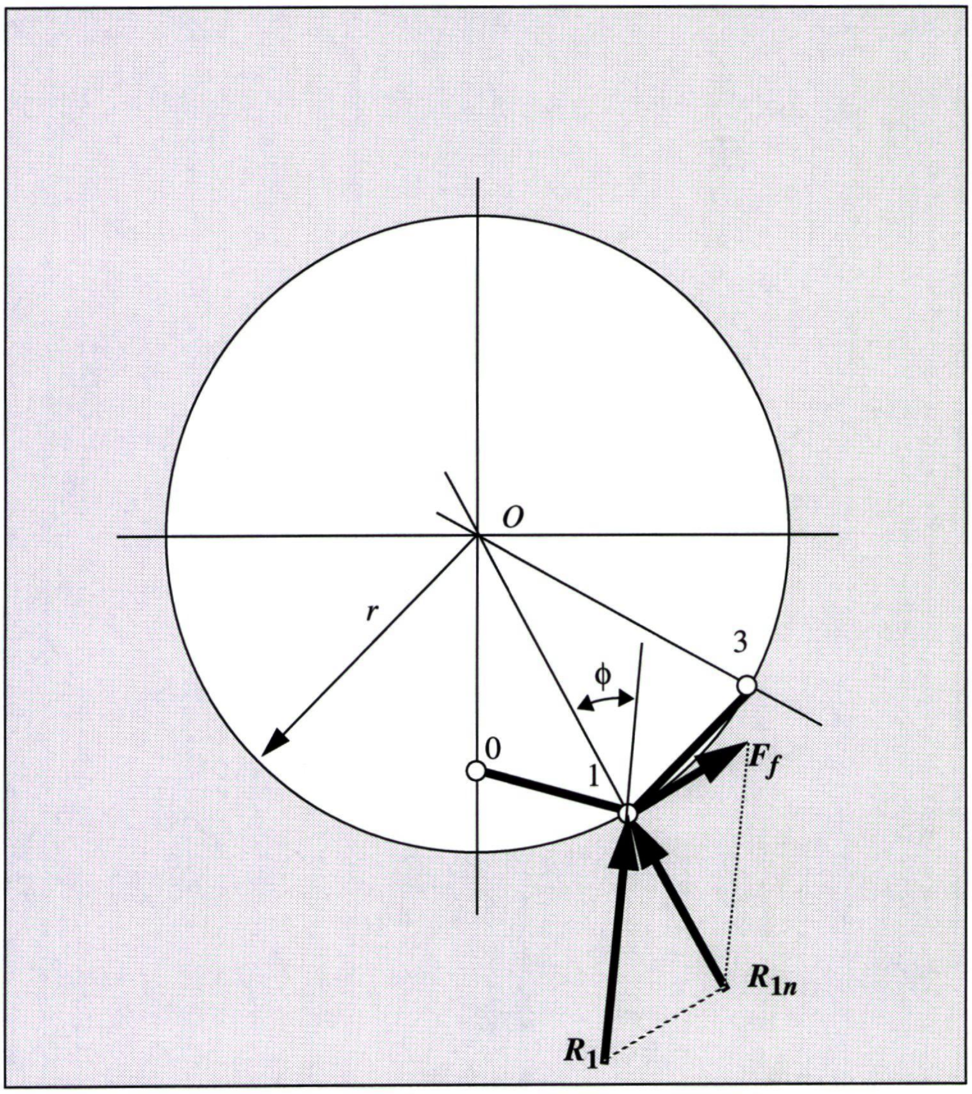

Figure 6.2 Total Reaction Force at Node 1

Comparing Equation (6.2)and Equation (6.3) we obtain

$$\tan\phi = \mu \qquad (6.4)$$

Thus the angle ϕ is called as the friction angle. The friction angle defines the direction of the total reaction force at the inter-surface, and the friction angle is decided by the coefficient of friction at the inter-surface.

For the discrete model, when buckling occurs, the nodes which contact the rigid boundary have a tendency to move along the rigid boundary toward the position where buckling takes place. Because of the existence of friction resistance force at the inter-face, the total reaction force R_1 at node 1 will act at the direction which has the angle ϕ with the radius line as shown in Figure 6.2.

6.5 Equilibrium Analysis

Figure 6.3 is the free body diagram of link $\overline{10}$, where R_0 is the reaction force of the point obstacle to the node 0, R_1 is the reaction force of the rigid boundary to node 1, P_{31} is the reaction force of link $\overline{31}$ to link $\overline{10}$, F is the reaction force of link $\overline{02}$ to link $\overline{01}$ and M_1 and M_0 are reaction moments at node 1 and node 0 respectively. Because of the frictional resistance force at node 1, the total reaction force R_1 has a angle ϕ with the normal line of the rigid boundary. P_{31} acts along a line which has an angle γ with link $\overline{31}$. The angle γ can be determined by equilibrium analysis of link $\overline{31}$ which will be done later.

For the equilibrium in the vertical direction we obtain

$$\frac{R_0}{2} + R_1 \cos(\alpha - \phi) - P_{31} \sin(\beta - \gamma) = 0 \qquad (6.5)$$

Thus

$$\frac{R_0}{2} = P_{31} \sin(\beta - \gamma) - R_1 \cos(\alpha - \phi) \qquad (6.6)$$

At the instant of buckling, the ring intends to lift off the boundary. Thus the critical condition for the buckling is that the reaction force R_0 at this moment vanishes, i.e. $R_0 = 0$. Then we have

$$P_{31} = R_1 \frac{\cos(\alpha - \phi)}{\sin(\beta - \gamma)} \qquad (6.7)$$

Considering the free body diagram of link $\overline{01}$ as shown in Figure 6.3 in the critical condition and taking moments about point 1, we have

$$M_0 + M_1 - F\frac{\delta}{2} = 0 \qquad (6.8)$$

where M_0 and M_1 are reaction moments at node 0 and 1 caused by the changes of angle between two links connected at these points and they have the same values as described in Equations (5.18) and (5.19).

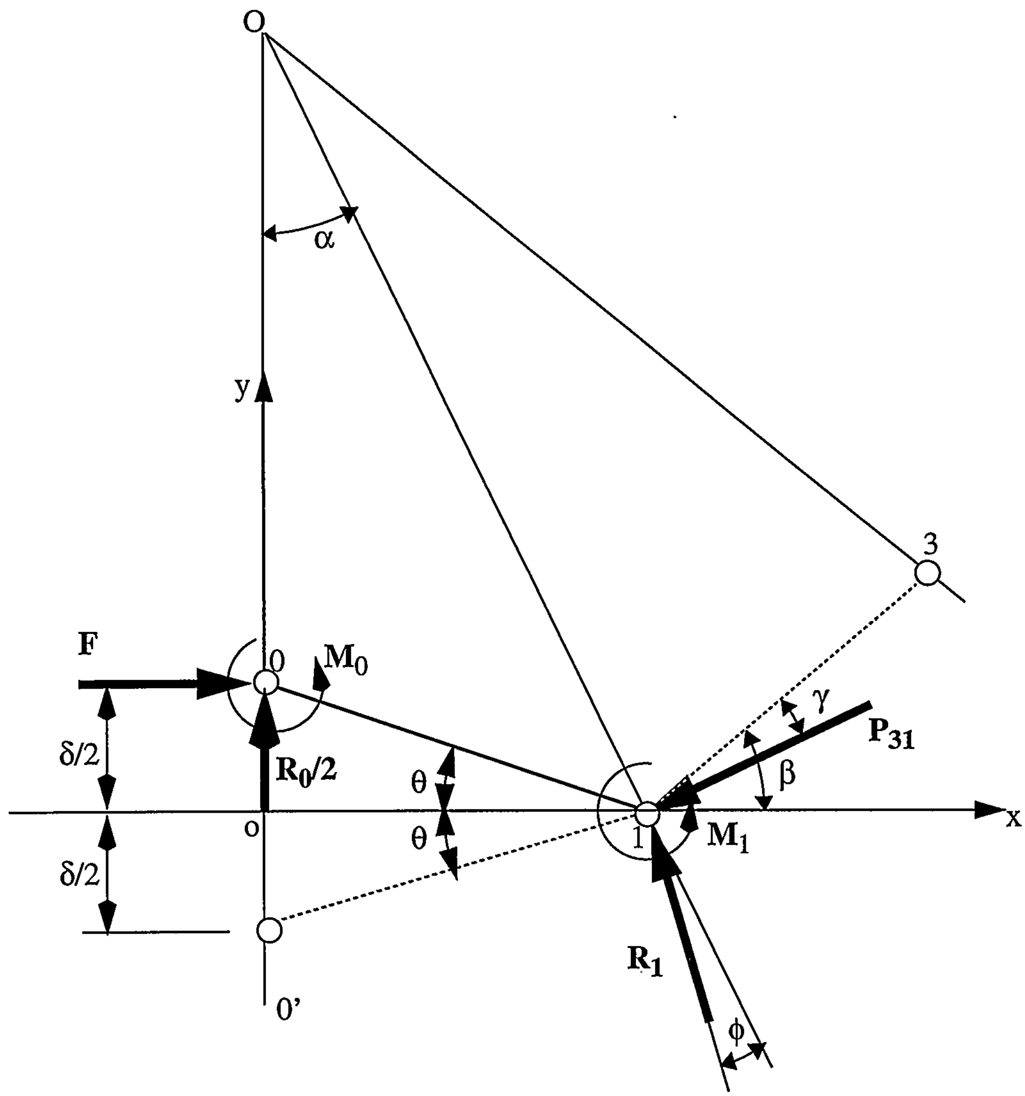

Figure 6.3 Free Body Diagram of link $\overline{01}$

There is only horizontal reaction force F at point 0 because of the symmetric condition. There are two forces at node 1, R_1 and P_{31}. P_{31} is the reaction force of link $\overline{13}$ to link $\overline{10}$ and R_1 is the total reaction force of the rigid boundary toward node 1. From the force equilibrium equation in the horizontal direction

$$F - [P_{31}\cos(\beta-\gamma) + R_1\sin(\alpha-\phi)] = 0 \tag{6.9}$$

Substituting Equation (6.7) into Equation (6.9) we obtain

$$F = P_{31}[\cos(\beta-\gamma) + \sin(\beta-\gamma)\tan(\alpha-\phi)] \tag{6.10}$$

Bringing Equation (5.18), (5.19) and (6.9) into Equation (6.8) yields

$$2k\theta + 4k\theta - P_{31}[\cos(\beta-\gamma) + \sin(\beta-\gamma)\tan(\alpha-\phi)]\frac{\delta}{2} = 0 \tag{6.11}$$

Then

$$P_{31} = \frac{12k\theta}{\delta[\cos(\beta-\gamma) + \sin(\beta-\gamma)\tan(\alpha-\phi)]} \tag{6.12}$$

Bring Equation (5.13) into Equation (6.12) we have

$$P_{31} = \frac{12EI\theta}{r\delta\alpha[\cos(\beta-\gamma) + \sin(\beta-\gamma)\tan(\alpha-\phi)]} \tag{6.13}$$

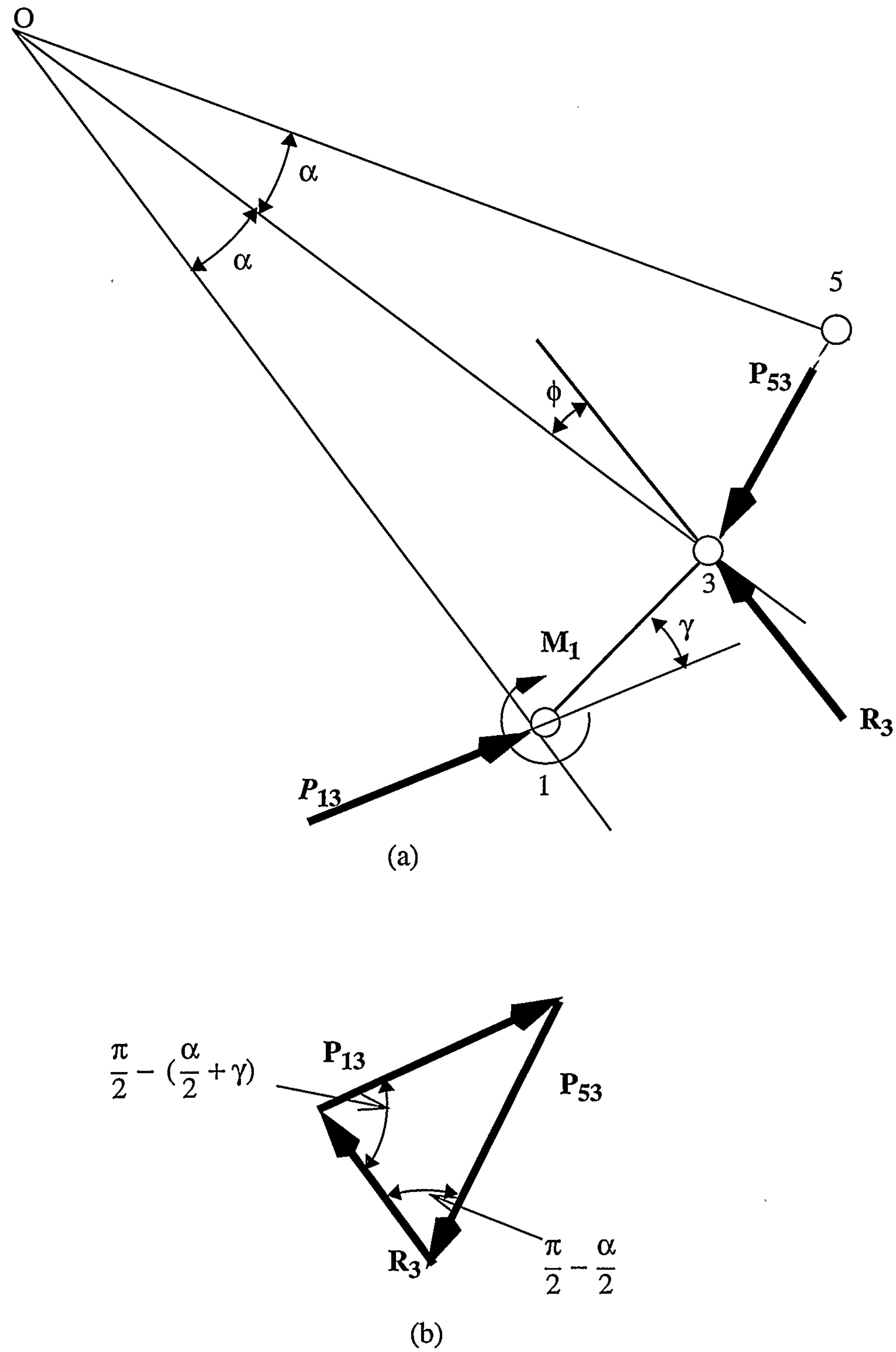

Figure 6.4 Free Body Diagram of Link $\overline{13}$

Bring Equation (5.31) into Equation (6.13) yields

$$P_{31} = \frac{EBt^3\theta}{r\delta\alpha\,[\cos(\beta-\gamma) + \sin(\beta-\gamma)\tan(\alpha-\phi)]} \tag{6.14}$$

As shown in Figure 6.4 for the equilibrium at node 3 we must have

$$P_{53} = P_{13}\frac{\cos(\frac{\alpha}{2}+\gamma-\phi)}{\cos(\frac{\alpha}{2}+\phi)} \tag{6.15}$$

Because P_{13}=P_{31}, we get

$$P_{53} = \frac{1}{2}\frac{Bt^3E}{r\delta}\frac{\cos(\frac{\alpha}{2}+\gamma-\phi)}{\cos(\frac{\alpha}{2}+\phi)\left[\cos(\frac{3}{2}\alpha-\gamma) + \sin(\frac{3}{2}\alpha-\gamma)\tan(\alpha-\phi)\right]} \tag{6.16}$$

Also in Figure 6.4 taking the moments about node 3 we have

$$M_1 - P_{13}l\sin\gamma = 0 \tag{6.17}$$

Because P_{13}=P_{31} and M_1=$2k\theta$, we get

$$2k\theta - P_{31}l\sin\gamma = 0 \tag{6.18}$$

Bringing Equation (6.12) into Equation (6.18) yields

$$3\alpha\sin\gamma - (1-\cos\alpha)\,[\cos(\beta-\gamma) + \sin(\beta-\gamma)\tan(\alpha-\phi)] = 0 \qquad (6.19)$$

For a given initial deflection δ, the angles α and β can be calculated from Equations (5.18) and (5.19). Then from Equation (6.26) angle γ can be determined.

As shown in Figure 6.5, we have

$$P_{75} = P_{53}\left[\frac{\cos\left(\frac{\alpha}{2}-\phi\right)}{\cos\left(\frac{\alpha}{2}+\phi\right)}\right] \qquad (6.20)$$

It should be pointed out that only P_{13} deviates from acting axially along link $\overline{13}$ by an angle γ, while P_{53} and P_{75} are constrained to lie along link $\overline{53}$ and link $\overline{75}$ (see Figures 6.4 - 6.5). This is because there is a reaction moment M_1 at node 1 (see Figure 6.4) and a deviation angle γ is needed to balance the moment M_1. There are no reaction moments at nodes 3 and 5, thus P_{53} and P_{75} should be constrained to lie along link $\overline{53}$ and link $\overline{75}$ for equilibrium purposes. In the same manner, the force acting at the end of the half ring should be

$$P = P_{53}\left[\frac{\cos\left(\frac{\alpha}{2}-\phi\right)}{\cos\left(\frac{\alpha}{2}+\phi\right)}\right]^{n} \qquad (6.21)$$

where

$$n = \frac{\pi}{2\alpha} - 2 \qquad (6.22)$$

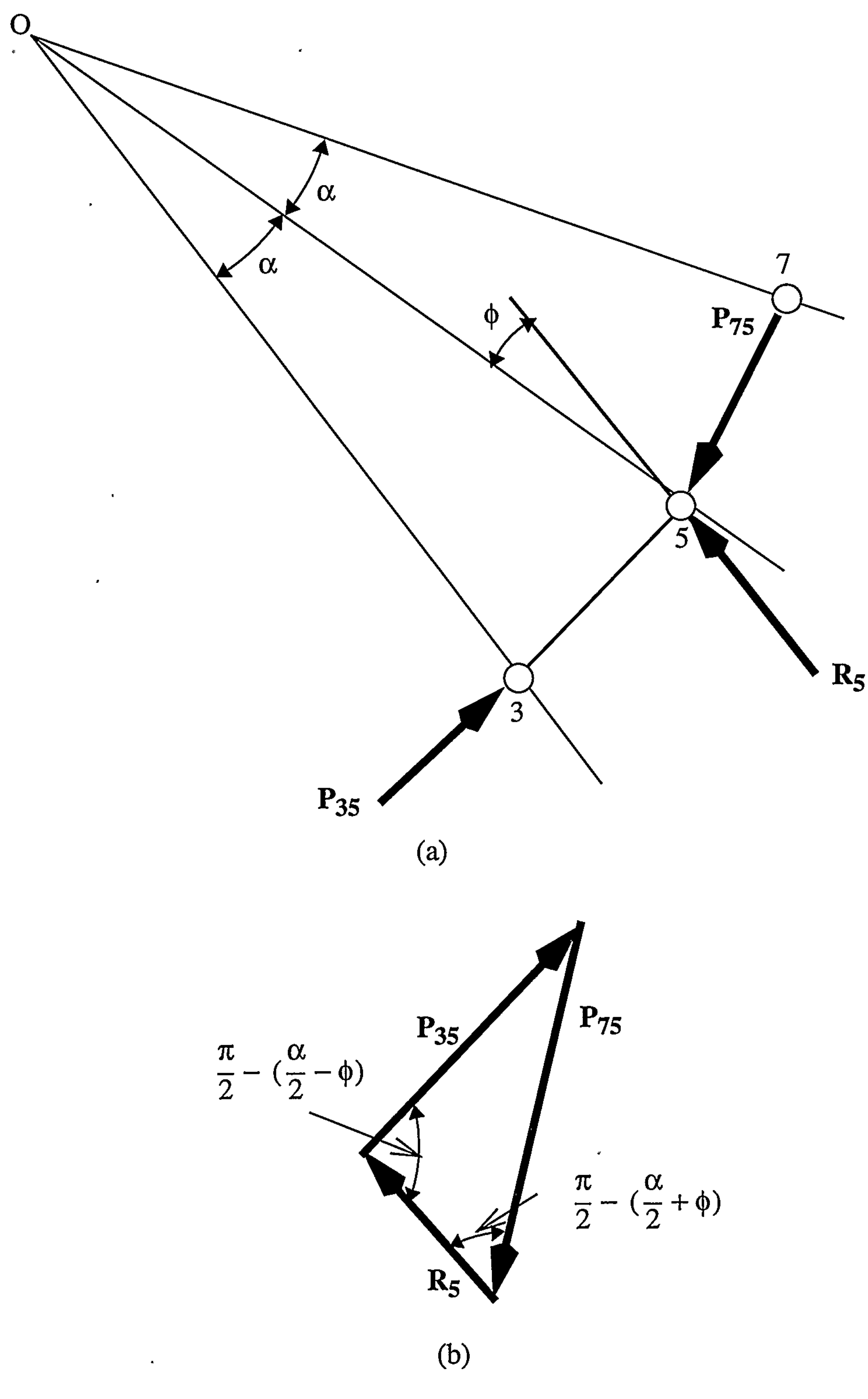

Figure 6.5 Free Body Diagram of Link $\overline{35}$

Let

$$C_f = \frac{\cos\left(\frac{\alpha}{2}+\gamma-\phi\right)\left[\frac{\cos\left(\frac{\alpha}{2}-\phi\right)}{\cos\left(\frac{\alpha}{2}+\phi\right)}\right]^n}{\cos\left(\frac{\alpha}{2}+\phi\right)\left[\cos\left(\frac{3}{2}\alpha-\gamma\right)+\sin\left(\frac{3}{2}\alpha-\gamma\right)\tan\left(\alpha-\phi\right)\right]} \tag{6.23}$$

Bringing Equations (6.16) and (6.23) into (6.21) we obtain

$$P = \frac{1}{2}EBt\left(\frac{r}{t}\right)^{-1}\left(\frac{\delta}{t}\right)^{-1}C_f \tag{6.24}$$

Then

$$\frac{\sigma}{E} = \frac{1}{2}\left(\frac{r}{t}\right)^{-1}\left(\frac{\delta}{t}\right)^{-1}C_f \tag{6.25}$$

6.6 Comparison with the Results from the Frictionless Model

Comparing Equation (6.25) with Equation (5.33) it can be seen that only difference the two equations have is the coefficients C_f and C_α. But if ϕ=0, we have $C_f = C_\alpha$. Then Equation (6.25) reduces to Equation (5.33). It means that Equation (6.25) is a general formulation of the buckling compression stress of a ring confined in a rigid boundary and the frictionless model is just a special case of the friction model.

From Equation (6.23) it can be seen that C_f is affected both by the half center angle α and the friction coefficient μ. But a detailed study shows that in a small α region, C_f

is mainly affected by the friction coefficient μ. Figure 6.6 is a diagram of C_f as affected by α. It shows that for a given value of μ the changes of C_f with α are very small and for a small value of μ, when $\mu = 0.0 - 0.6$, the changes are insignificant. Figure 6.7 is the relationship of C_f with μ. It shows that different values of μ will significantly change the value of C_f. Therefore C_f is referred to as the friction effect coefficient and its value is mainly determined by the friction coefficient μ.

6.7 Summary

From the preceding analysis and comparison it can be seen that the friction plays an important role in the buckling behaviour of a thin elastic ring confined in a rigid boundary. Friction resistance force at the interface increases the stability of a ring and thus has a positive effect on the critical buckling compression stress of the ring. The larger of the friction resistance force is, the larger the critical compression stress. The friction discrete model is closer to practice situation than the frictionless discrete model. The frictionless discrete model is just a special case of the friction discrete model.

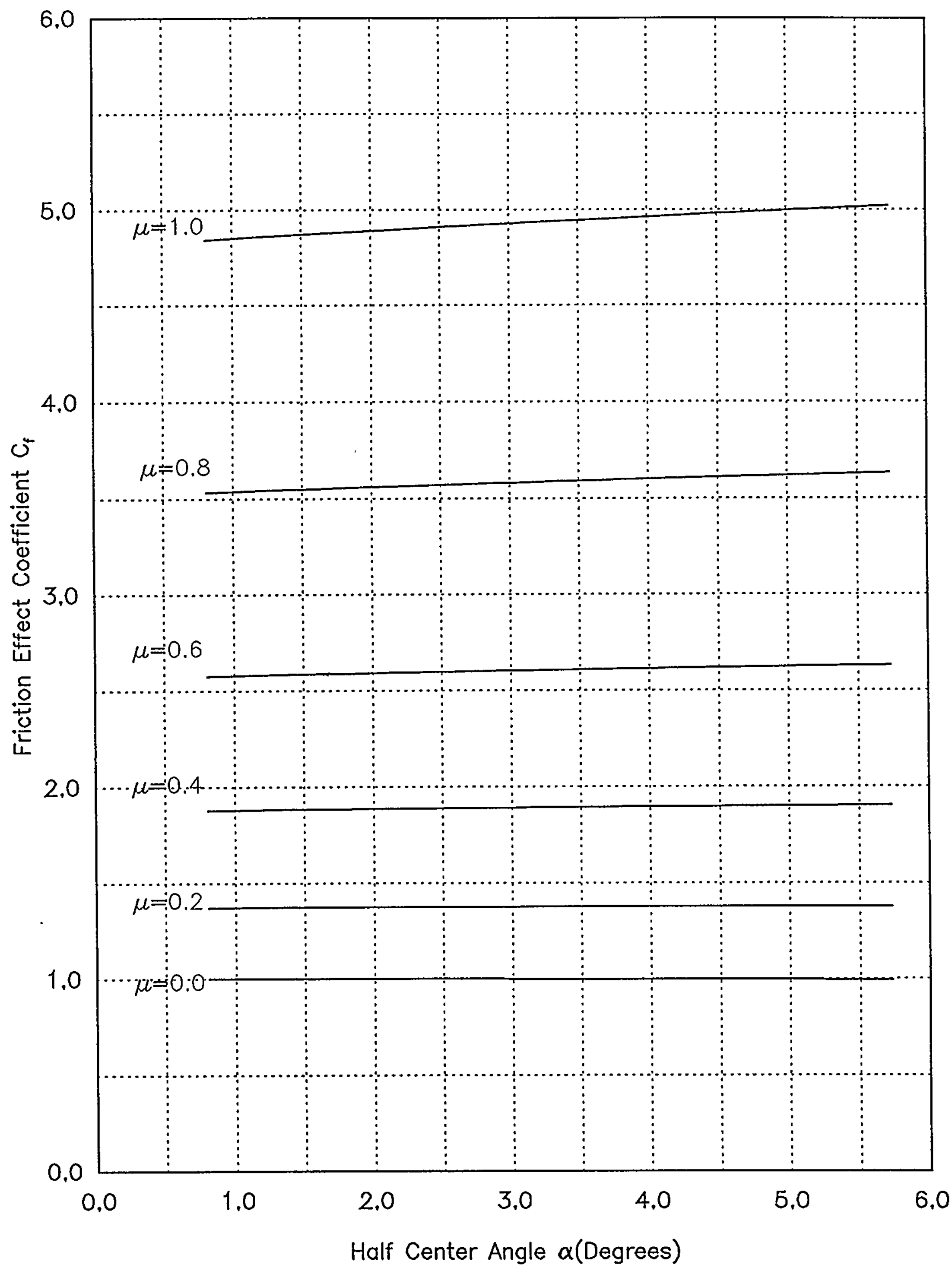

Figure 6.6 Relationship of the Friction Effect Coefficient C_f with the Half Center Angle α

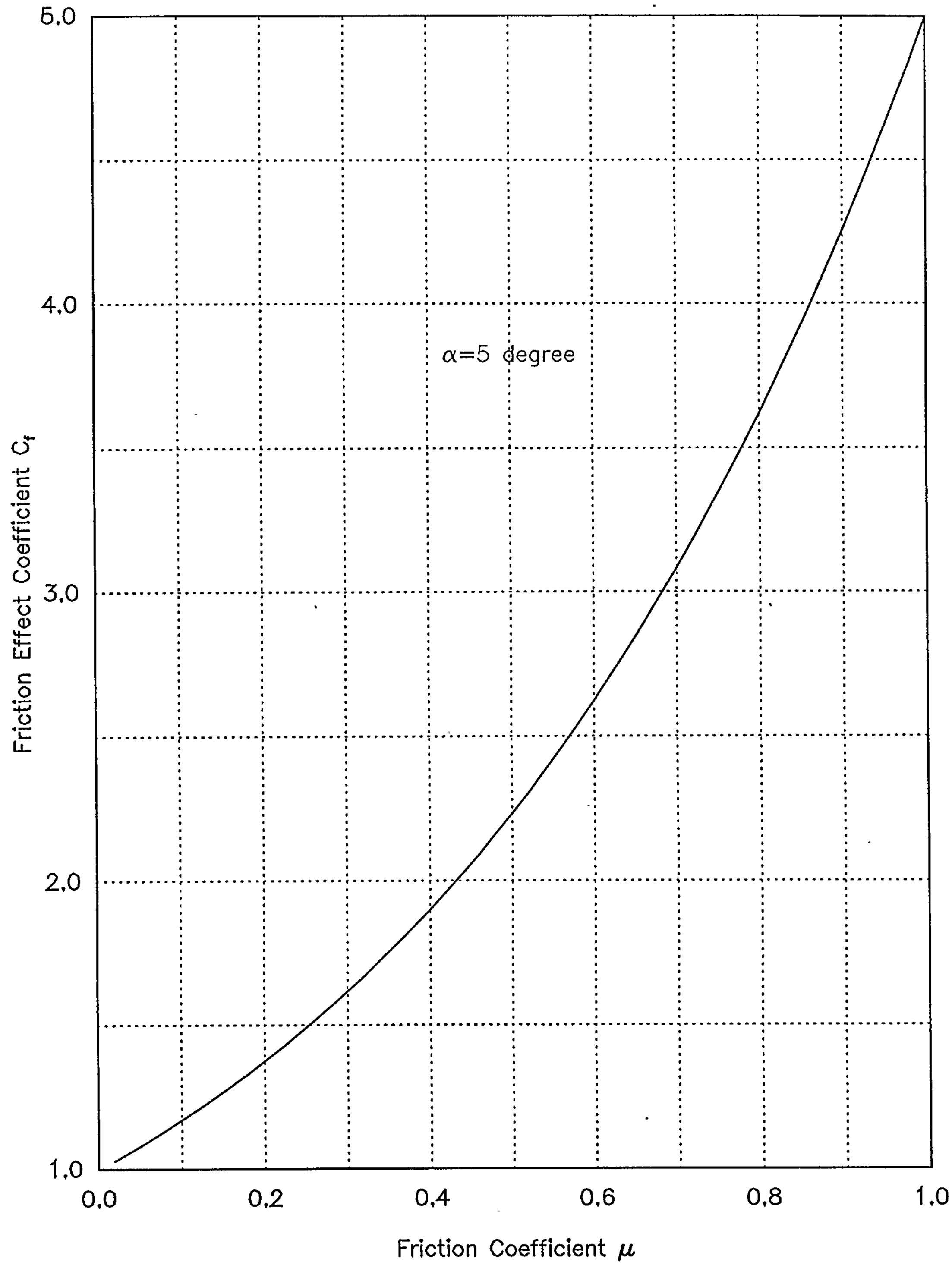

Figure 6.7 Relationship of the Friction Effect Coefficient C_f with the Friction Coefficient μ

Chapter 7

EXPERIMENTAL ARRANGEMENT

7.1 Introduction

In Chapter 4-6, various models were developed. These models described the buckling behaviour of a thin ring confined within a rigid boundary and can be used to predict the buckling load in certain conditions. These models are helpful to understand the problem and explore the properties that otherwise may be difficult to determine. But these models have to be verified by experiments. A fundamental relationship of the critical buckling compression stress with geometry, imperfection and material property was developed in Chapter 4 by using the dimensional analysis method. The undetermined coefficients in this relationship need to be determined by experimental methods. In this chapter, an experimental apparatus will be described based on the loading situation and applicability. Experiments were carried out to explore the characteristics of buckling behaviours by using different materials, different geometries and different lubricants.

7.2 Experimental Apparatus

An initial deflection of the ring can be introduced by an external disturbance or by an imperfection in the rigid boundary. An imperfection in the rigid boundary is much easier to control and is much more reliable than an external disturbance in the experimental process. Therefore an imperfection in the rigid boundary was imposed to create an initial centre deflection of the ring. Nevertheless, an initial deflection of a ring due to an imperfection can also be considered to be a combination effect of the geometric imperfection and the external disturbances. To stimulate the point imperfection on the rigid confinement a wire with diameter δ was inserted between the ring and the rigid confinement as shown in Figure 7.1. By changing the diameter of the wire, different initial centre deflections can be imposed on the ring.

In reality the hoop compression force P of a ring is introduced by a pressure between the ring and the outside boundary. The pressure is set up by a designed interference fitting or radius mismatch between the ring and the rigid confinement as described in Chapter 3. Assume the radius of the ring is r_1 and the radius of the rigid confinement is r. The difference of the two radii is

$$\Delta r = r_1 - r \tag{7.1}$$

Then the pressure q at the interface between the ring and the rigid confinement will be given by (see Chapter 3)

$$q = AE\frac{\Delta r}{r^2} \tag{7.2}$$

where A is the cross-section area of the ring, E is the elastic modulus of the material. From Equation (7.2) it can be seen that different pressures can be obtained by changing the dimension mismatch Δr. But it is very difficult to obtain a specific and exact

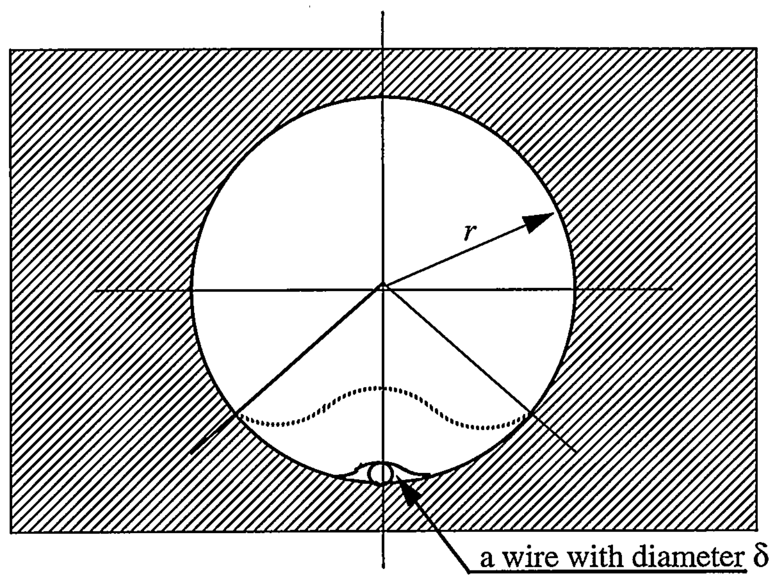

Figure 7.1 Insert a wire in between a Ring and a Rigid Confinement to Simulate a Point Imperfection on the Confinement

pressure between the ring and the boundary by designing the mismatched radii because variations or tolerances are unavoidable in machine shop practice. On the other hand, in order to get the critical pressure for a given initial centre deflection on the ring the continuous change of the radius mismatch is required. To obtain one critical pressure, a considerable number of specimens should be used. This makes the experiment very expensive and nearly practically impossible. Therefore the dimension mismatch method can only be used to check a specific rule or criteria. For a large scale of experimental investigation, an alternative method must be considered. This alternative method can be developed from the following analysis.

As shown in Figure 7.2 an assembly of the ring and the rigid boundary was cut in half. There is a vertical compression load P acting at each end of the half ring. In the frictionless situation, this vertical compression load P (per unit width) is related to the pressure q at the interface between the ring and the rigid confinement by the following formulation[53]

$$P = rq \tag{7.3}$$

From Equation (7.3) it can be seen that the different pressures can be obtained by changing the end compression load P. On the other hand, for a specific vertical displacement at the end of the ring, a corresponding end vertical compression load, P can be obtained. And subsequently a pressure, q at the interface between the ring and the rigid boundary can be found. If the end vertical displacement could change continuously, the end compression load would also change continuously. In this way, different pressures can be achieved by applying different vertical displacement at the end of the

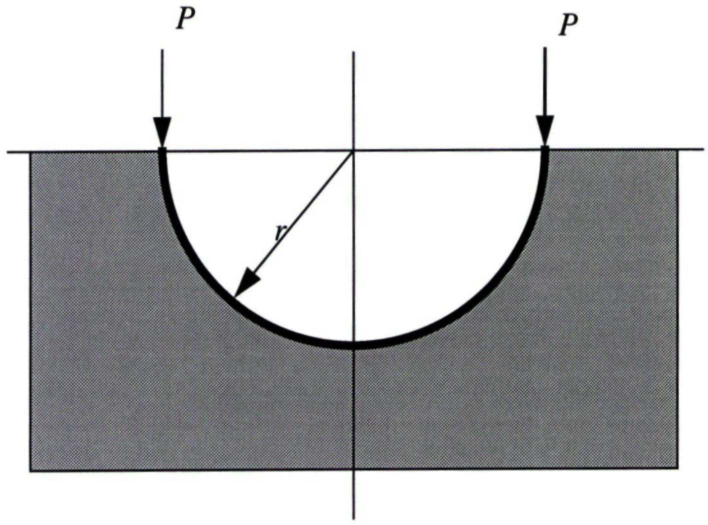

Figure 7.2 A Half ring and Rigid Confinement Assembly

half ring. For a given initial centre deflection of the ring, we can continuously change the end vertical compression load by imposing a continuously changed end displacement until the corresponding critical buckling compression load is reached. Thus to obtain a critical load only one specimen is needed. This method is obviously more efficient, economical and practical than the dimension mismatch method.

Based on the preceding analysis, an experimental apparatus was designed. Figure 7.3 is a picture of the experimental apparatus. The experimental apparatus is schematically shown in Figure 7.4. In Figure 7.4, the rigid support (1) is a steel block with a half circular curvature and is considered as a rigid confinement. The machined surface of the rigid support was polished in order to reduce the friction between the ring and the support. Three rigid supports with different radii were used. The loading head (2) consists of a steel bar and two load transfer plates. The two plates can slide along the steel bar. The specimen is item (3). The ends of the specimen are fixed by the two plates as shown. The plates are fastened together by two bolts. By adjusting the position of the plates on the load head, the portion of the specimen at the outside the rigid support can be made coincidental with the tangent of the half circular rigid support. A wire (4) is inserted at the bottom of the support to impose an initial deflection on the ring and to simulate a combination effect of the point imperfection and the outside disturbances. The apparatus was mounted in a materials testing machine MTS 810. The vertical load P can be measured and recorded continuously in response to the change of the end displacement.

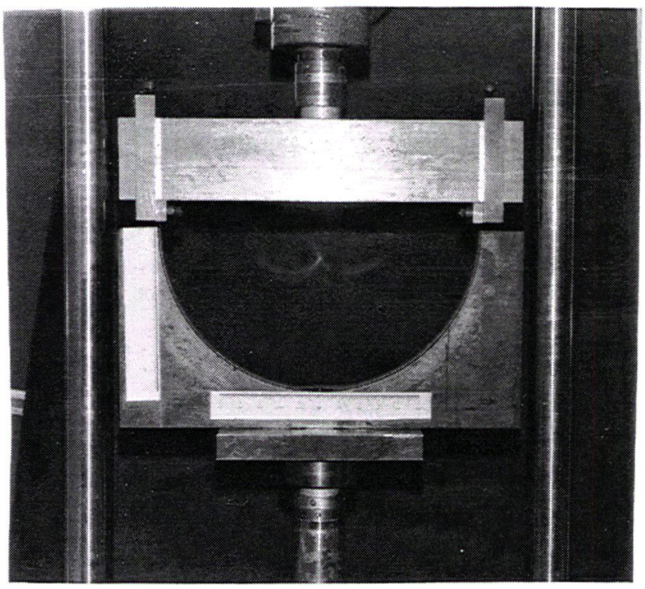

Figure 7.3 A Picture of the Experimental Apparatus

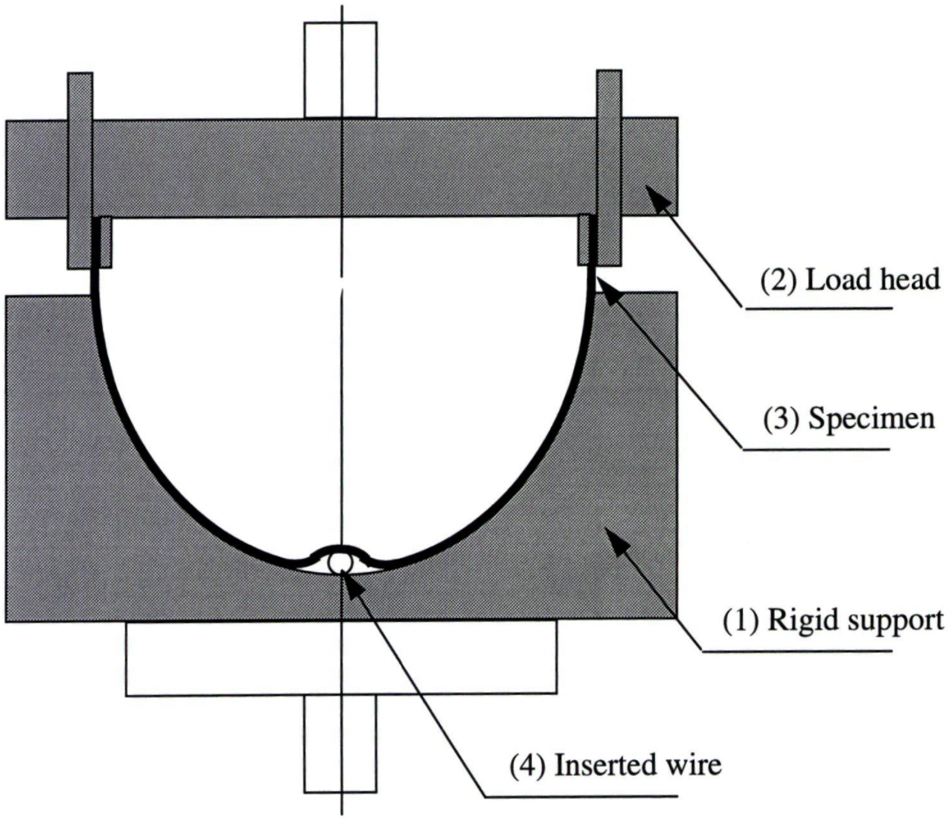

Figure 7.4 Schematic Diagram of the Experimental Apparatus

7.3 Specimens

The specimens were made from four different materials, Steel (Steel shim 1010), Aluminium (Aluminium shim 1100), Plastic (Polyvinyl Chloride) and Cardboard. Dimensions of specimens and the elastic moduli E are listed in Table 7.1. The moduli of elasticity of steel and aluminium were taken from [48]. The moduli of plastic and cardboard were measured by the author (see Appendix A). From different thicknesses of the materials and three different radii of the rigid supports a wide range of $(\frac{r}{t})$ ratios could be obtained.

Table 7.1(a) Test Materials' Elastic Moduli and Dimensions

Materials	Width B (mm)	Thickness t (mm)	E (GPa)
Plastic Sample1	25.00	0.51	2.10
Plastic Sample2	25.00	0.38	2.39
Plastic Sample3	25.00	0.25	2.37

Table 7.1(b) Test Materials' Elastic Moduli and dimensions

Materials	Width B (mm)	Thickness t (mm)	E (GPa)
Steel Sample1	12.50	0.51	210
Steel Sample2	12.50	0.38	210
Steel Sample3	12.50	0.25	210

Table 7.1(c) Test Materials' Elastic Moduli and Dimensions

Materials	Width B (mm)	Thickness t (mm)	E (GPa)
Aluminium Sample1	12.50	0.51	78
Aluminium Sample2	12.50	0.38	78
Aluminium Sample3	12.50	0.25	78

Table 7.1(d) Test Materials' Elastic Moduli and Dimensions

Materials	Width B (mm)	Thickness t (mm)	E (GPa)
Cardboard	25.00	0.60	4.15

The three rigid support's radii are listed in Table 7.2. The diameters of the wires used to simulate the imperfections of the rigid boundary are listed in Table 7.3.

Table 7.2 Radii of Rigid Supports

Rigid Support No.	Radius r (mm)
1	203.2
2	152.4
3	101.6

Table 7.3 Diameters of Inserted Wires

mm

$\delta 1$	$\delta 2$	$\delta 3$	$\delta 4$	$\delta 5$	$\delta 6$	$\delta 7$	$\delta 8$
3.20	2.10	1.85	1.65	0.75	0.65	0.40	0.20

7.4 Experimental Procedure

The tests were conducted on a MTS model 810 under displacement control mode. First, a specimen was bent elastically into position and pressed against the surface of the rigid boundary by imposing displacement on both ends. The component was then unloaded and a wire was inserted between the specimen and the rigid boundary as shown in Figure 7.4. The component was reloaded until buckling occurred. The displacement-load curve was recorded on an X-Y recorder for both loading and unloading processes.

Figure 7.5 is a typical displacement-load curve recorded during testing. Along curve B-C-D-E the end vertical displacement is increasing. Thus the curve B-C-D-E is called the loading curve. Along curve E-F-B the end displacement is decreasing. This portion of the curve E-F-B is called the unloading curve. From B to C the compression load P increases as the end displacement increases. The ring is in the stable equilibrium state. When the compression load reaches the critical point P_C, the specimen will suddenly jump to the large deflection position and the compression load drops rapidly from P_C to P_D in a very short interval of time. Buckling occurs at point C. After this occurrence, the load will slowly decrease as the end displacement increases continually. When the curve reaches point E, the end displacement was reversed. From E to F the load increases slowly as the end displacement decreases but when the end displacement decreases to a certain point, the specimen will suddenly jump back to the unbuckled position and the load increases to P_F instantly. For a specific material the jump-back always occurs at the same point for the same specimen even if the buckling point is different for the different initial deflection. This suggests that if the end compression load P is below the load P_F at which the snap-back occurs, there is only one possible stable state which is the unbuckled state. If the load exceeds this point, there are two possible stable states, which are the original unbuckled state and the buckled large deflection state. Whether or not the specimen buckles when the load reaches this point depends on the magnitude of the imperfections or the external disturbances. This observation agrees with results from literature reviews in Chapter 2.

7.5 Summary

Based on equilibrium analysis an experimental apparatus was developed. Although the design of this apparatus is very simple, it is a powerful tool for experimental investigation of buckling behaviours of a ring confined within a rigid boundary.

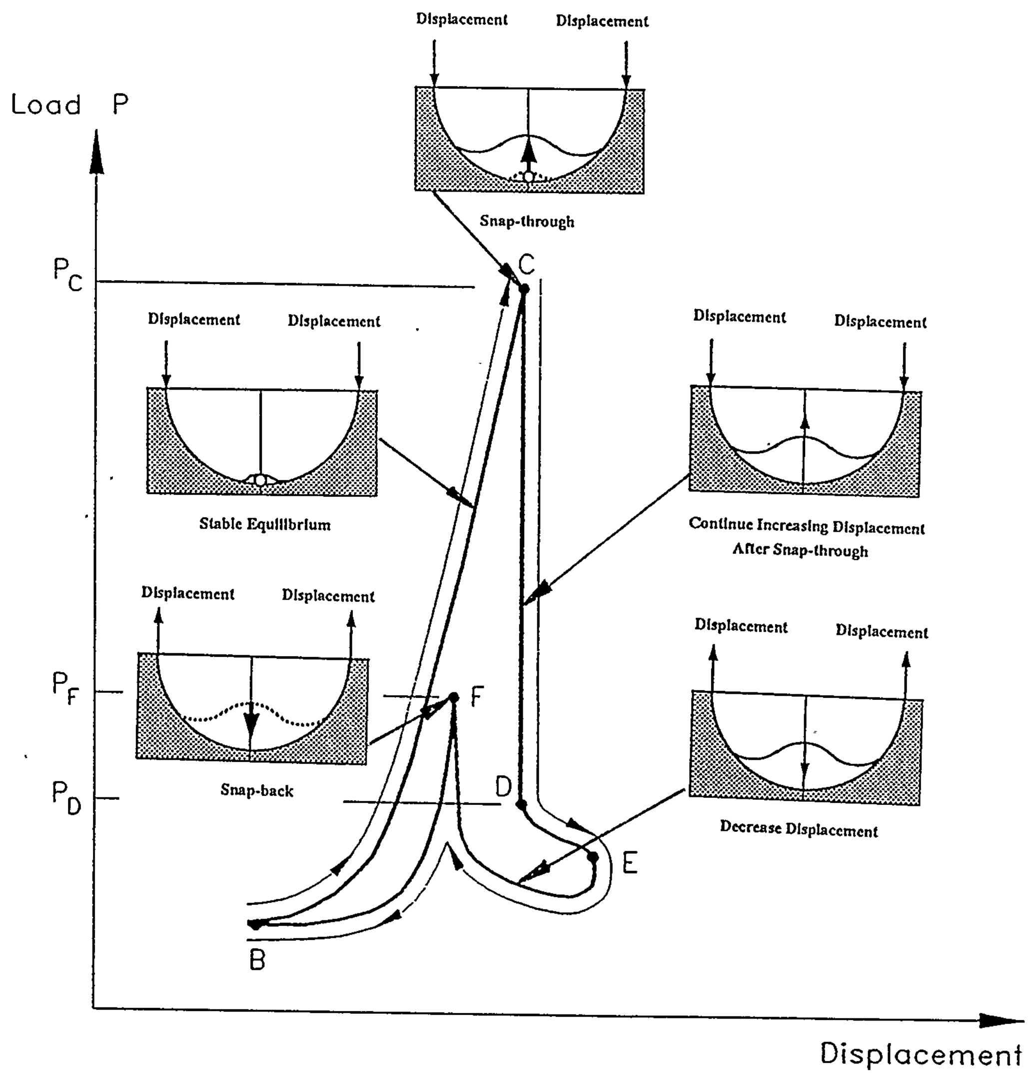

Figure 7.5 Loading and Unloading Curve

Chapter 8

EXPERIMENTAL RESULTS AND DISCUSSIONS

8.1 Introduction

In this chapter, experimental results for various materials and geometry will be discussed. First the three undetermined numbers in the buckling function developed in Chapter 4 will be derived from the experimental data. Then all the experimental results will be compared with the discrete element model results. Friction effects and local plastic deformation will also be discussed in detail.

8.2 Experimental Results

At each experimental point a minimum of four specimens was tested. The experimental data at each point showed a amount of scatter. The average values at each point were calculated and used to derive the unknown quantities in Equation (4.10) and to compare with the discrete element model results. Table 8.1 -- Table 8.10 are average $\frac{\sigma_c}{E} \times 10^3$ values from different materials.

Table 8.1 Ratio of σ_c/E for Plastic Sample1

$(\sigma/E) \times 10^3$

r/t	δ/t						
	6.27	4.12	3.63	3.24	1.47	1.27	0.78
200	1.70	2.53	2.93	3.10	6.30		
300	1.30	1.87	2.11	2.42	5.45	6.21	
400	0.92	1.36	1.55	1.73	3.92	4.54	6.75

Table 8.2 Ratio of σ_c/E for Plastic Sample2

$(\sigma/E) \times 10^3$

r/t	δ/t						
	8.42	5.53	4.87	4.34	1.97	1.71	1.05
267	1.12	1.56	1.71	1.95	4.11		
400	0.77	1.15	1.28	1.36	2.98	3.42	5.14
533	0.49	0.73	0.87	0.98	2.24	2.48	3.90

Table 8.3 Ratio of σ_c/E for Plastic Sample3

$(\sigma/E) \times 10^3$

r/t	δ/t						
	12.80	8.40	7.40	6.60	3.00	2.60	1.60
400	0.48	0.69	0.77	0.86	1.42	1.53	
600	0.30	0.49	0.51	0.58	1.17	1.28	
800	0.24	0.35	0.41	0.46	0.91	1.02	1.44

Table 8.4 Ratio of σ_c/E for Aluminium Sample1

$(\sigma/E) \times 10^3$

r/t	δ/t					
	6.22	3.94	3.50	3.11	1.38	1.18
200	0.35	0.53	0.57	0.65	1.22	1.29
300	0.30	0.45	0.52	0.62	1.13	1.27
400	0.38	0.57	0.63	0.71	1.27	1.38

Table 8.5 Ratio of σ_c/E for Aluminium Sample2 $(\sigma/E)\times 10^3$

r/t	δ/t					
	8.29	5.25	4.67	4.15	1.84	1.57
267	0.30	0.44	0.50	0.54	1.11	1.28
400	0.28	0.42	0.48	0.52	1.05	1.14
533	0.34	0.48	0.54	0.62	1.24	1.32

Table 8.6 Ratio of σ_c/E for Aluminium Sample3 $(\sigma/E)\times 10^3$

r/t	δ/t					
	12.44	7.87	7.01	6.22	2.76	2.36
400	0.16	0.23	0.28	0.30	0.57	0.74
600	0.15	0.22	0.23	0.26	0.55	0.60
800	0.16	0.22	0.25	0.28	0.50	0.65

Table 8.7 Ratio of σ_c/E for Steel Sample1 $(\sigma/E)\times 10^3$

r/t	δ/t						
	12.60	9.33	6.22	3.94	3.50	3.11	1.38
200			0.65	0.99	1.15	1.23	2.37
300			0.58	0.85	0.99	1.07	1.85
400	0.23	0.31	0.49	0.73	0.88	0.93	1.60

Table 8.8 Ratio of σ_c/E for Steel Sample2 $(\sigma/E)\times 10^3$

r/t	δ/t					
	8.29	5.25	4.67	4.15	1.84	1.57
267	0.53	0.78	0.87	0.98	1.76	1.93
400	0.42	0.72	0.79	0.86	1.56	1.99
533	0.35	0.39	0.41	0.43	0.71	0.82

Table 8.9 Ratio of σ_c/E for Steel Sample3

$(\sigma/E) \times 10^3$

r/t	δ/t					
	12.44	7.87	7.01	6.22	2.76	2.36
400	0.28	0.42	0.47	0.55	1.00	1.04
600	0.21	0.29	0.37	0.44	0.79	0.83
800	0.14	0.19	0.21	0.23	0.41	0.46

Table 8.10 Ratio of σ_c/E for Cardboard

$(\sigma/E) \times 10^3$

r/t	δ/t					
	5.27	3.33	2.97	2.63	1.17	1.00
170	1.14	1.75	1.82	1.97		
253	1.08	1.58	1.64	1.85	2.93	3.43

r/t	δ/t								
	17.92	11.89	8.94	5.92	3.81	3.06	1.43	1.17	0.28
338	0.27	0.50	0.63	0.91	1.25	1.55	2.12	2.60	3.83

8.3 Buckling Function and Verification

In Chapter 4 a relationship of the critical buckling compression stress σ_c with the elastic modulus E and two dimensionless variables $(\frac{r}{t})$ and $(\frac{\delta}{t})$ were derived by using the dimensional analysis method (see Equations (4.9),(4.10) and (5.1))

From Equation (5.1) it can be seen that the critical buckling compression stress σ_c is proportional to the elastic modulus of the ring material. But the critical buckling compression stress σ_c can not be completely determined unless the three numbers C, b and

d are known. Thereafter, the three unknown numbers C, b and d will be determined by using the least squares method for the different materials.

Only experimental data in Table 8.1-Table 8.3 were used to derive the three undetermined numbers in the buckling function (8.1). The reason for this is that the buckling function was derived under the total elastic material assumption. In experiments, local plastic deformation was observed for all materials except the plastics. That is why initially only data from plastic materials were used. This initial analysis using a multi-variable least square method resulted in the following three numbers.

$$C = 1.9970 \qquad b = -0.9917 \qquad d = -0.9499 \tag{8.1a}$$

The 99 percent confidence intervals for the three parameters are [57,58]

$$\begin{aligned} \mathrm{CI}\,(C) &= [1.9414, 2.0843] \\ \mathrm{CI}\,(b) &= [-1.0318, -0.9508] \\ \mathrm{CI}\,(d) &= [-0.9921, -0.9077] \end{aligned}$$

With 0.01 lever of significance we can accept that

$$C = 2.00 \qquad b = -1.00 \qquad d = -0.95 \tag{8.1b}$$

Thus the buckling function for the plastic becomes

$$f\left[\left(\frac{r}{t}\right), \left(\frac{\delta}{t}\right)\right] = 2.00\left(\frac{r}{t}\right)^{-1.00}\left(\frac{\delta}{t}\right)^{-0.95} = \frac{\sigma_c}{E} \tag{8.2}$$

To test the validity of Equation (8.2), according to Chapter 4, first $(\frac{\delta}{t})$ is held constant at a value of 4.34 and a component equation is determined by the least square method from the data in Table 8.2

$$f\left[(\frac{r}{t}), 4.34\right] = 0.4939 \times (\frac{r}{t})^{-0.9885} \quad (8.3)$$

Then $(\frac{r}{t})$ is held constant at a value of 400 and another component equation can be determined from the data in Table 8.2

$$f\left[400, (\frac{\delta}{t})\right] = 0.5483 \times 10^{-2} (\frac{\delta}{t})^{-0.9222} \quad (8.4)$$

Similarly another two component equations can be determined from the data in Table 8.2

$$f\left[(\frac{r}{t}), 4.87\right] = 0.3768 \times (\frac{r}{t})^{-0.9605} \quad (8.5)$$

$$f\left[533, (\frac{\delta}{t})\right] = 0.4247 \times 10^{-2} (\frac{\delta}{t})^{-1.0098} \quad (8.6)$$

And

$$f[400, 4.34] = 1.36 \times 10^{-3} \qquad f[533, 4.87] = 0.87 \times 10^{-3} \quad (8.7)$$

$$f[400, 4.87] = 1.28 \times 10^{-3} \qquad f[533, 4.34] = 0.98 \times 10^{-3} \quad (8.8)$$

Using Equation (4.23) to test the validity of the prediction Equation (8.2), we have

$$\frac{f\left[400,\ (\frac{\delta}{t})\right]}{f[400, 4.34]} = 4.0316\,(\frac{\delta}{t})^{-0.9222} \qquad \frac{f\left[533,\ (\frac{\delta}{t})\right]}{f[533, 4.34]} = 4.3337\,(\frac{\delta}{t})^{-1.0098} \tag{8.9}$$

Figure 8.1 is the comparison of two equations in Equations (8.9). It is found that

$$\frac{f\left[400,\ (\frac{\delta}{t})\right]}{f[400, 4.34]} \approx \frac{f\left[533,\ (\frac{\delta}{t})\right]}{f[533, 434]} \tag{8.10}$$

Using Equation (4.24) to conduct another test, we obtain

$$\frac{f\left[(\frac{r}{t}), 4.34\right]}{f[400, 4.34]} = 363.16\,(\frac{r}{t})^{-0.9885} \qquad \frac{f\left[(\frac{r}{t}), 4.87\right]}{f[400, 4.87]} = 294.37\,(\frac{r}{t})^{-0.9605} \tag{8.11}$$

Figure 8.2 is the comparison of two equations in Equations (8.11). It is also found that

$$\frac{f\left[(\frac{r}{t}), 4.34\right]}{f[400, 4.34]} \approx \frac{f\left[(\frac{r}{t}), 4.87\right]}{f[400, 4.87]} \tag{8.12}$$

From the preceding test, it is concluded that the form of the prediction Equation (8.2) is valid.

Figure 8.3 is a comparison of the dimensional analysis fitted curves with the experimental data. Figure 8.4 is the comparison of Equation (8.2) with Lo and Chan's theoretical results. The experimental data are in good agreement with the curves of Equation (8.2) in Figure 8.3. But the curves of Equation (8.2) are well above Lo and Chan's theoretical results. This is due to the friction effect which will be discussed later.

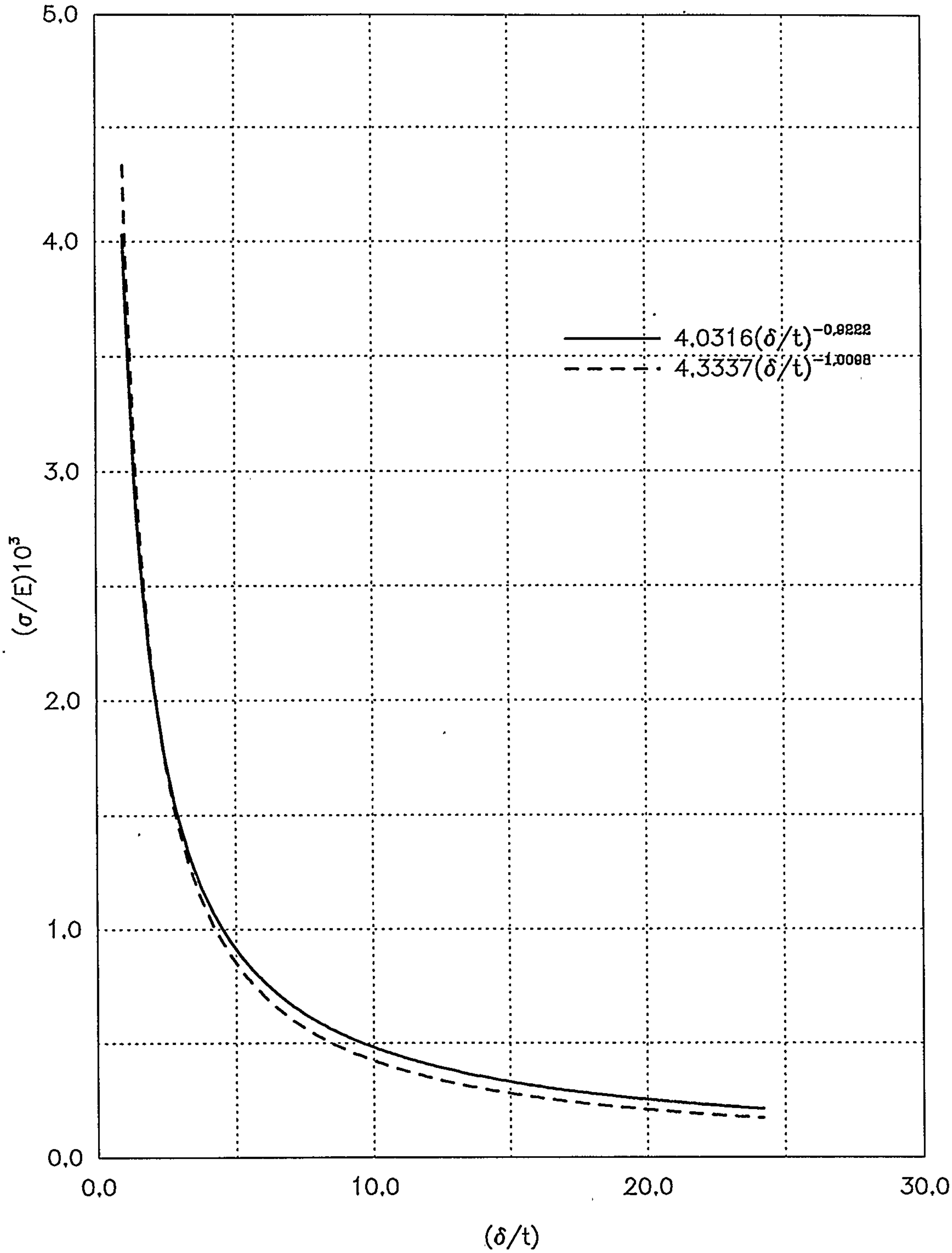

Figure 8.1 Validation Test for the Prediction Equation with (δ/t) as a Variable

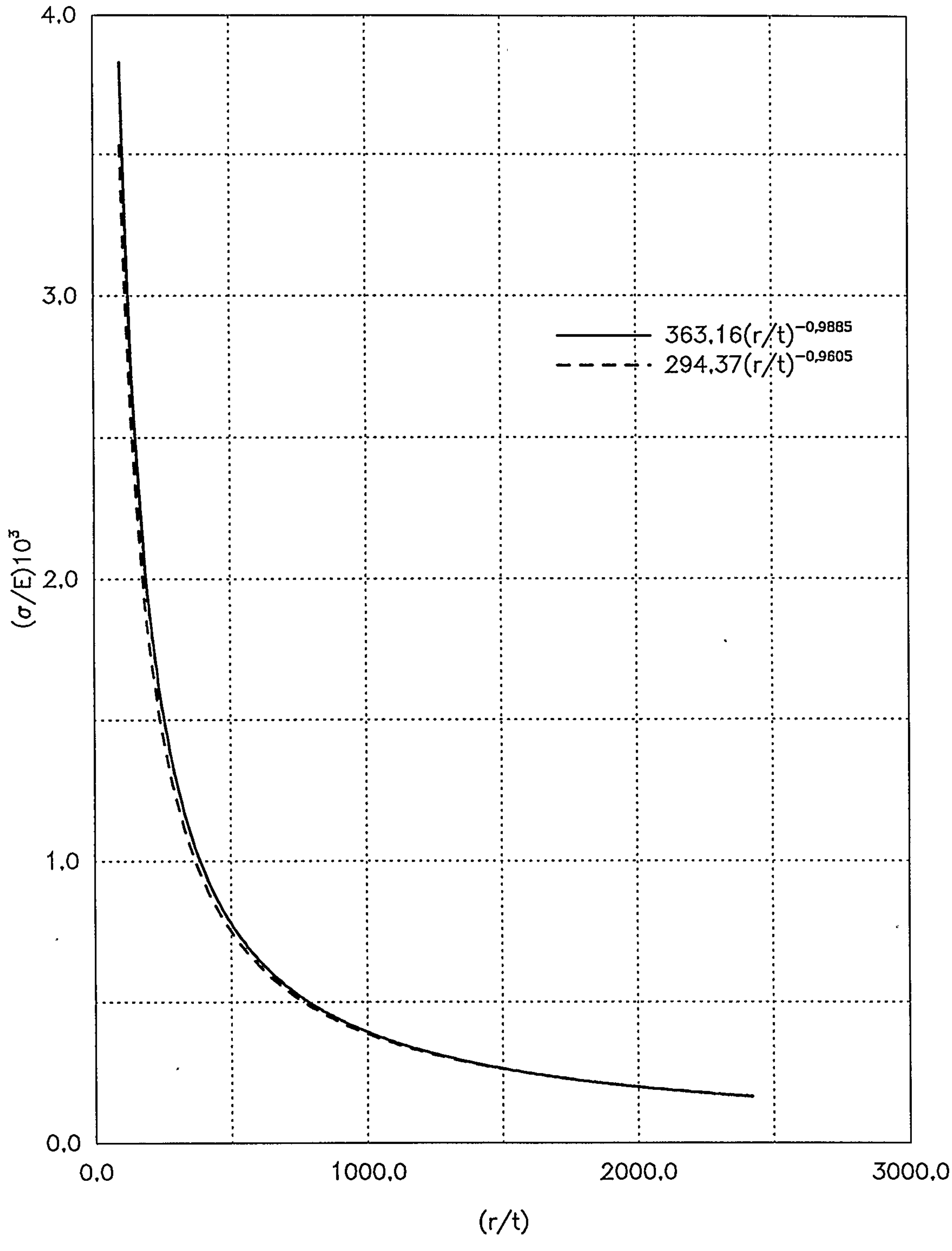

Figure 8.2 Validation Test for the Prediction Equation with (r/t) as a Variable

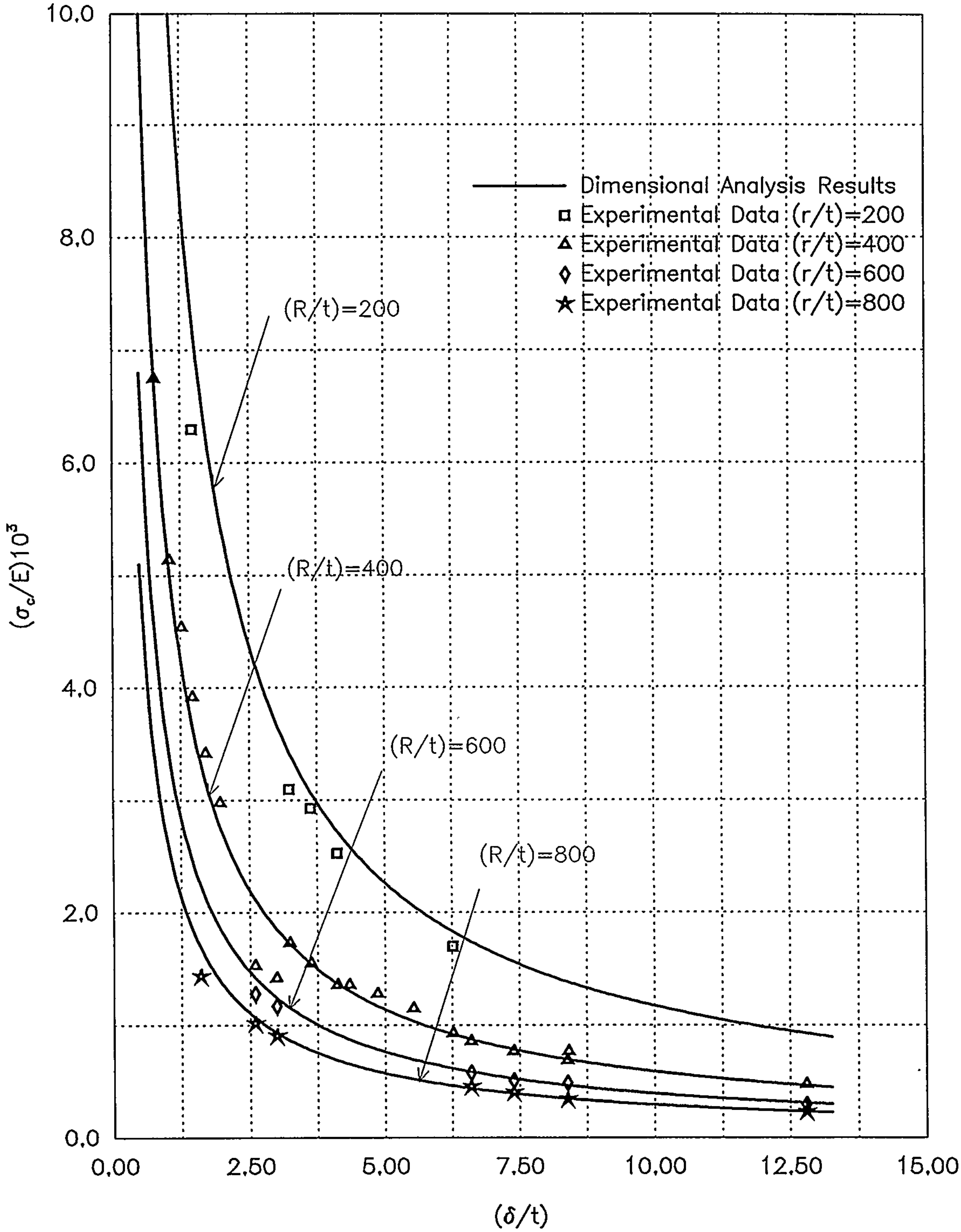

Figure 8.3 Comparison of Experimental Data with Dimensional Analysis Fitting Curves

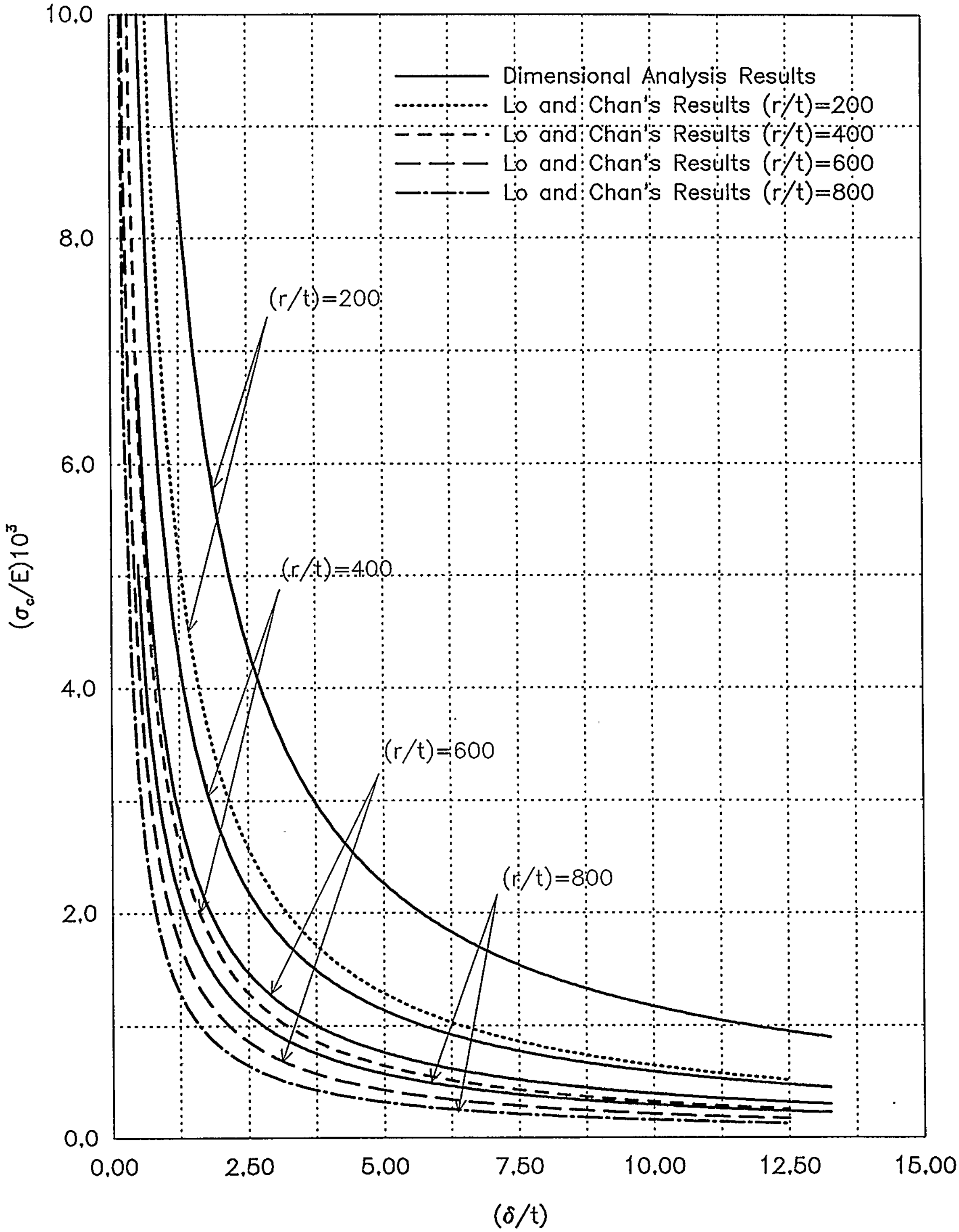

Figure 8.4 Comparison of Dimensional Analysis Fitting Curves with Lo and Chan's Results

8.4 Comparison with Discrete Element Model for Plastics Materials

Figure 8.5 -Figure 8.13 are comparisons of the experimental data for plastic materials with the results of the discrete element model analysis.

Comparing Equation (8.2) with Equation (5.33) and Equation (6.25) it is found that the exponents of two dimensionless variables $(\frac{r}{t})$ and $(\frac{\delta}{t})$ are in a very good agreement with the discrete element model results and the exponents b and d are both approximately -1.

The coefficient C in Equation (8.2) is 2.00. In Equation (5.33) the coefficient C is approximately 1/2. It is obvious that the coefficient value from the experimental data is not in agreement with the frictionless discrete element model. This indicates that the friction resistance must exist in the experiment. It also indicates that the friction factor has a large effect on the coefficient and a little effect on the exponents of the buckling function.

The friction coefficient μ can be determined analytically by comparing Equation (8.2) with Equation (6.25). Let

$$\frac{1}{2}C_f = 2.00 \tag{8.13}$$

Solving Equation (8.13) for $\alpha = 5°$, we obtain

$$\mu \approx 0.87 \tag{8.14}$$

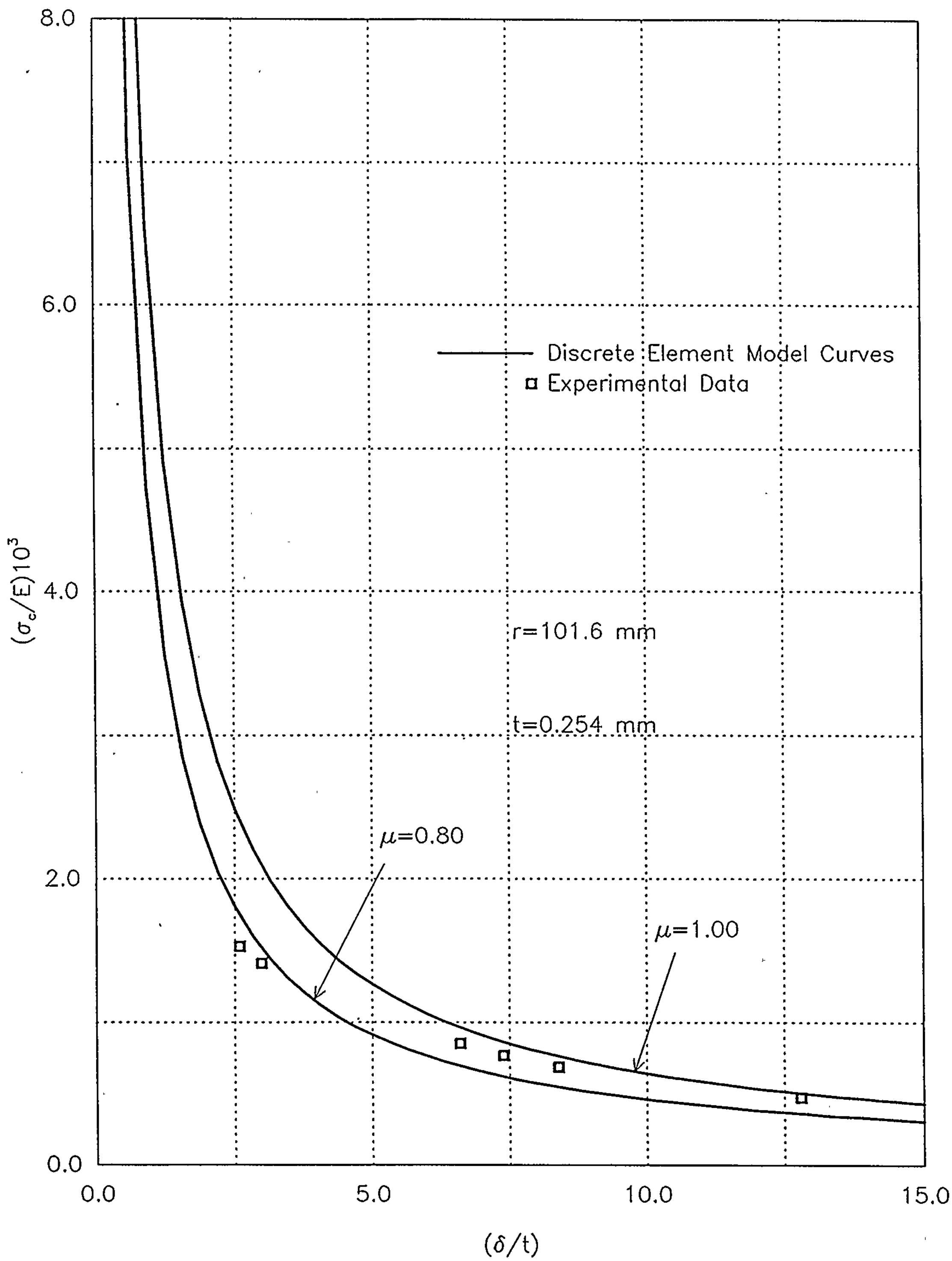

Figure 8.5 Comparison of Experimental Results with Discrete Element Model Result for Plastic

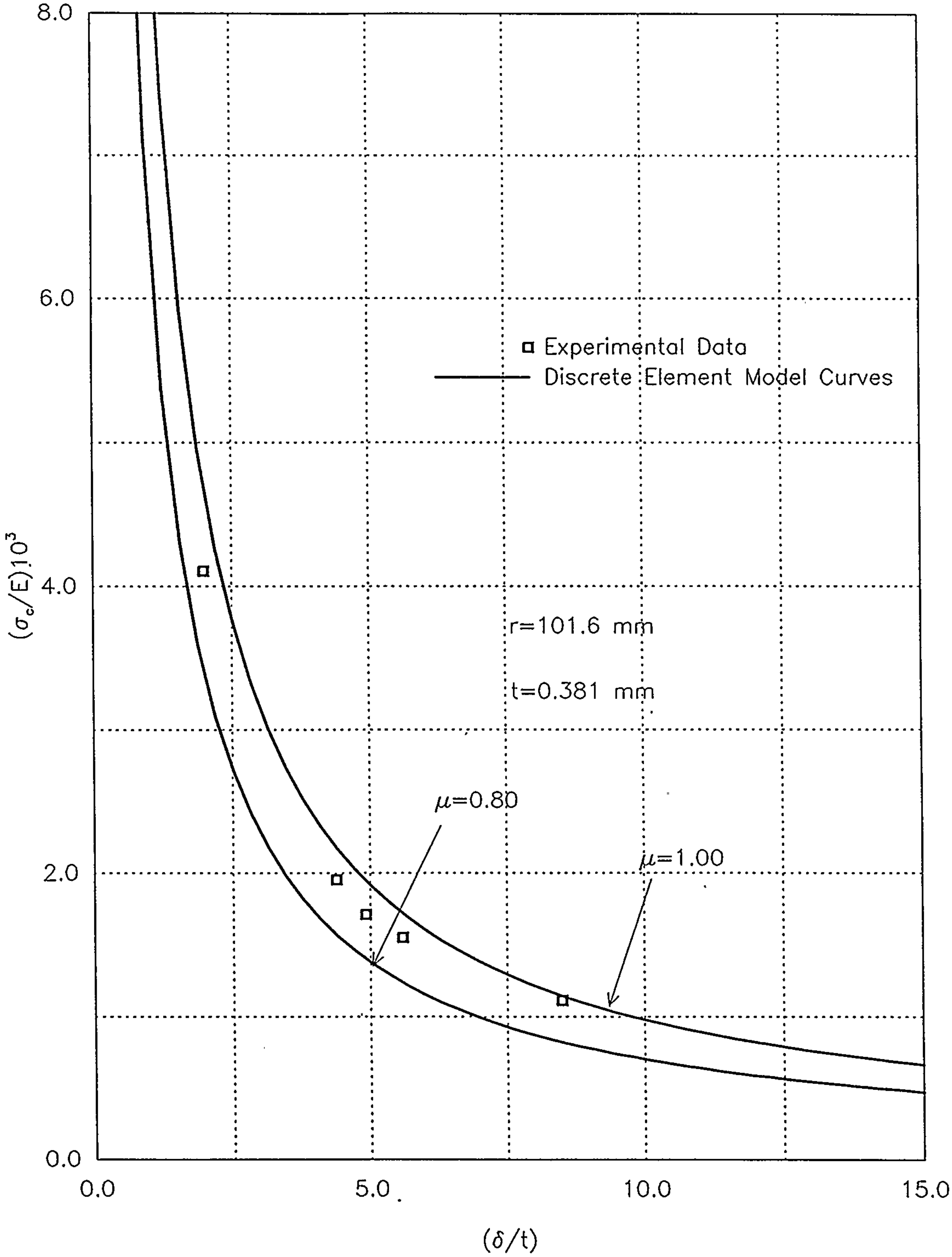

Figure 8.6 Comparison of Experimental Results with Discrete Element Model Results for Plastic

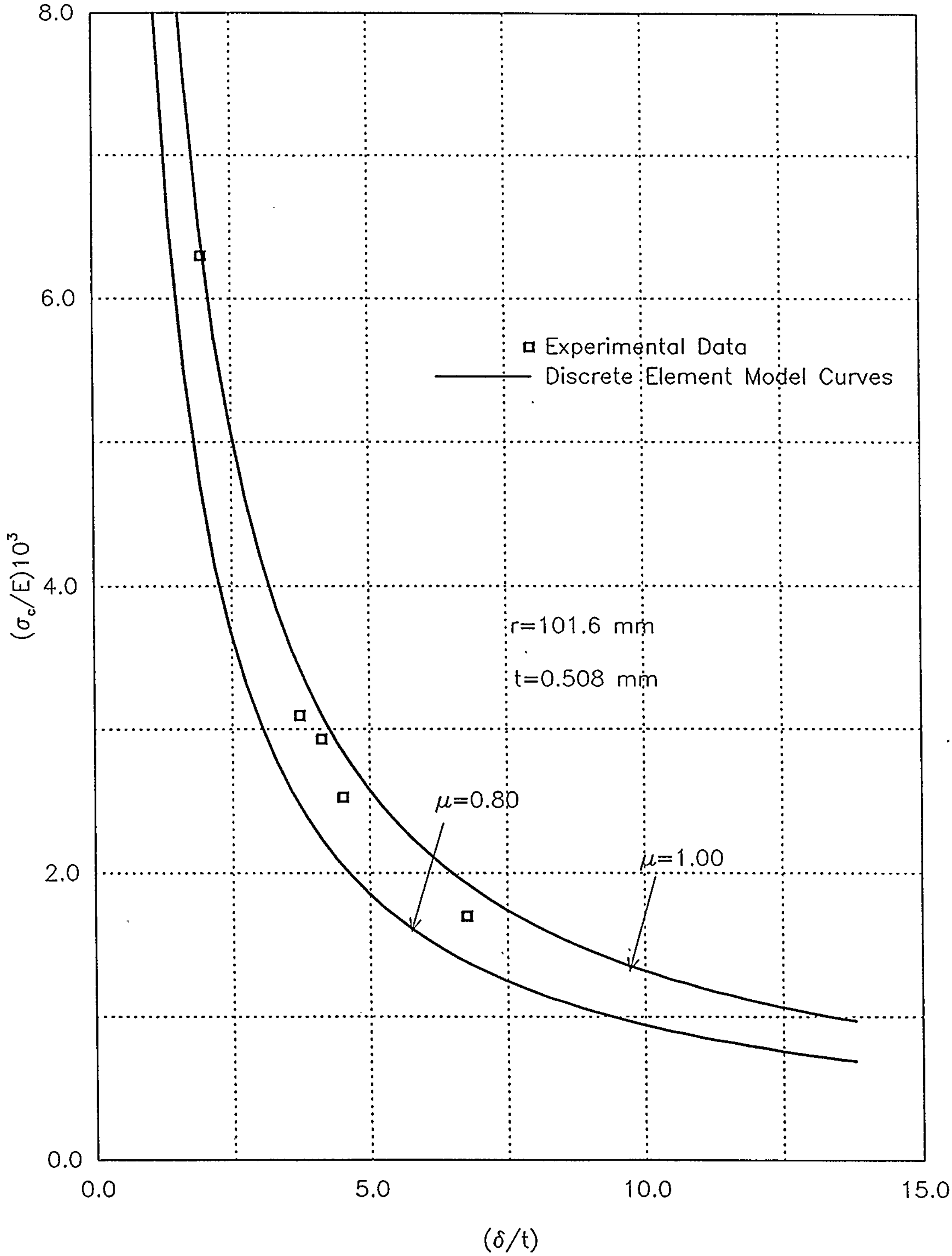

Figure 8.7 Comparison of Experiemntal Results with Discrete Element Model Results for Plastic

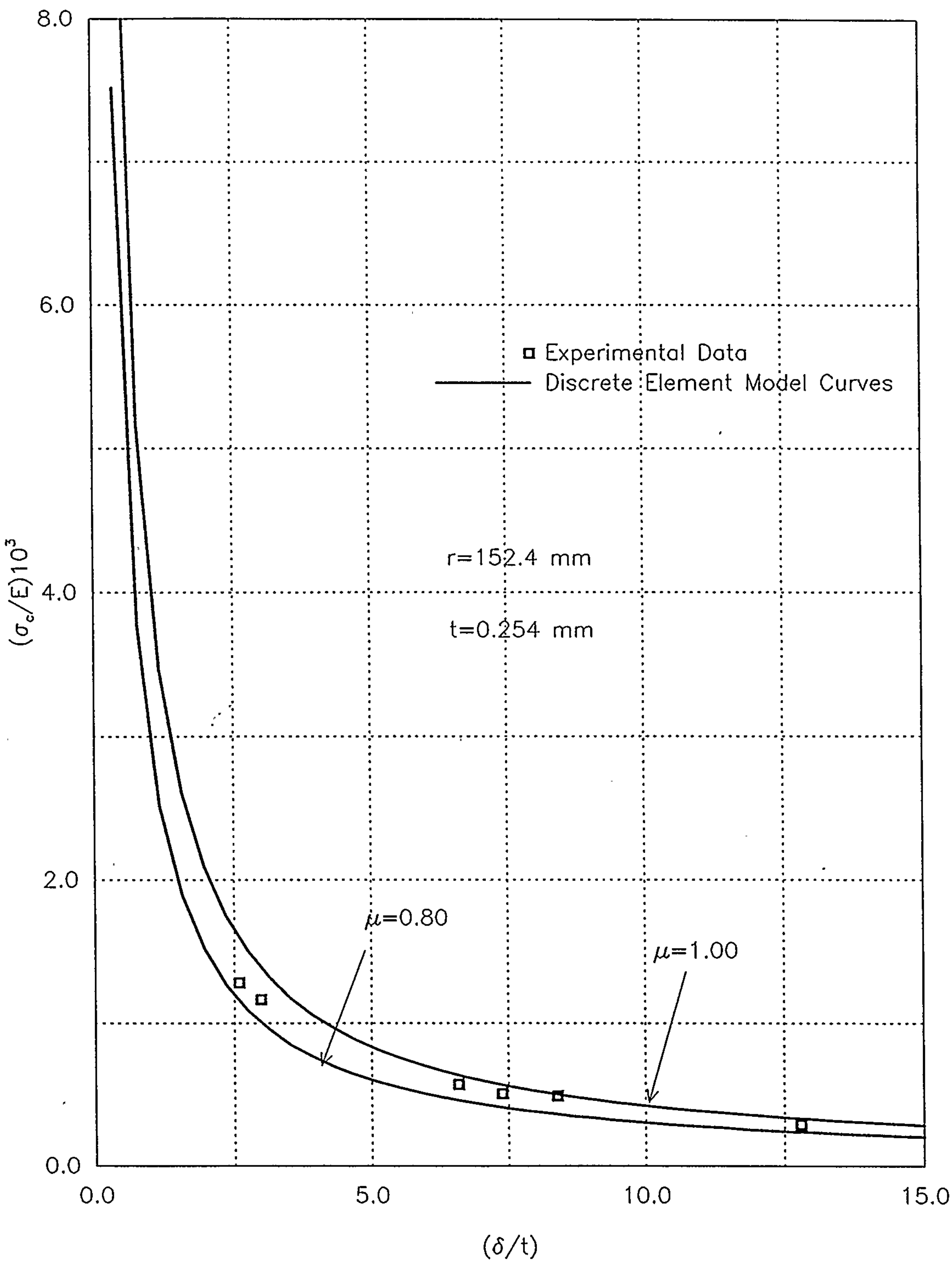

Figure 8.8 Comparison of Experimental Results with Discrete Element Results for Plastic

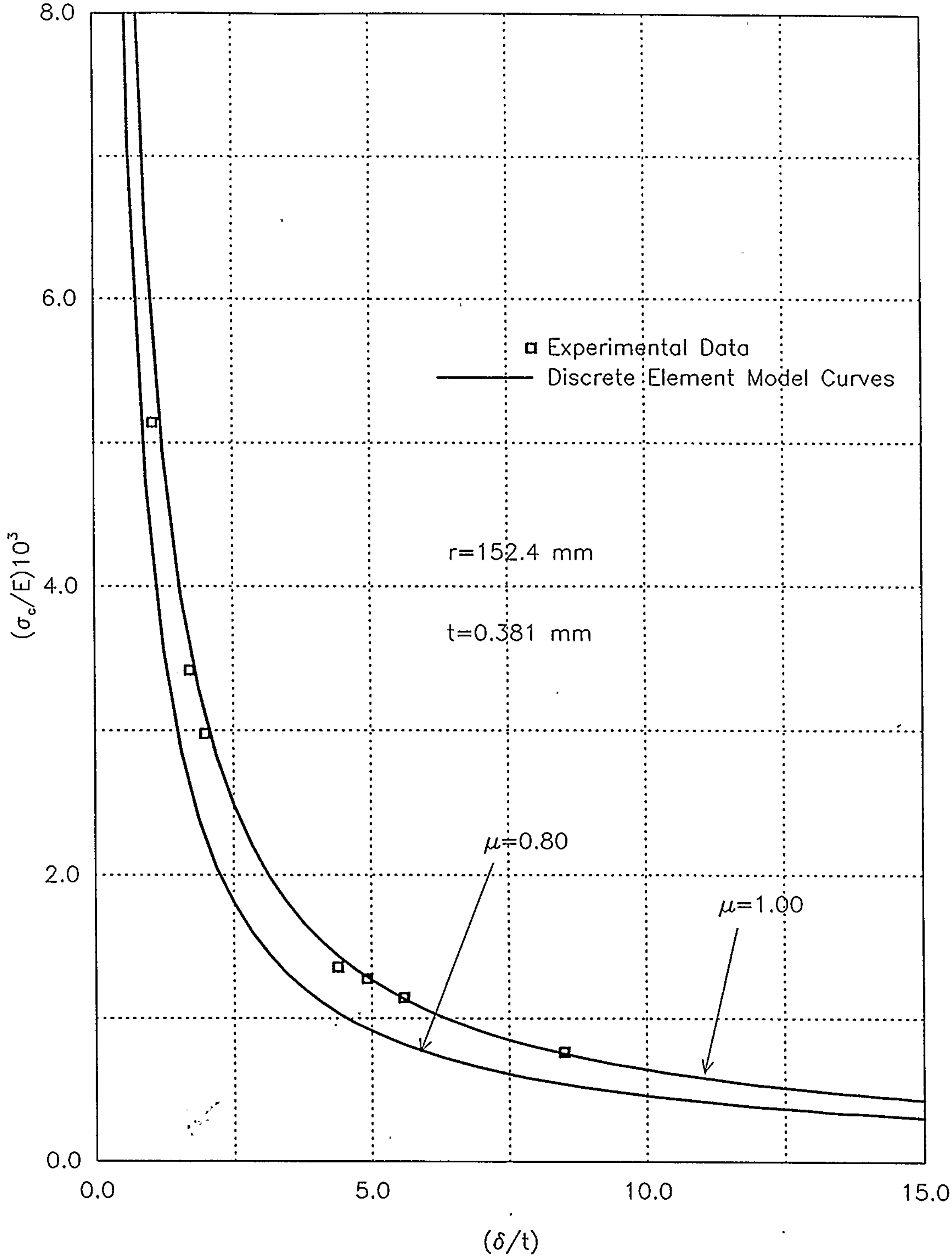

Figure 8.9 Comparison of Experimental Results with Discrete Element Results for Plastic

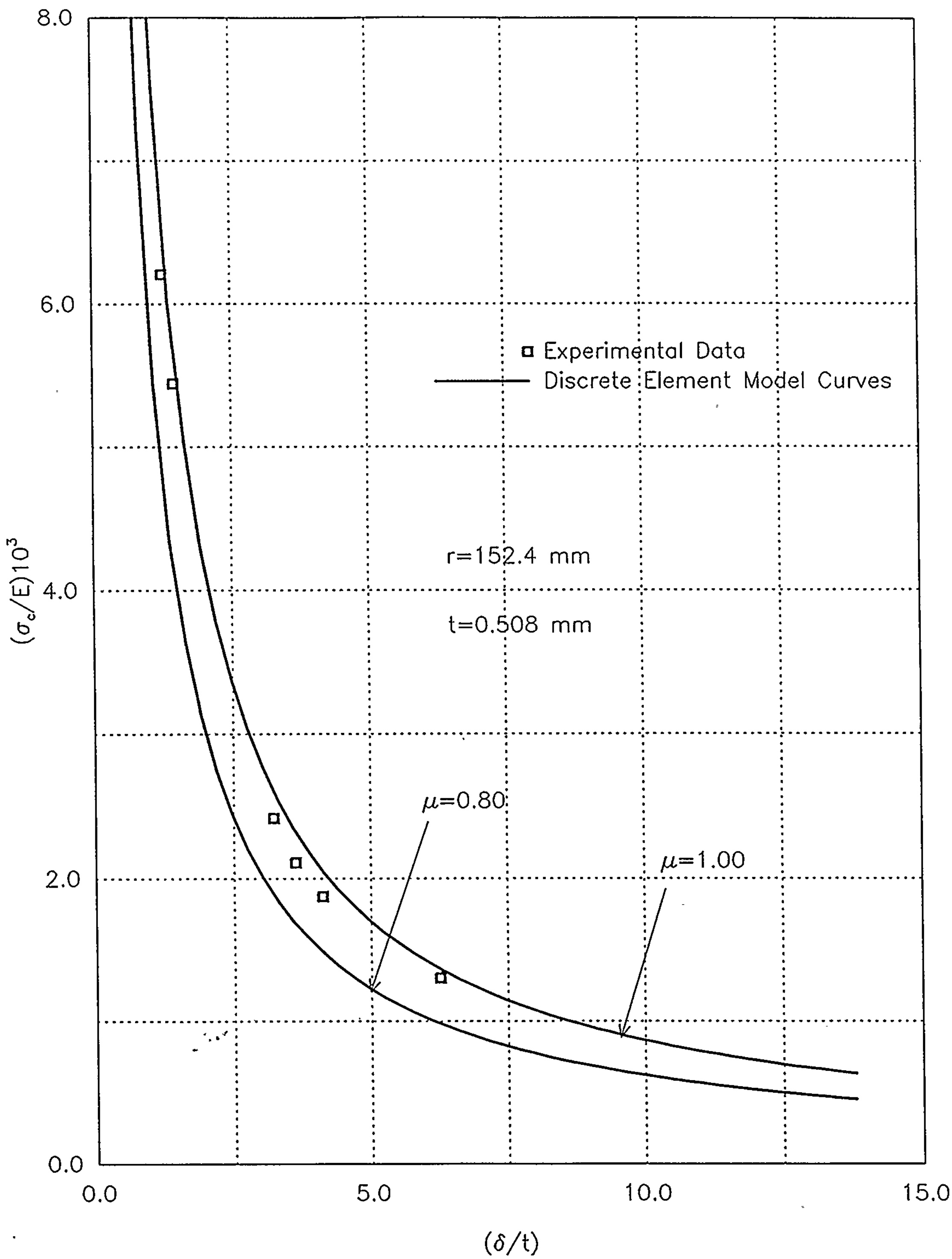

Figure 8.1·0 Comparison of Experimental Results with Discrete Element Model Results for Plastic

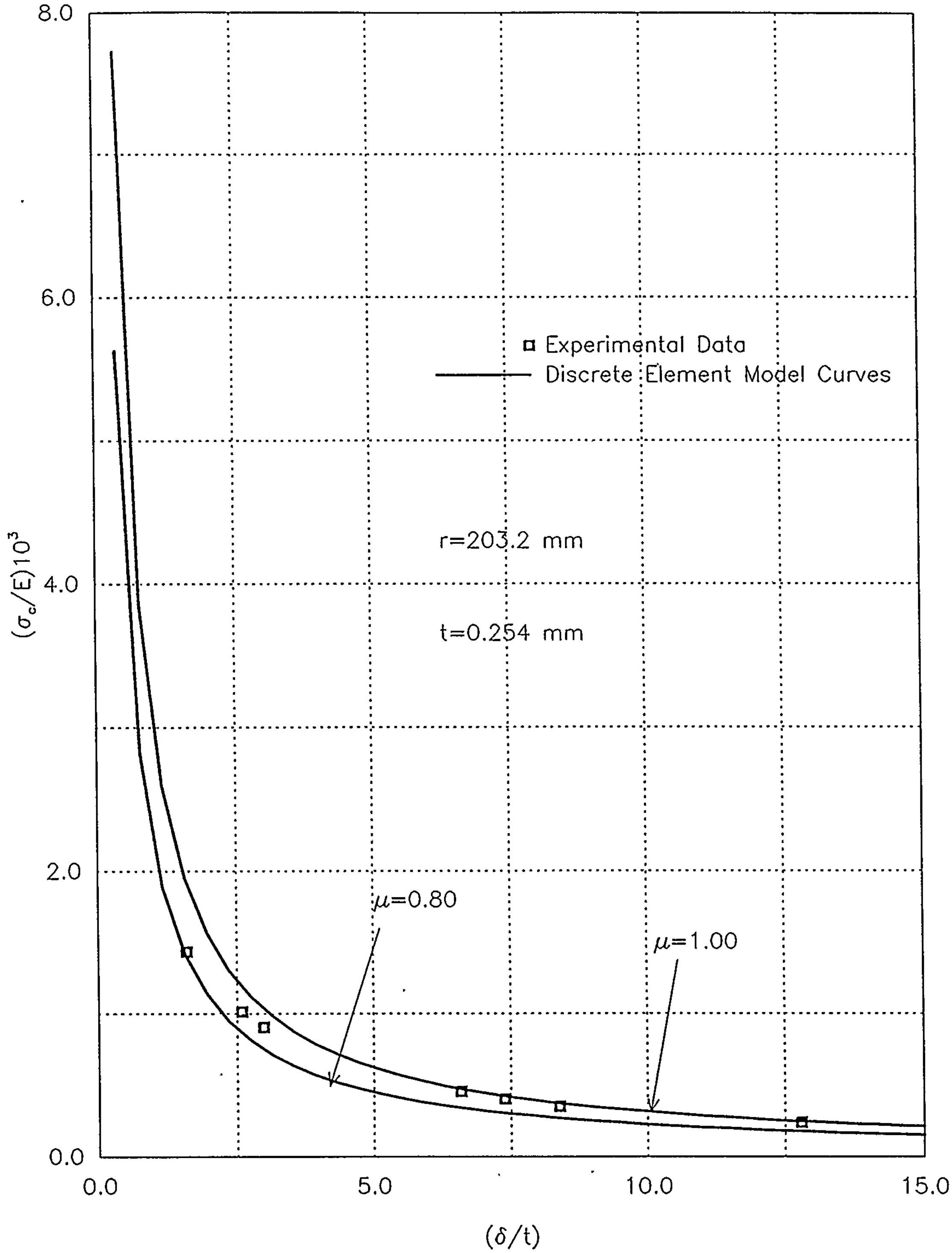

Figure 8.11 Comparison of Experimental Results with Discrete Element Model Results for Plastic

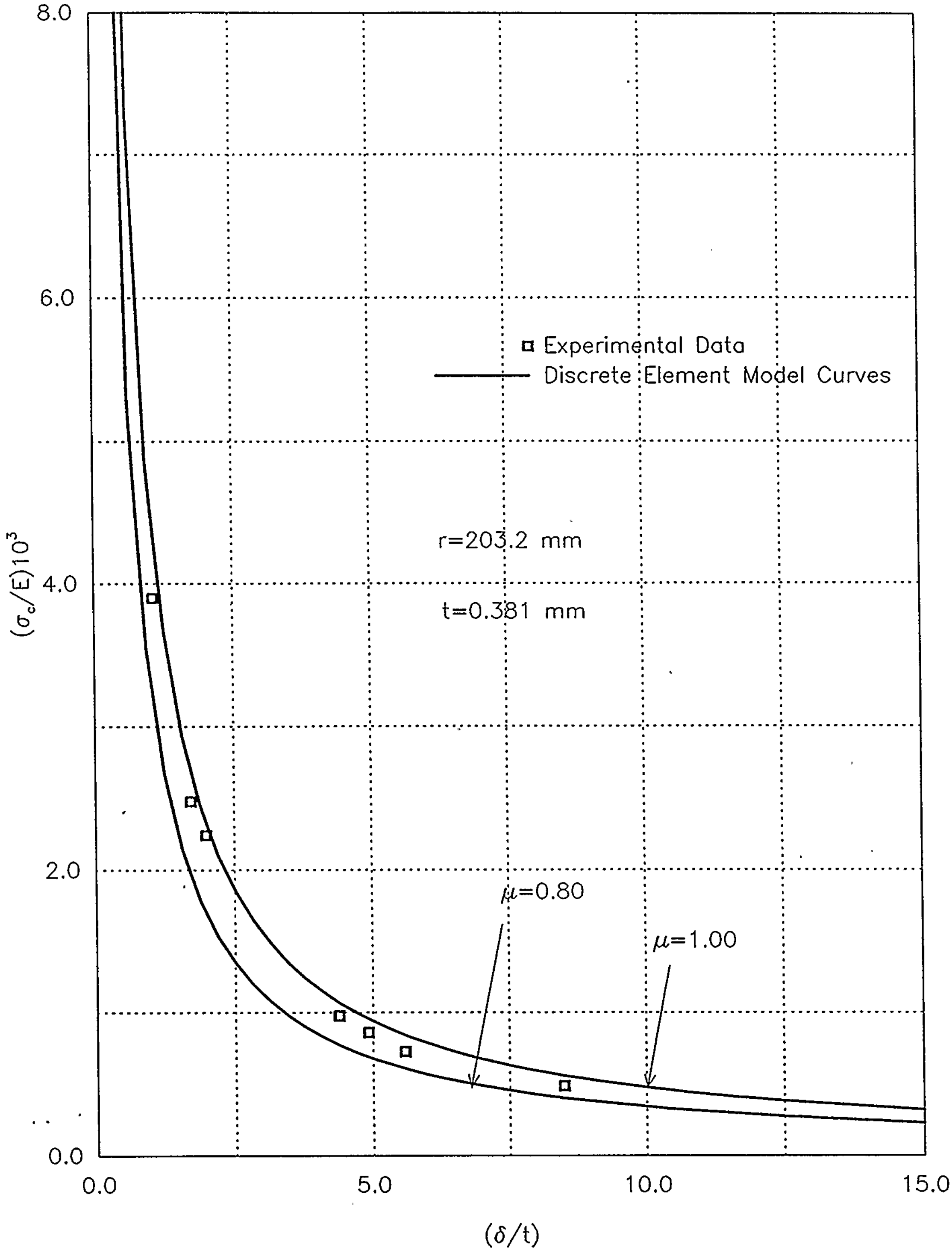

Figure 8.12 Comparison of Experimental Results with Discrete Element Model Results for Plastic

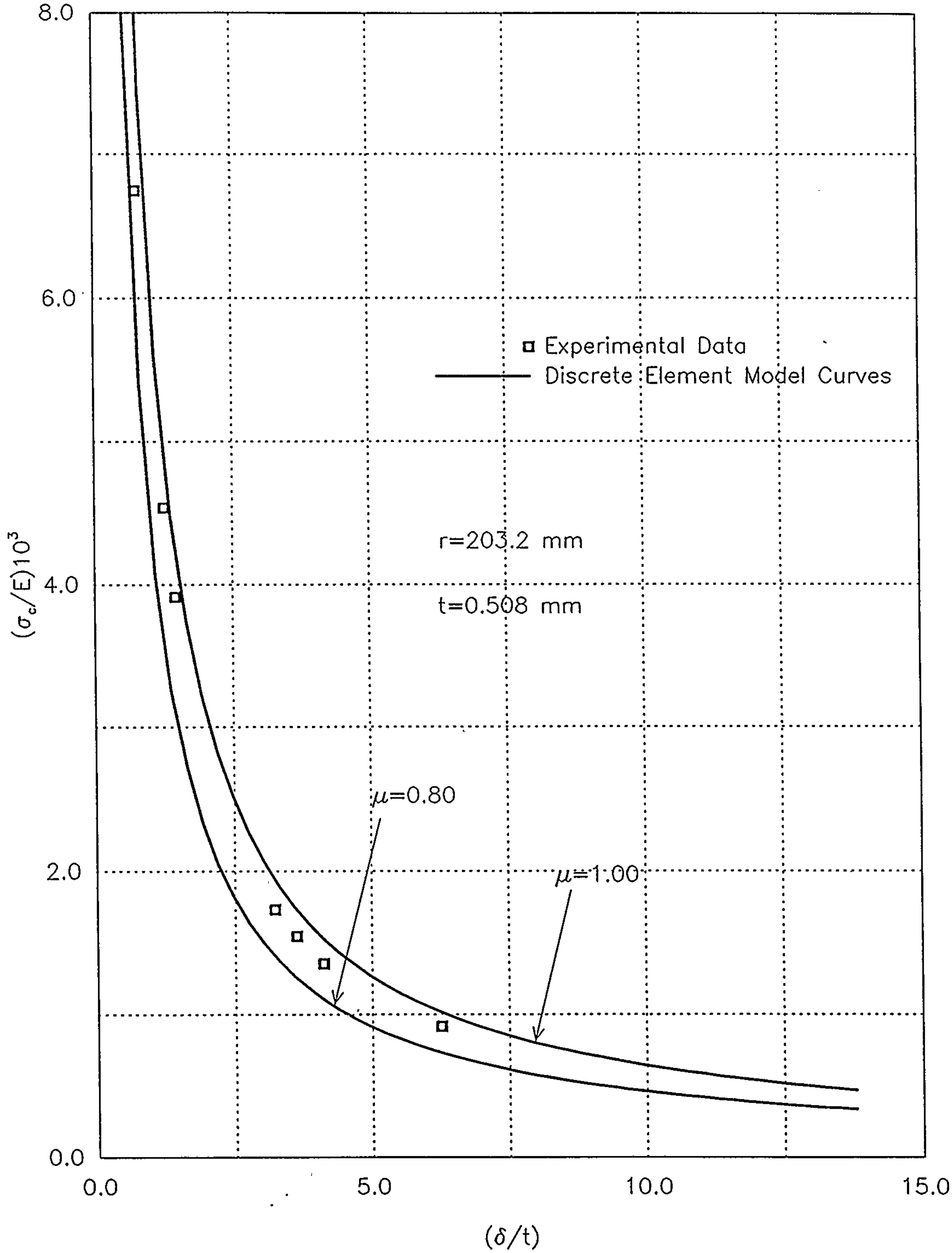

Figure 8.13 Comparison of Experimental Results with Discrete Element Model Results for Plastic

From Figure 8.5 - Figure 8.13 it can be seen that the experimental data of plastic materials are scattered in the region of $\mu = 0.8 - 1.0$. The friction coefficient measured as found in Appendix B is $\mu = 0.79 \sim 1.14$.

8.5 Comparison with Discrete Element Model for Other Materials

For materials other than plastics, some local plastic deformations were observed in the experiments. The plastic deformation will affect both the coefficient C and the exponents b and d of the buckling function.

For Aluminium, the three undetermined numbers are

$$C = 5.6269 \qquad b = -0.2110 \qquad d = -0.8730 \tag{8.15}$$

For Steel, the three undetermined numbers are

$$C = 296.50 \qquad b = -0.8367 \qquad d = -0.7752 \tag{8.16}$$

For Cardboard, the three undetermined numbers are

$$C = 67.133 \qquad b = -0.5581 \qquad d = -0.6465 \tag{8.17}$$

The measured friction coefficient μ for three materials are (see Appendix B):

Steel: $\mu = 0.24 \sim 0.34$

Aluminium: $\mu = 0.20 \sim 0.25$

Cardboard: $\mu = 0.17 \sim 0.22$

Figure 8.14 -Figure 8. 22 are the comparisons of the experimental data for steel with the discrete element model results. Figure 8.22-8.31 are the comparisons of the experimental data for aluminium with the discrete element model results. Figure 8.32-Figure 8.34 are the comparisons of the experimental data for cardboard with the discrete element model results.

Unlike plastic materials, the experimental data do not follow the curves of the discrete element model. In the large imperfection region the experimental data follow the discrete element model results quite well. But in the small imperfection region, the experimental data are at below the discrete element model results. This can be explained by the local plastic deformation observed in the experiments for these materials. At the large imperfection region, the critical load is relatively low and the plastic deformation is negligible, so that the experimental data are in good agreement with the theoretical analytical results. But in the small imperfection region, the critical load is relatively large and the local plastic deformations are very obvious and have a strong effect on the critical buckling load as the experimental data are well below the theoretical analysis results.

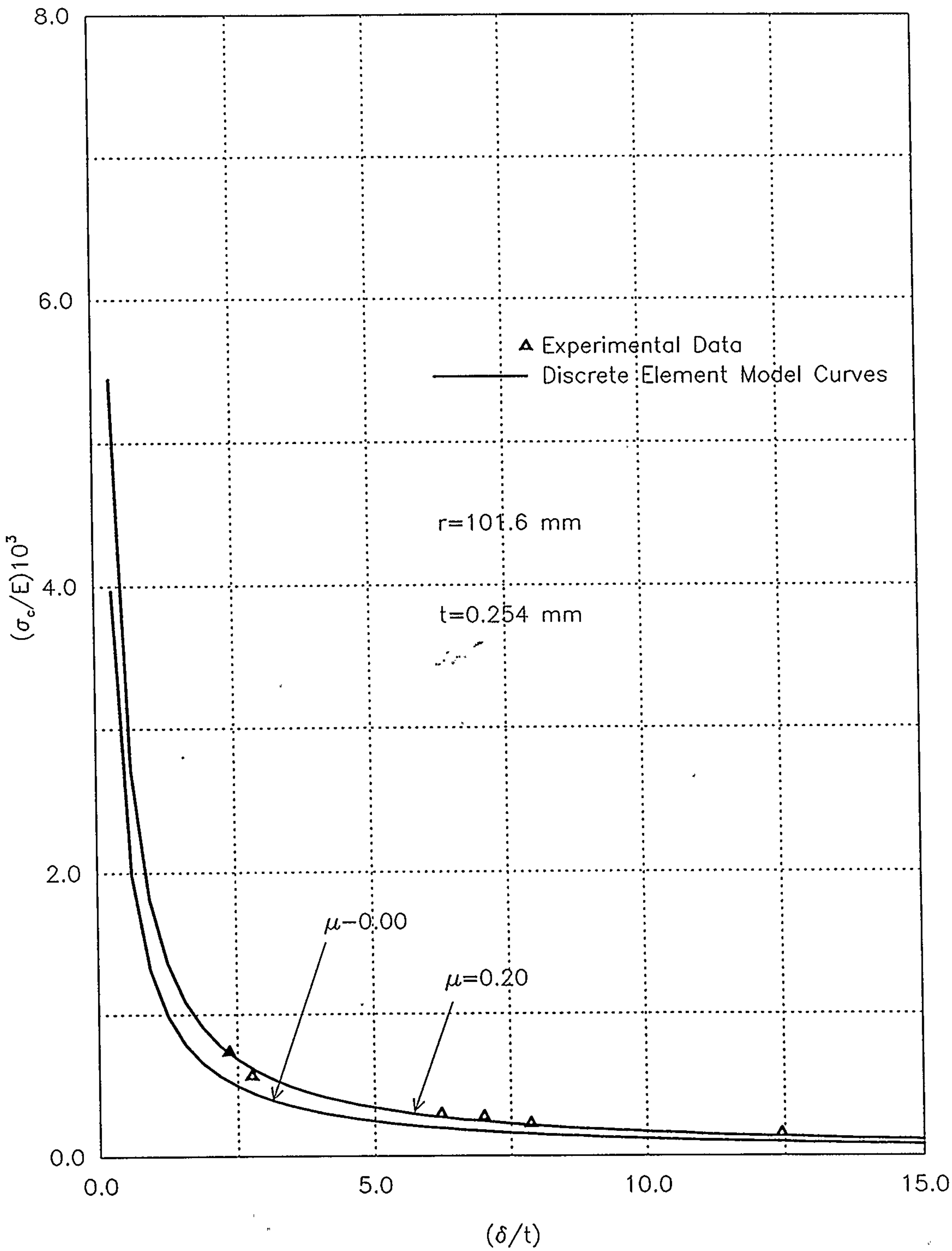

Figure 8.14 Comparison of Experimental Results with Discrete Element Model Results for Aluminium

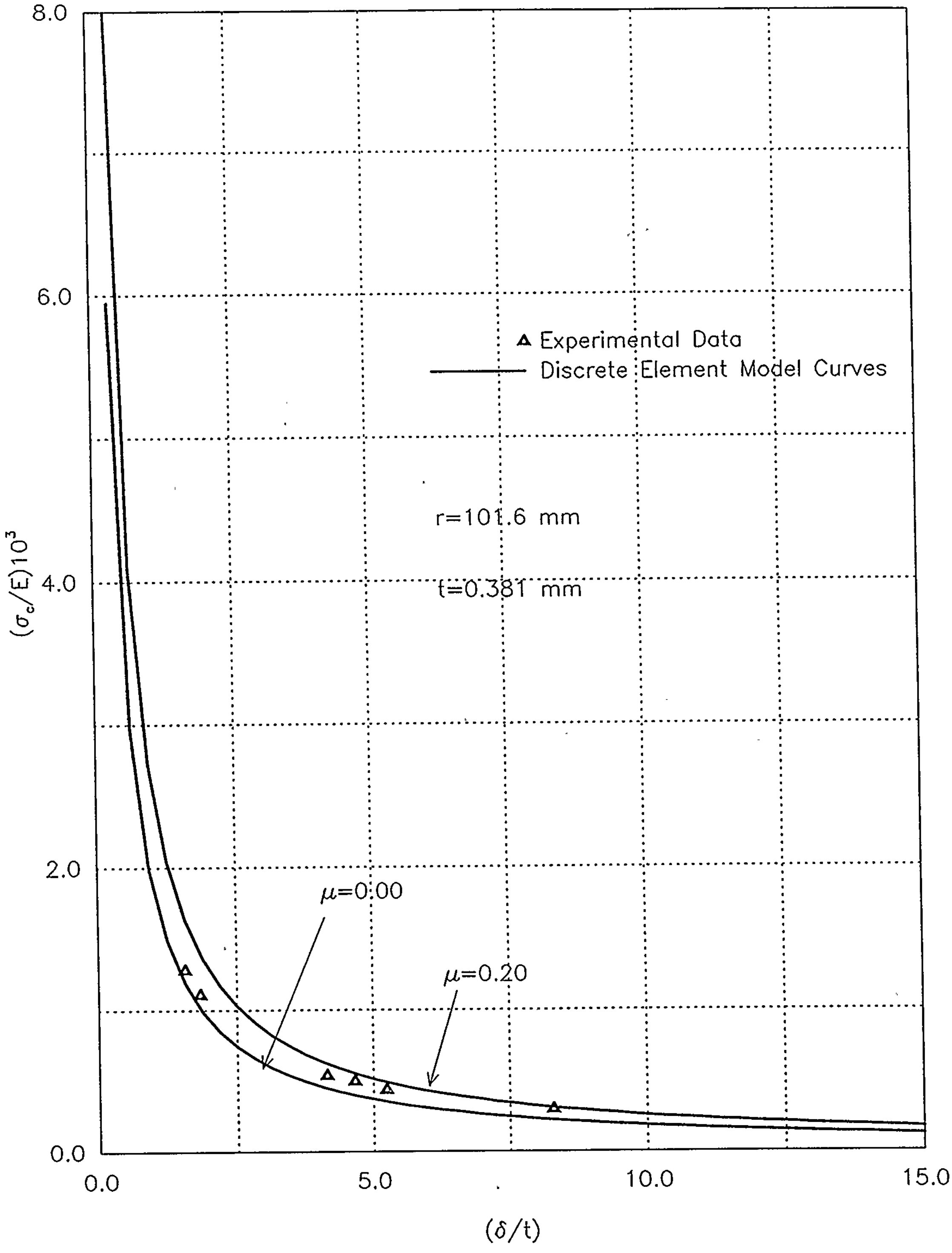

Figure 8.15 Comparison of Experimental Results with Discrete Element Model Results for Aluminium

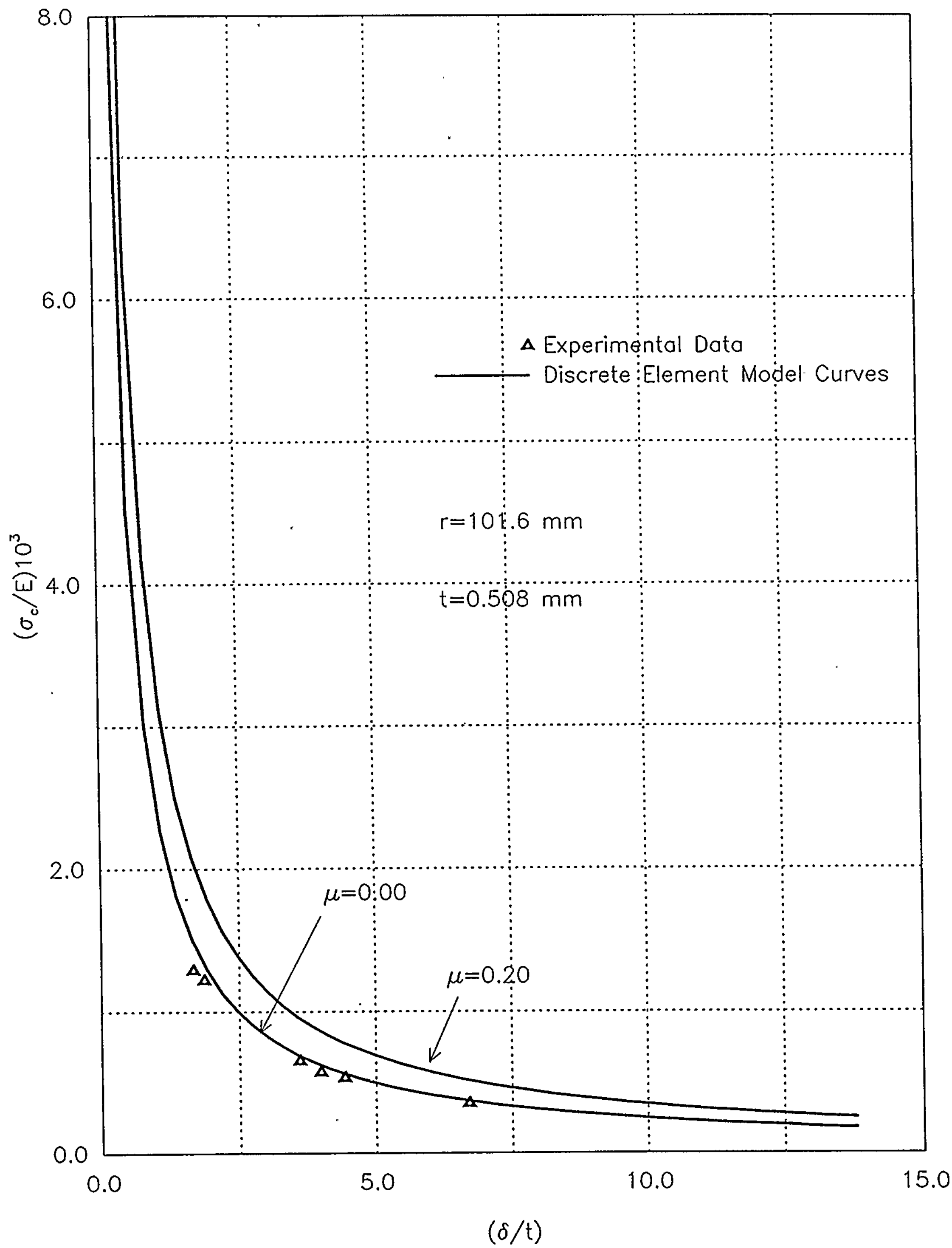

Figure 8.16 Comparison of Experiemntal results with Discrete Element Model Results for Aluminium

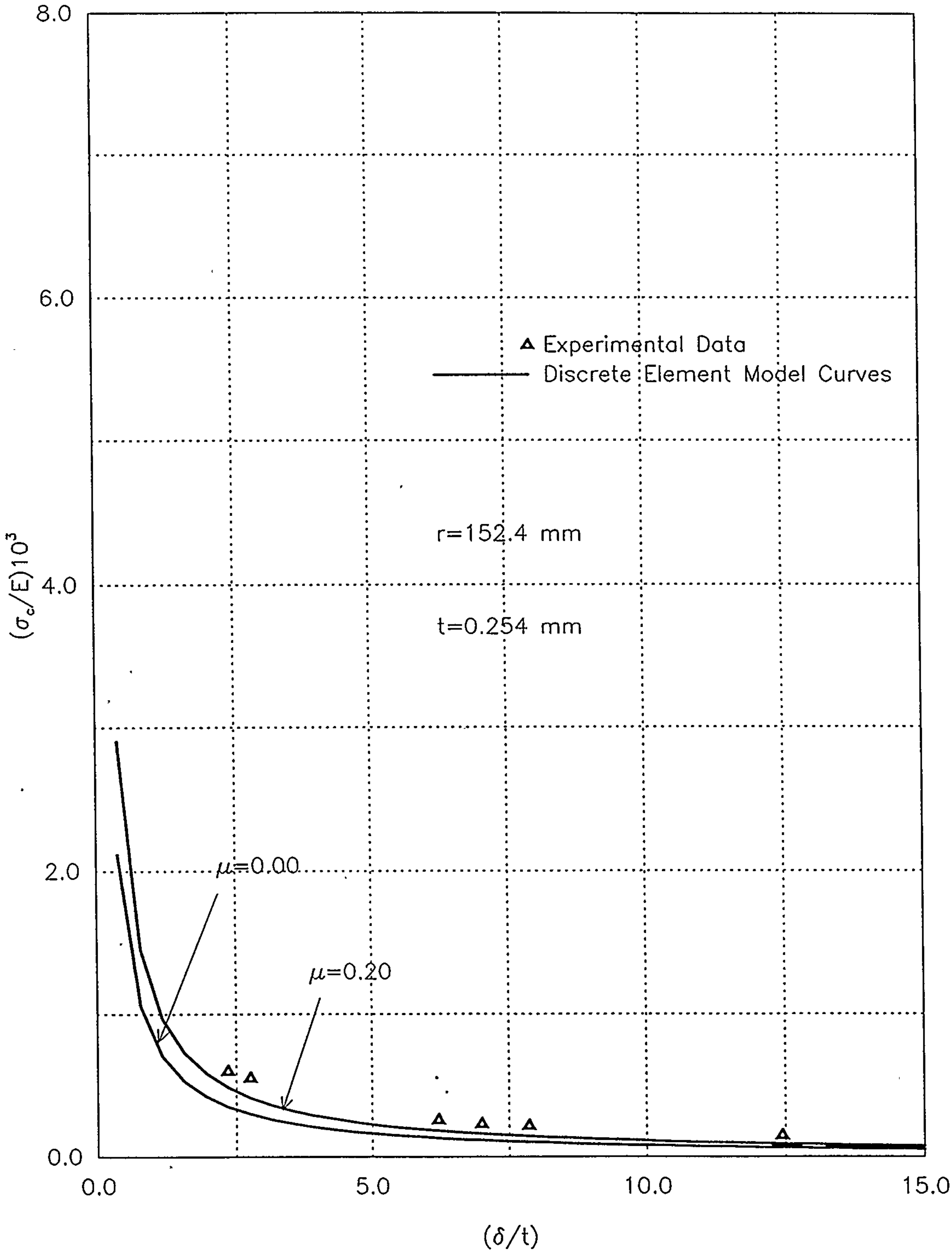

Figure 8.17 Comparison of Experimental Results with Discrete Element Model Results for Aluminium

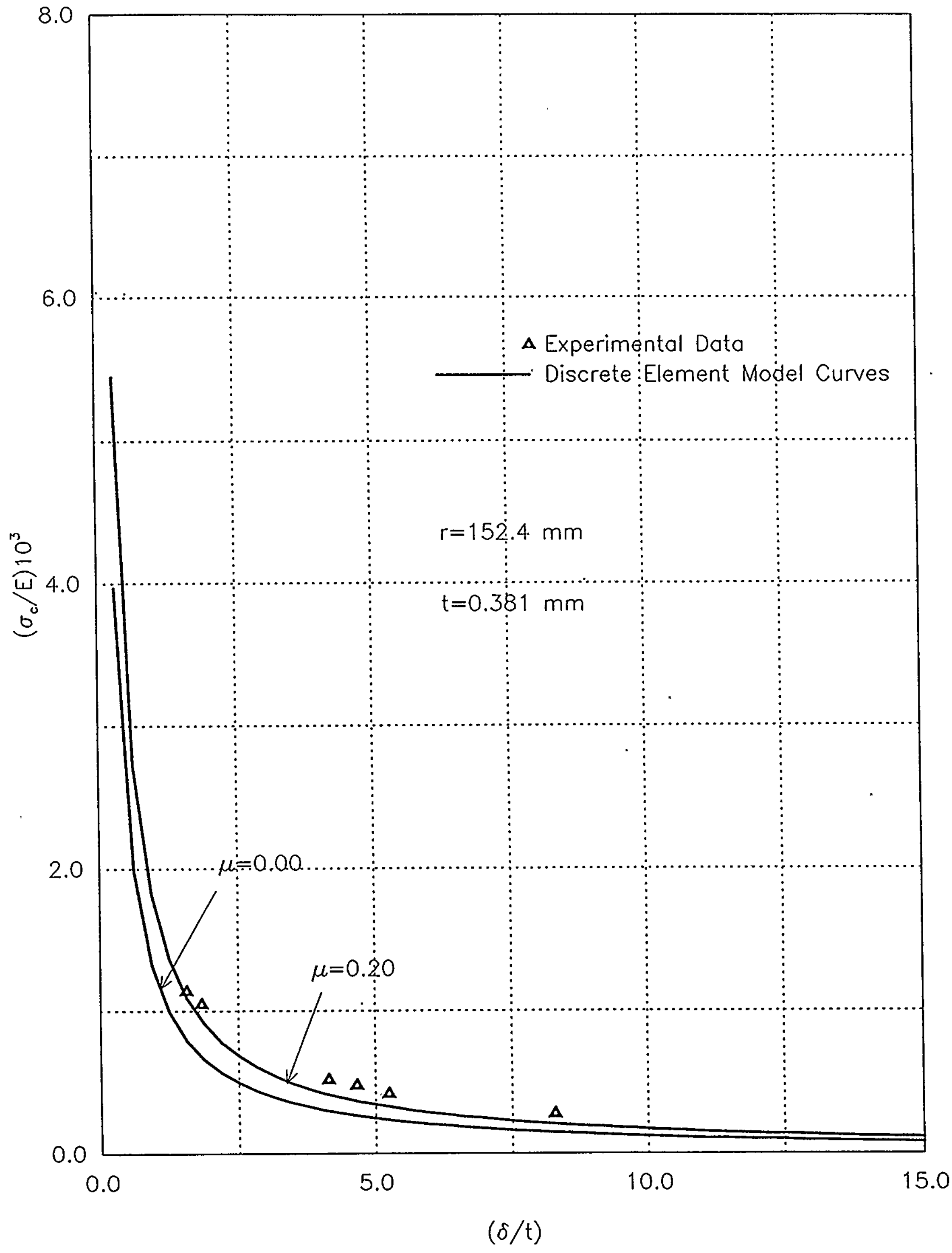

Figure 8.18 Comparison of Expermental Results with Discrete Element Model Results for Aluminium

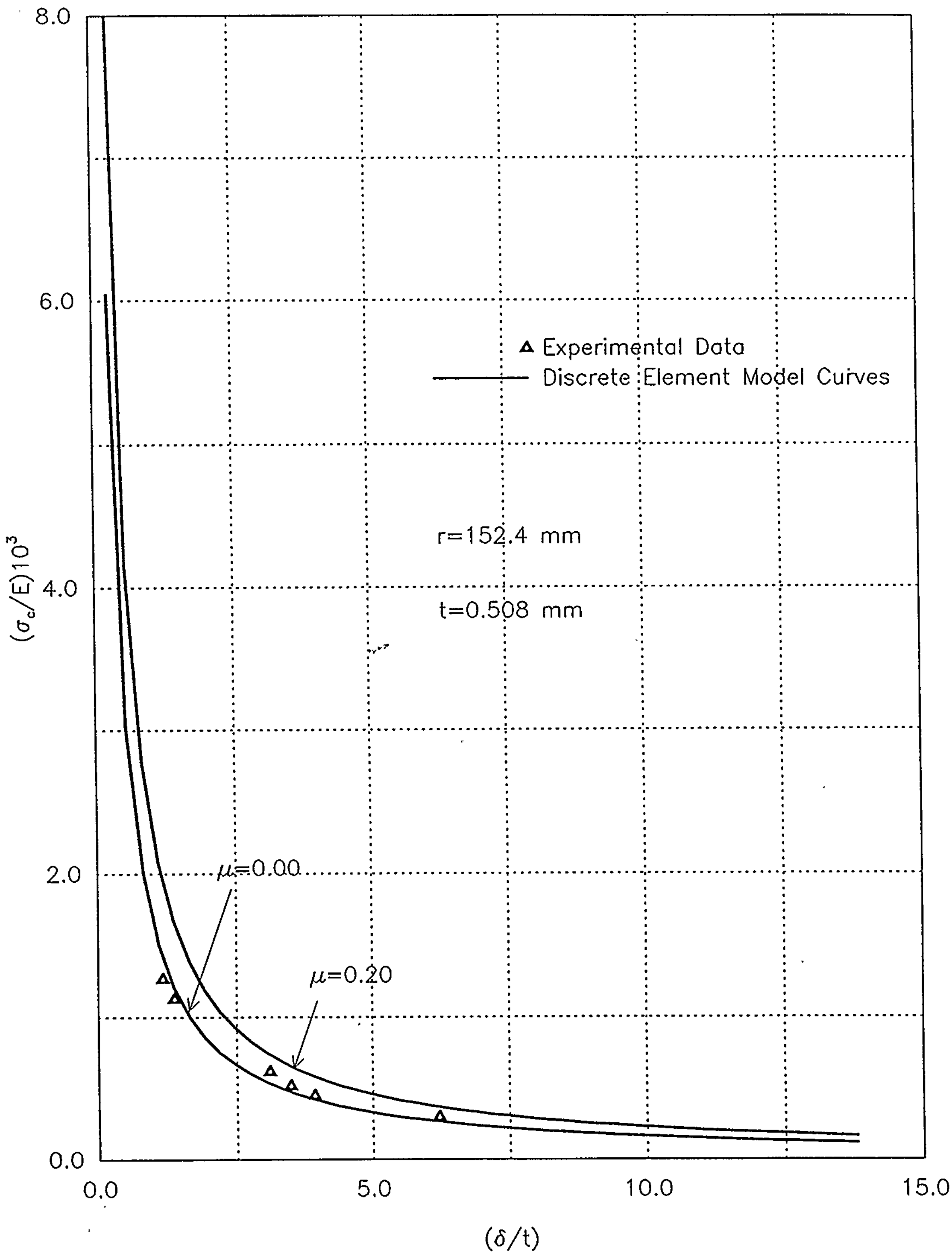

Figure 8.19 Comparison of Experimental Results with Discrete Element Model Results for Aluminium

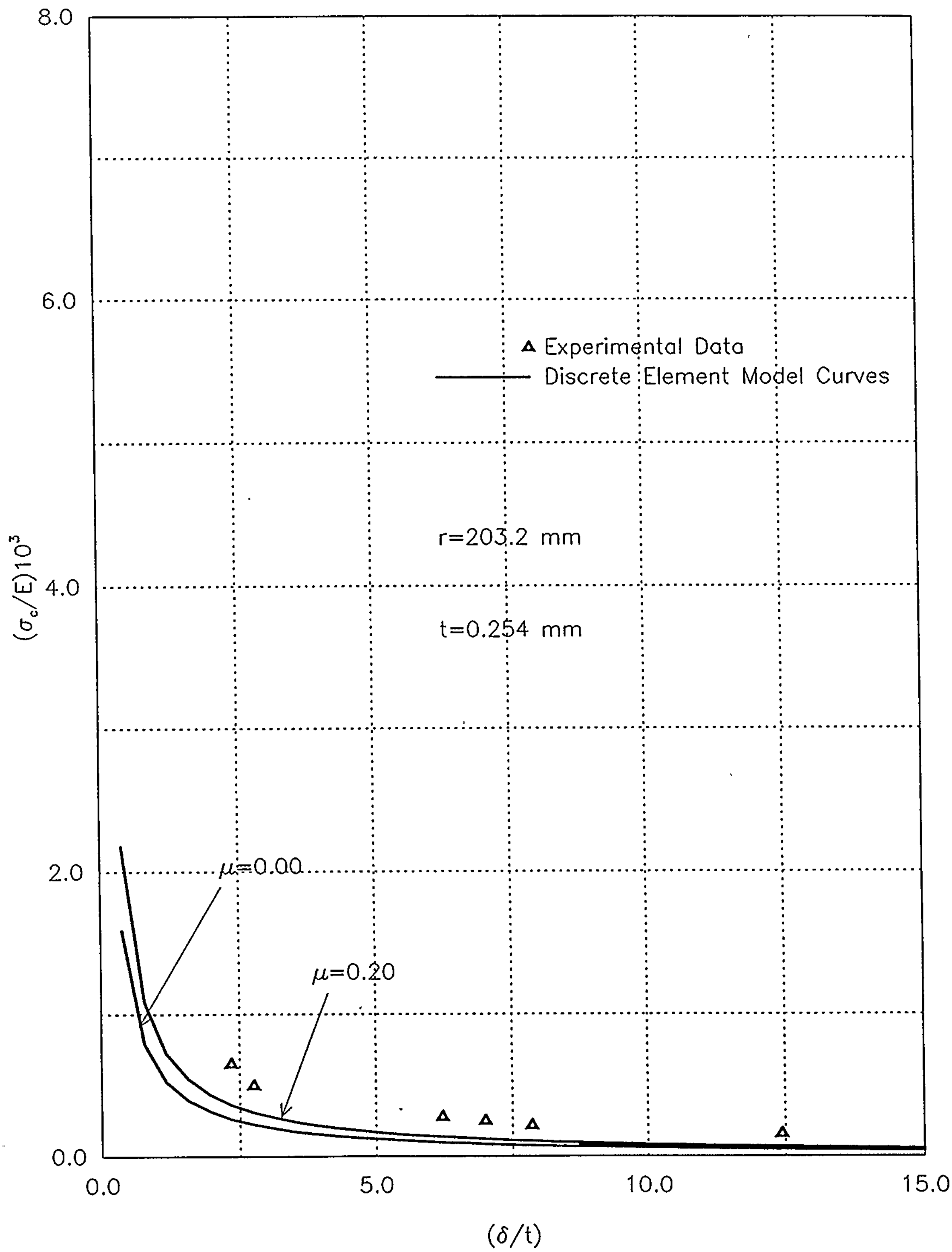

Figure 8.20 Comparison of Experimental Results with Discrete Element Model Results for Aluminium

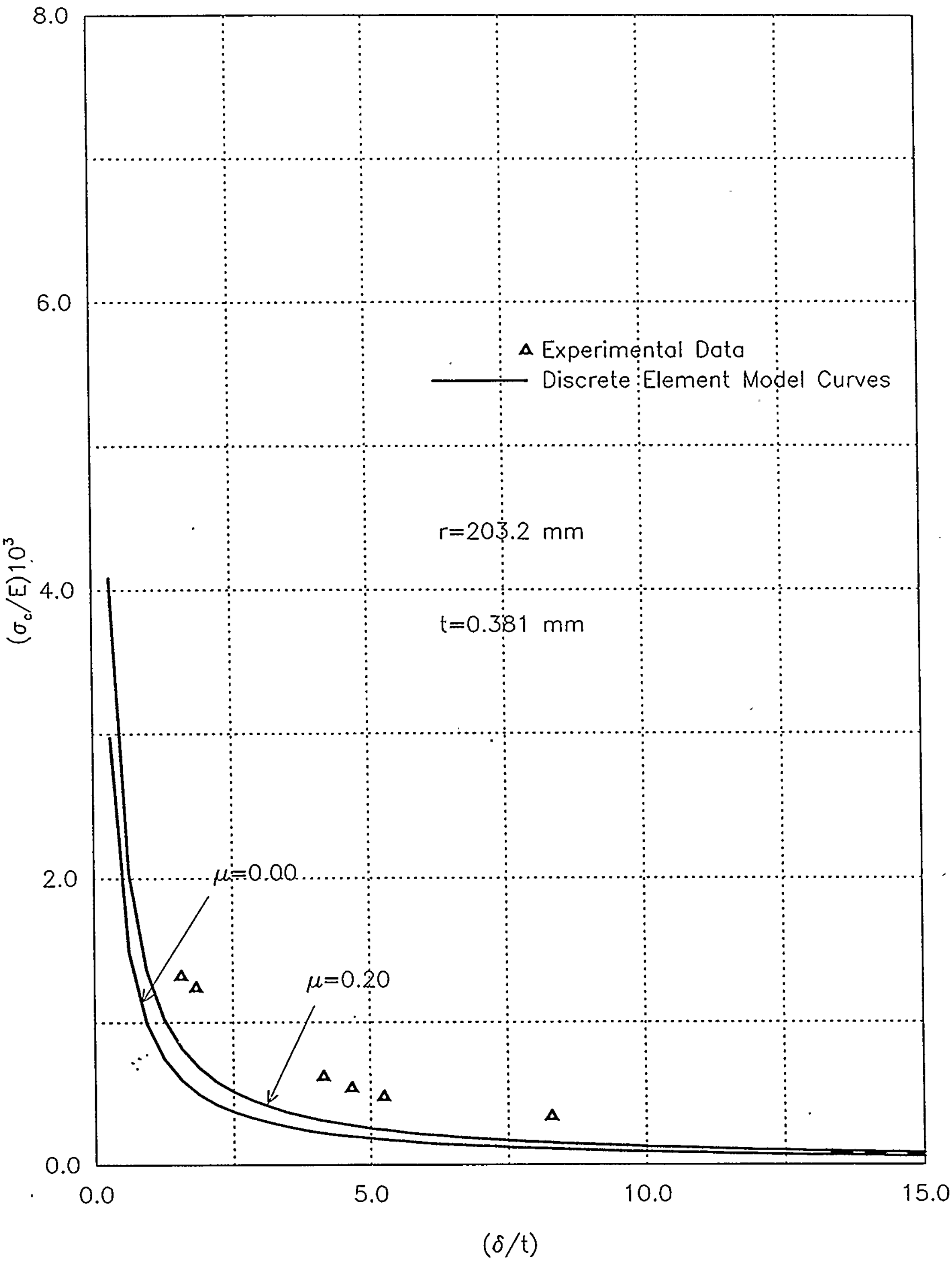

Figure 8.21 Comparison of Experimental Results with Discrete Element Model Results for Aluminium

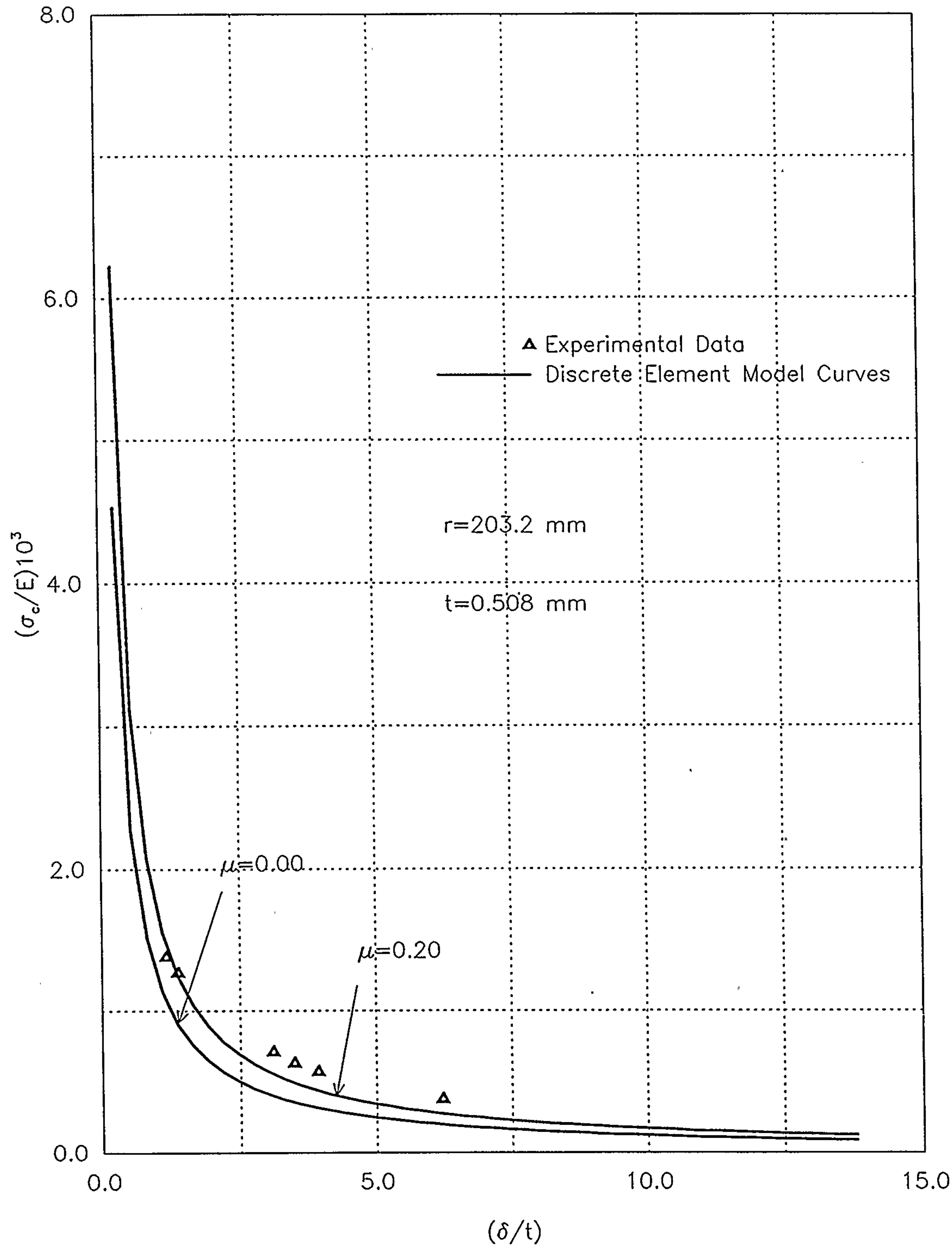

Figure 8.22 Comparison of Experimental Results with Discrete Element Model Results for Aluminium

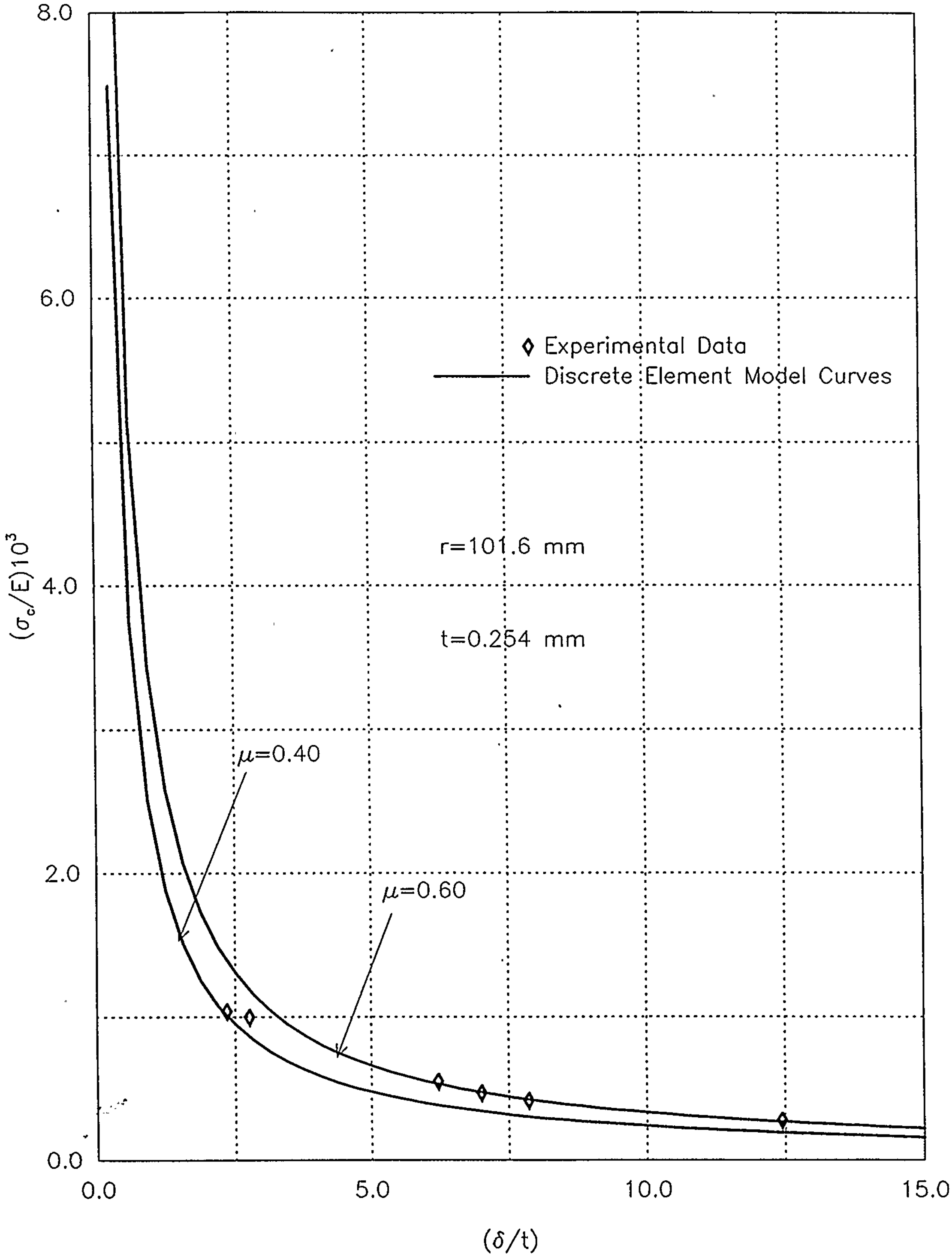

Figure 8.23 Comparison of Experimental Results with Discrete Element Model Results for Steel

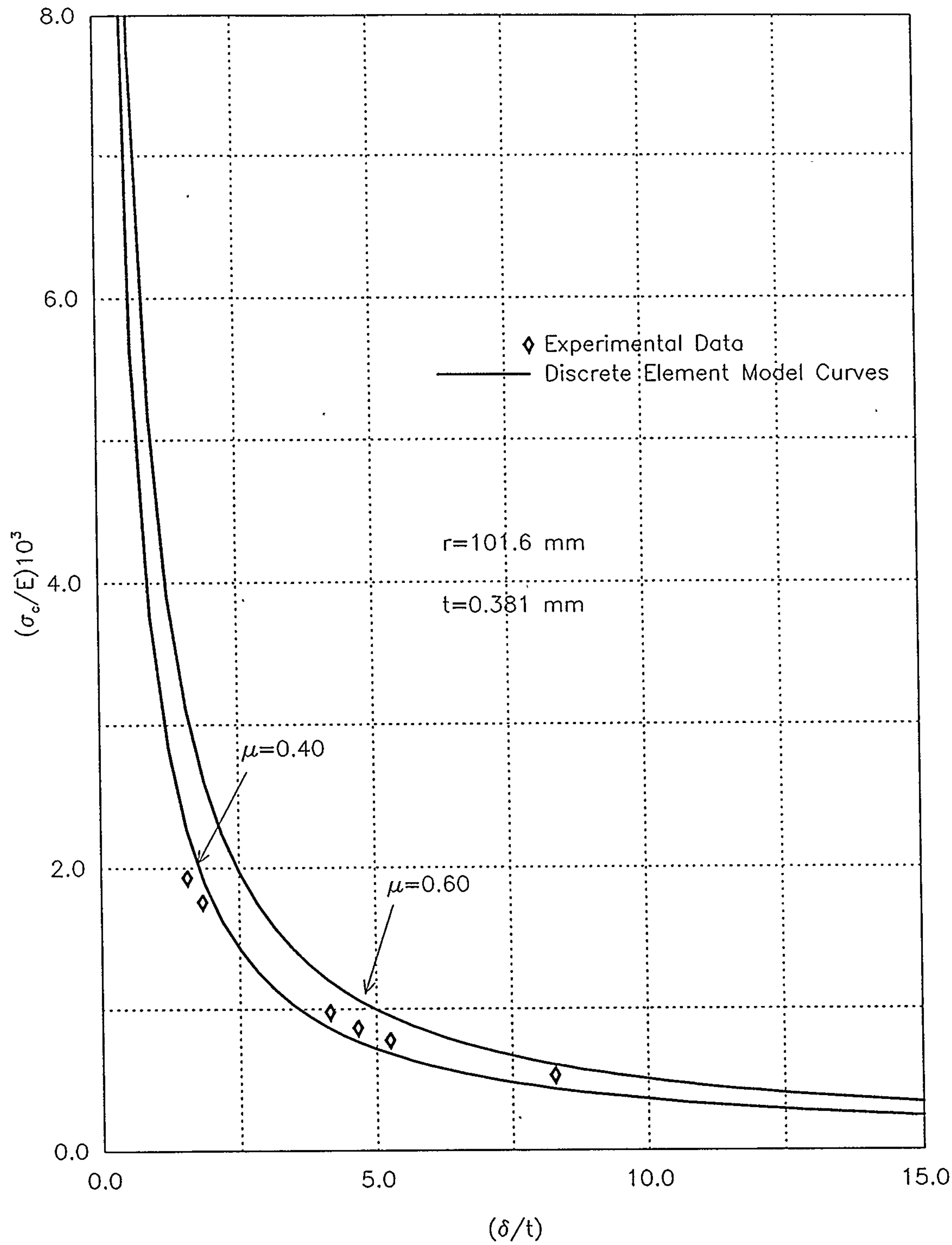

Figure 8.24 Comparison of Experimental Results with Discrete Element Model Results for Steel

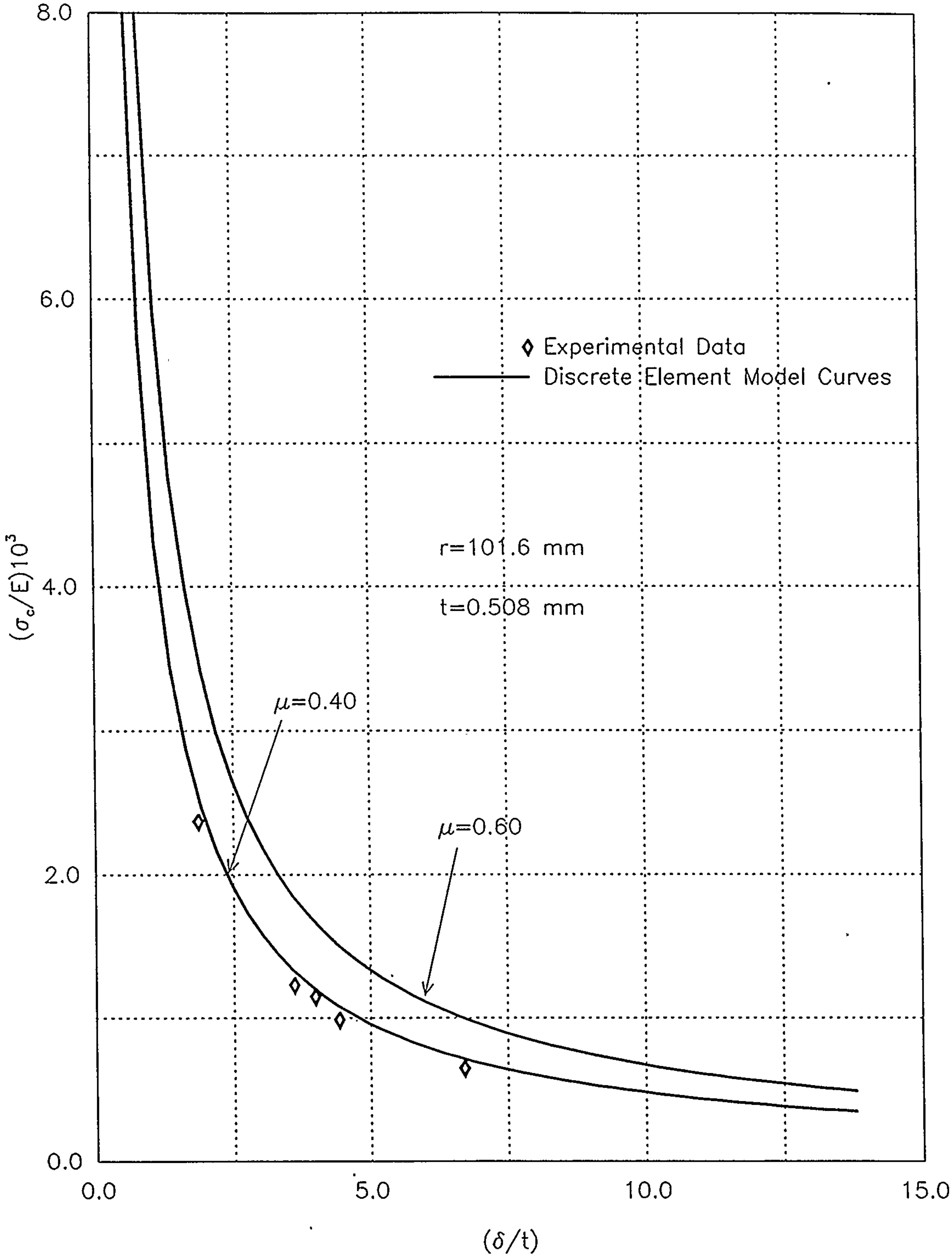

Figure 8.25 Comparison of Expermental Results with Discrete Element Model Results for Steel

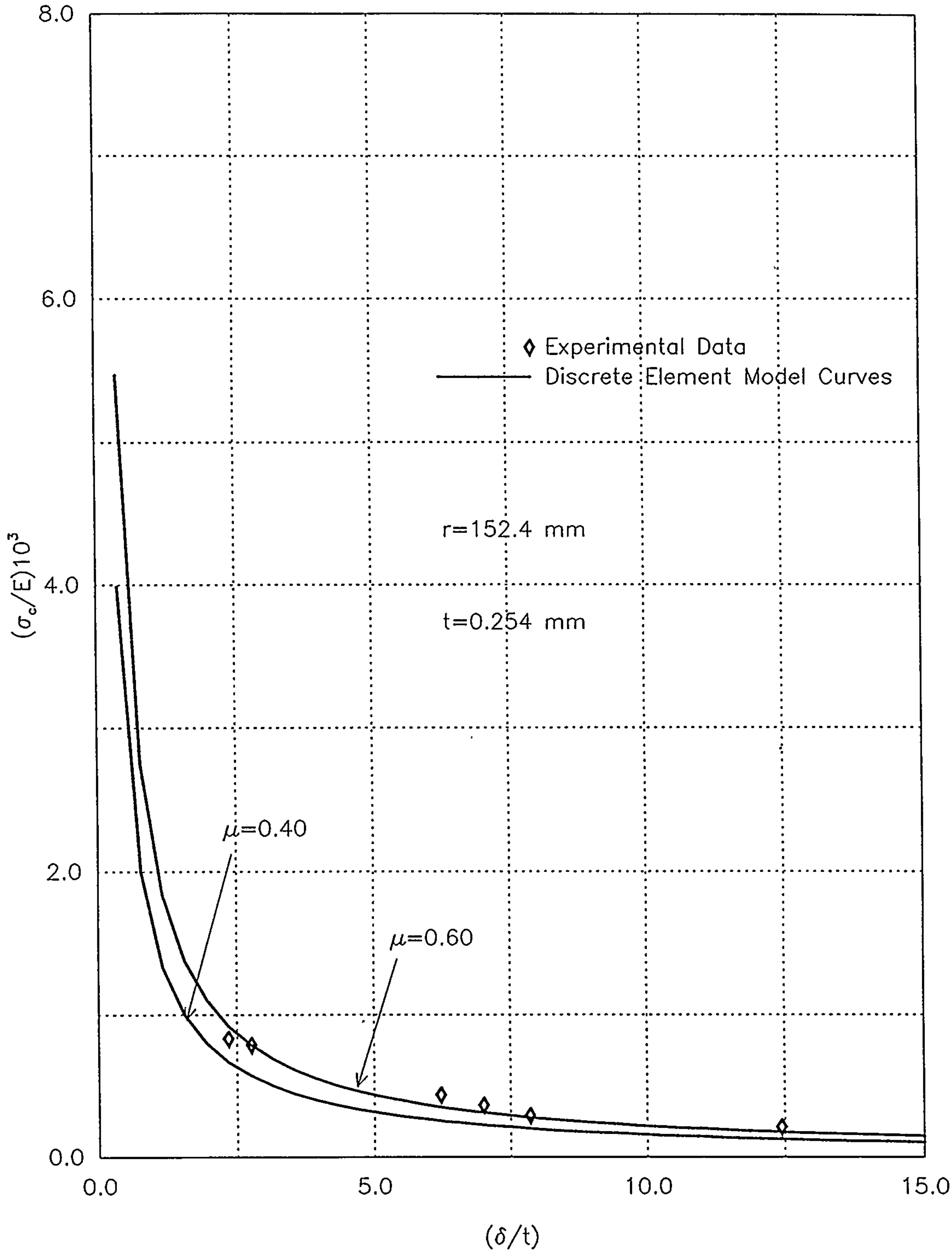

Figure 8.26 Comparison of Experimental Results with Discrete Element Model Results for Steel

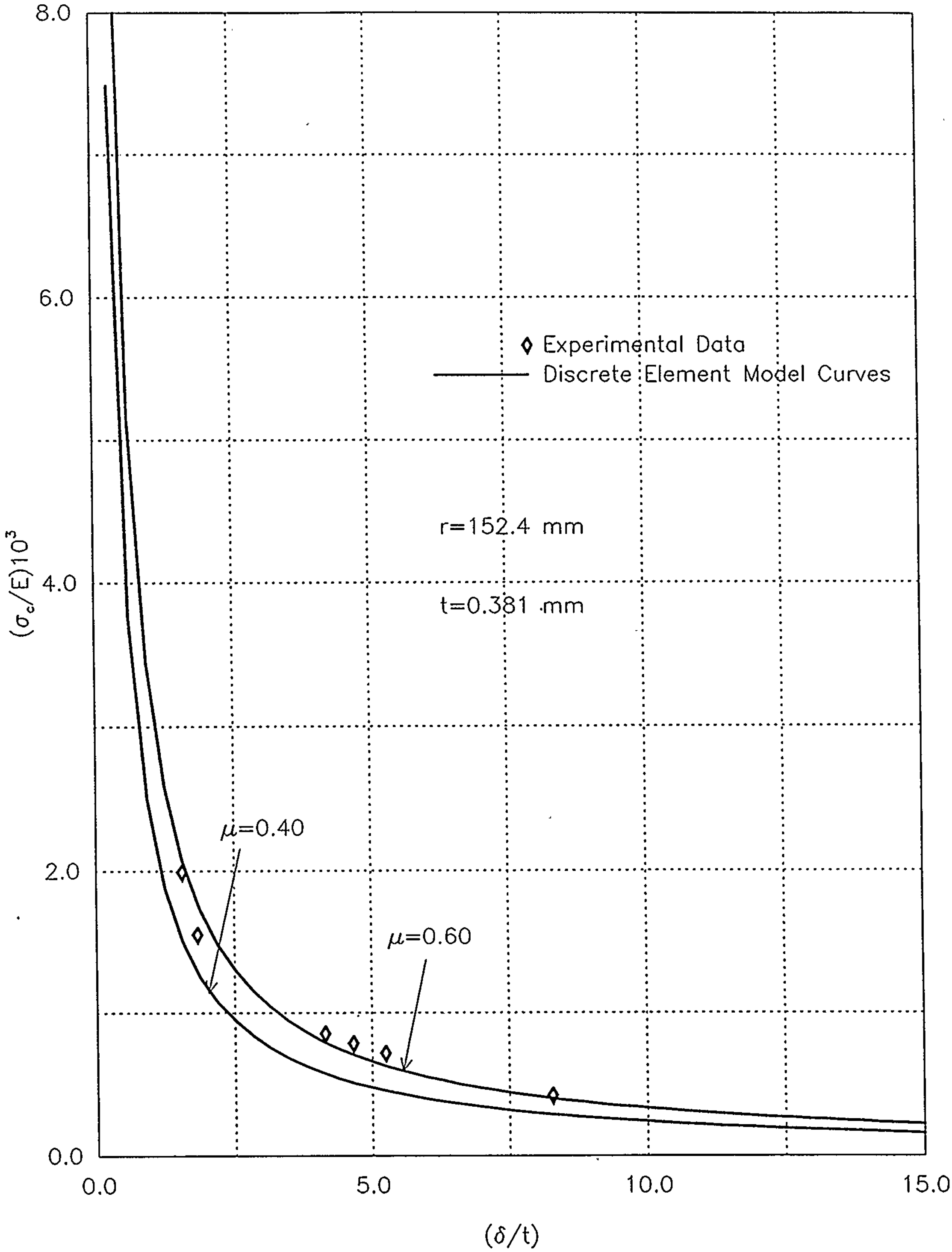

Figure 8.27 Comparison of Experimental Results with Discrete Element Model Results for Steel

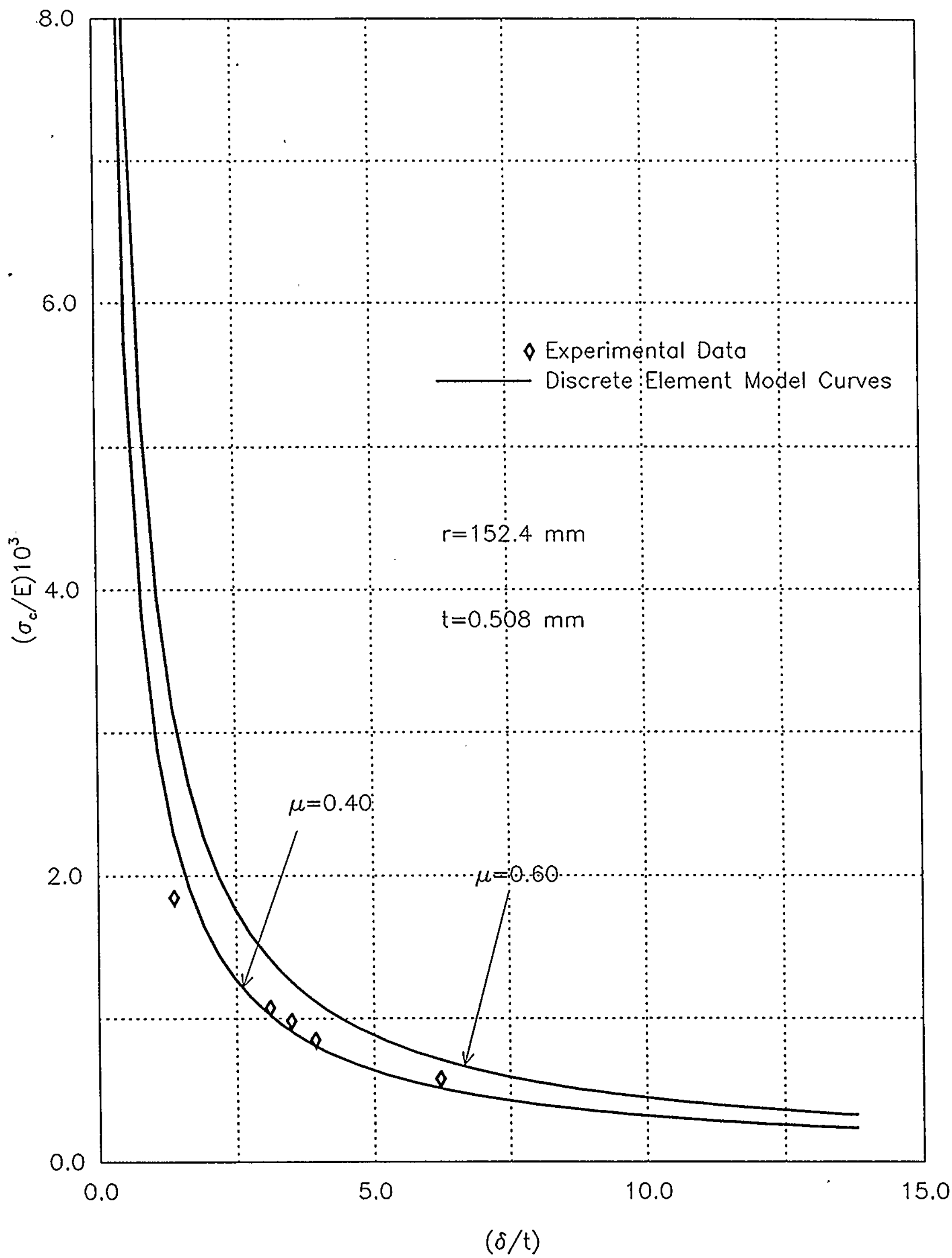

Figure 8.28 Comparison of Experimental Results with Discrete Element Model Results for Steel

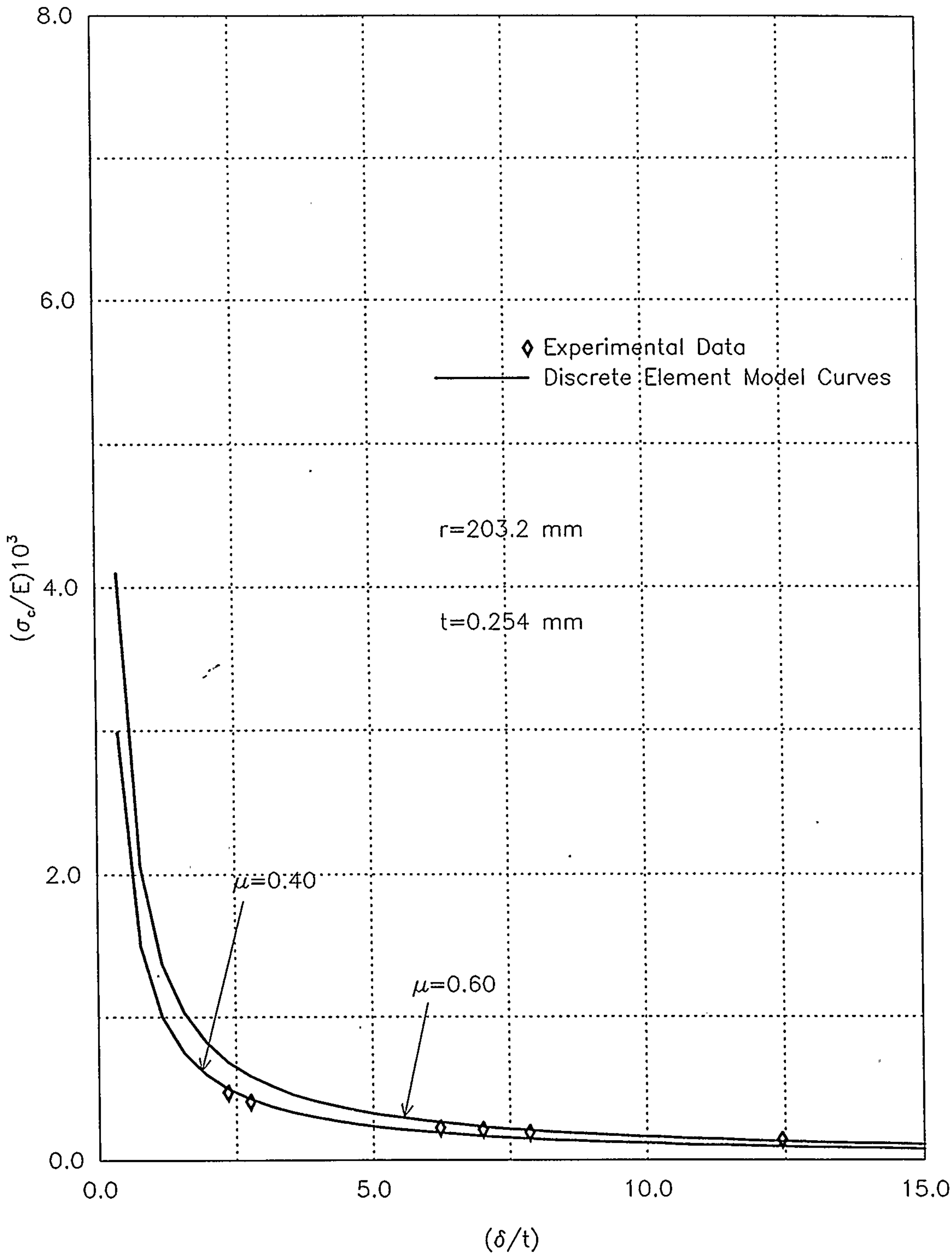

Figure 8.29 Comparison of Experimental Results with Discrete Element Model Results for Steel

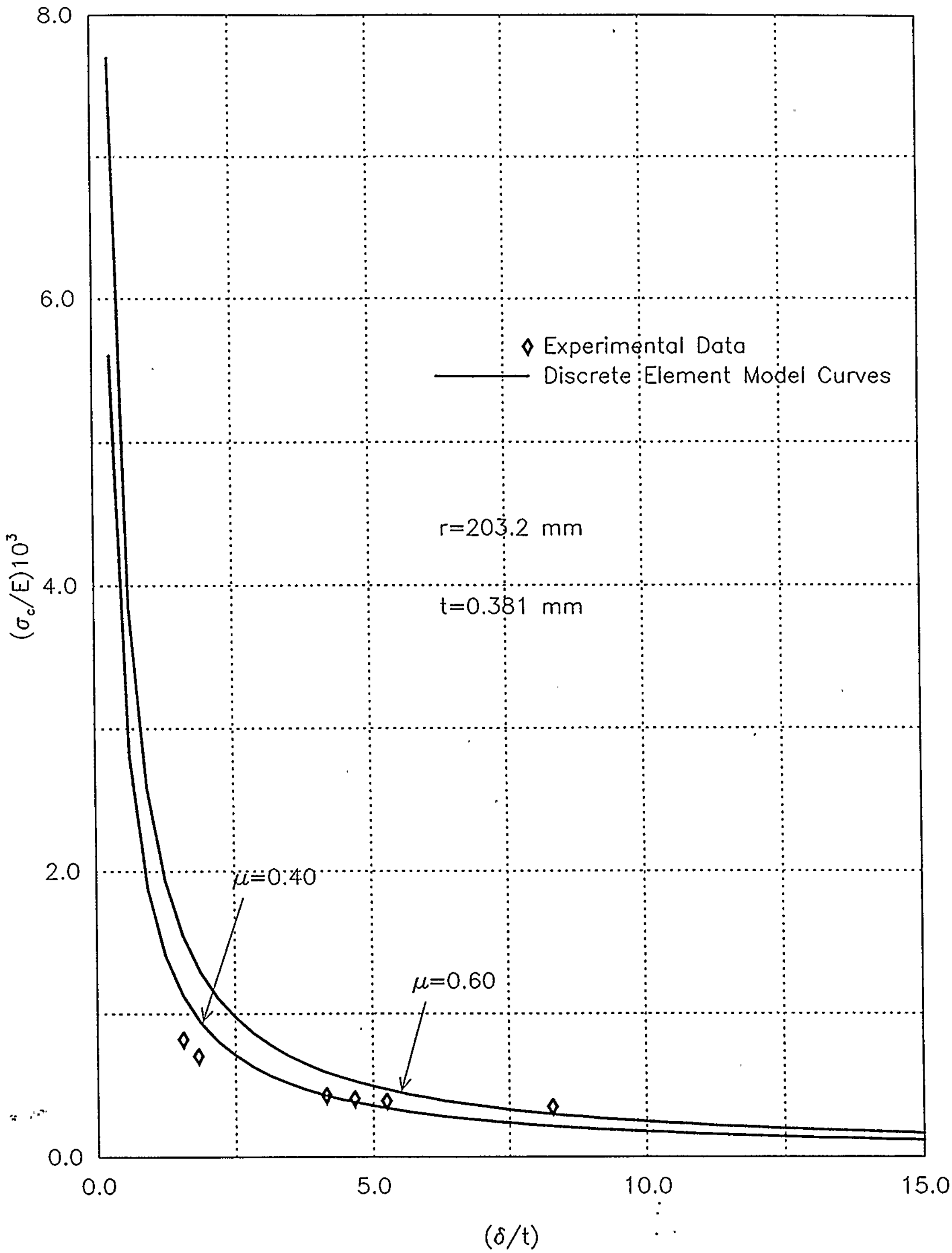

Figure 8.30 Comparison of Experimental Results with Discrete Element Model Results for Steel

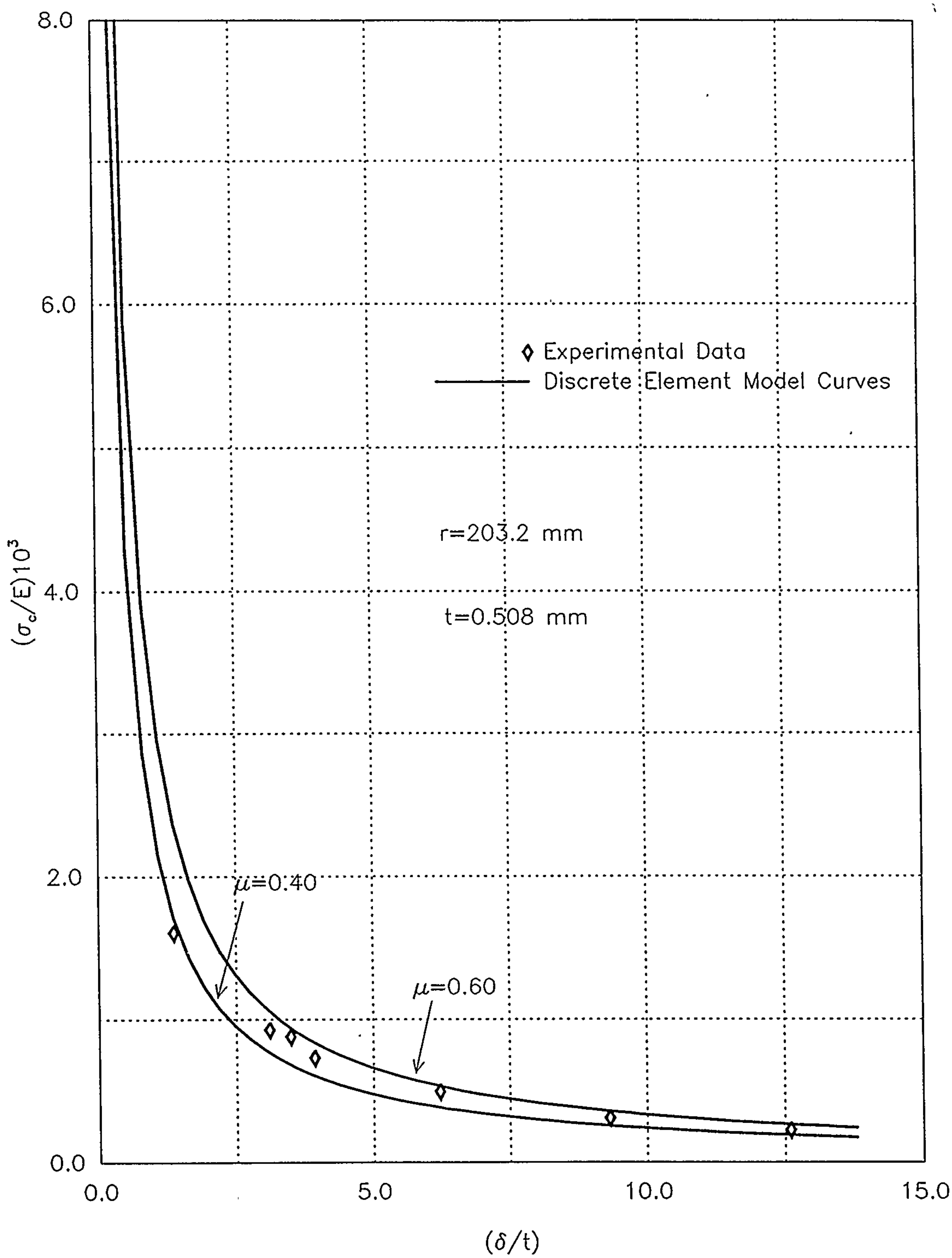

Figure 8.31 Comparison of Experimental Results with Discrete Element Model Results for Steel

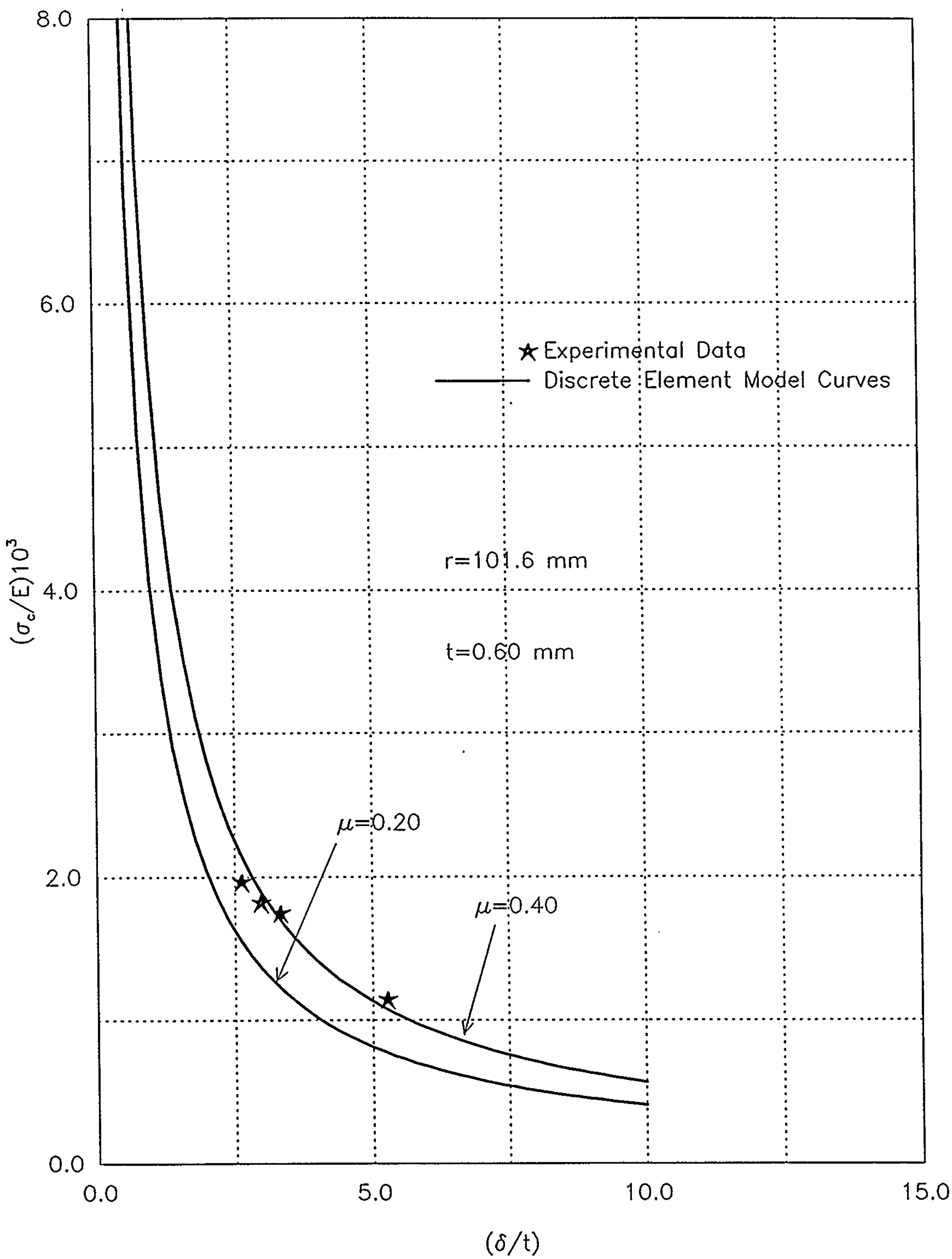

Figure 8.32 Comparison of Experimental Results with Discrete Element Model Results for Cardboard

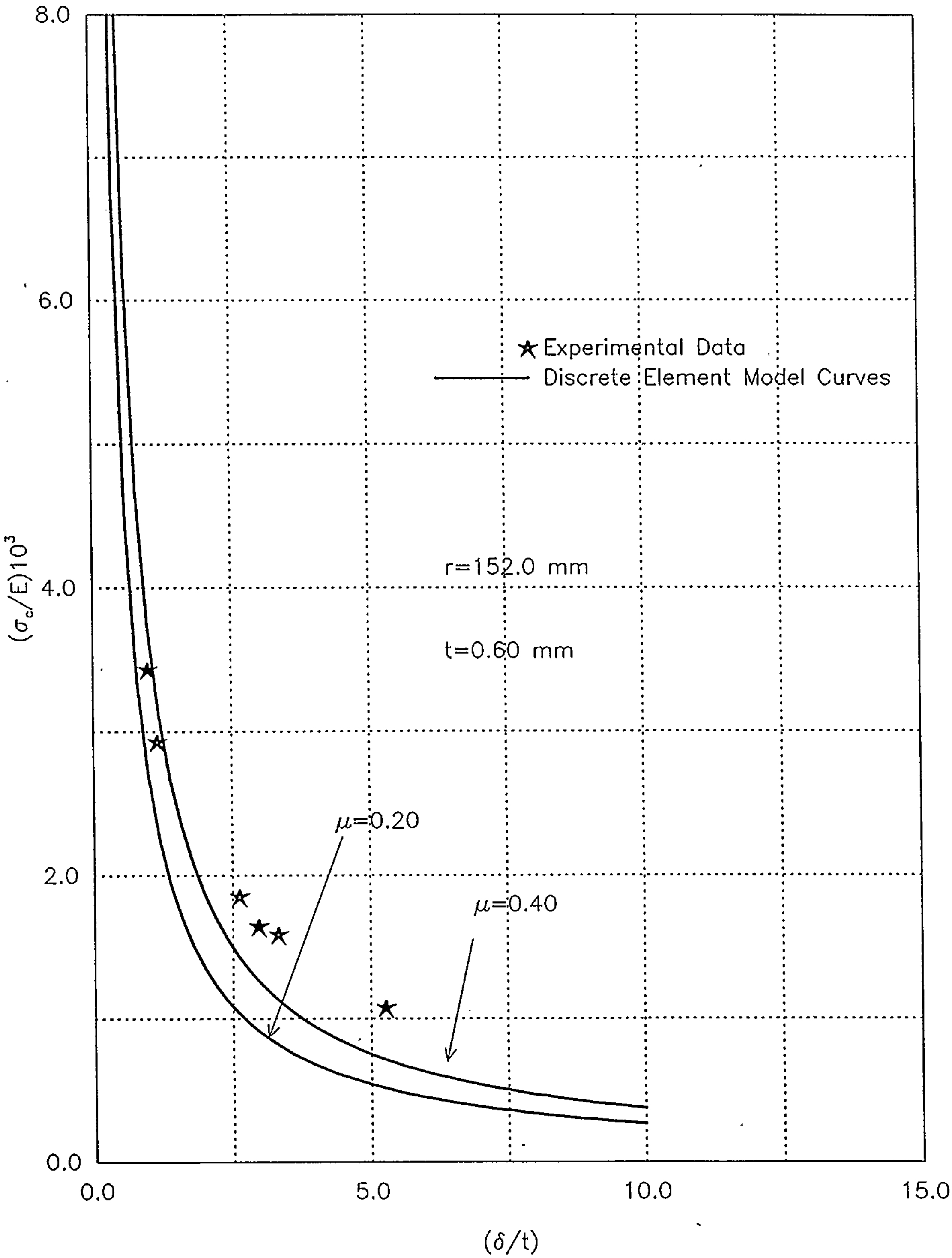

Figure 8.33 Comparison of Experimental Results with Discrete Element Model Results for Cardboard

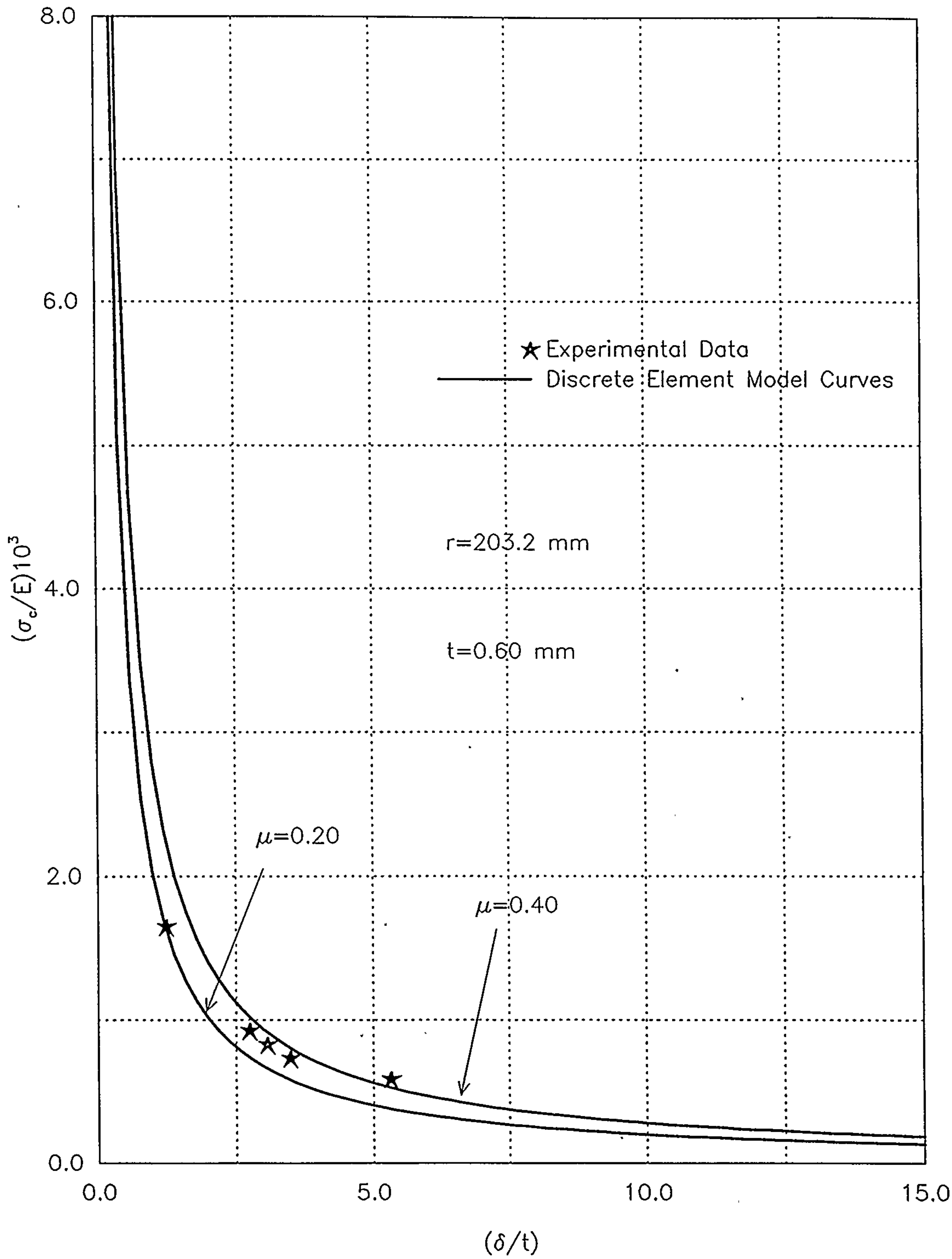

Figure 8.34 Comparison of Experimental Results with Discrete Element Model Results for Cardboard

8.6 Comparison of Results for Different Lubricants

The friction resistance is one of the major factors which influences the critical buckling stress. The friction coefficient is dependent on the materials. From preceding discussions it can be seen that for different materials, the friction coefficients are different. The friction coefficient is also dependent on the lubrication condition at the interface.

Figure 8.35 is a comparison of different lubrication conditions for the same plastic material. In the first case, no lubricant was used. In the second case, a light viscosity oil (Three-in-One Oil) was used at the interface. In the third case, a dry lubricant, Molybdenum (IV) sulphide was used. Comparing these three cases, it is surprising to find that the oil lubricant case appears to have the largest friction resistance instead of no lubricant case. The explanation is that the oil surface tension prevents the specimen from lifting off the rigid boundary. For the dry lubricant, there is no liquid surface tension. Therefore the smallest friction resistance case is the dry lubricant case.

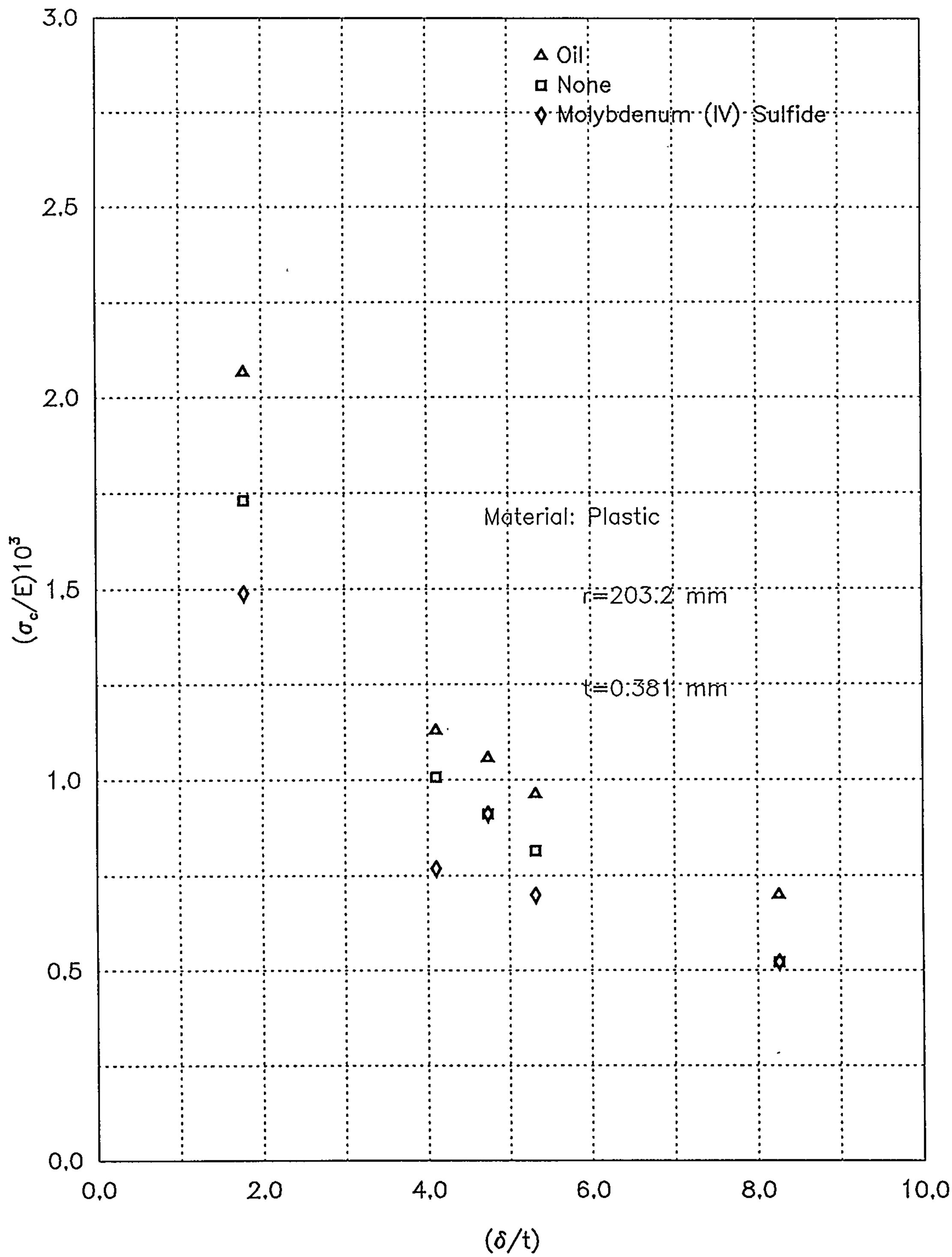

Figure 8.35 Comparison of Three Different Lubricants

8.7 Summary

From the experimental results and discussions, we find that the experimental data are in good agreement with the discrete element model results for plastic materials. For other materials the experimental data are in good agreement with the discrete element model results in the large imperfection region when accounting for friction but are not in agreement with the discrete element model results in small imperfection region. Local plastic deformation is the main factor which causes these discrepancies between the experimental data and the theoretical results. Friction coefficient has a strong effect on the critical buckling stress. But the friction resistance will only affect the coefficient of the buckling function. Local plastic deformation will affect both the coefficient and the exponents for the two dimensionless variables of the buckling function.

Chapter 9

FINITE ELEMENT ANALYSIS

9.1 Introduction

The finite element method is a powerful numerical analysis technique for obtaining approximate solutions to a wide variety of engineering problems. In this chapter, the finite element method is used to investigate the behaviour of a ring confined within a rigid boundary. First, a half ring model will be developed to simulate the discrete element models and the experimental model. ANSYS 4.4 was used to carry out the calculations. Then the results will be compared with the discrete element model results.

9.2 Model Description

The two dimensional beam element is used to establish the half ring model. As shown in Figure 9.1, from 0 to 10 degrees centre angle region the arc was divided into 1/4 degree per element. In this region the displacements and stresses change quickly because an initial deflection was caused by a point imperfection. From 10 to 20 degrees the arc was divided into 1 degree per element. Beyond 20 degrees the ring was divided into 10 degrees per element because in this region the changes of displacement and stress change are relatively small.

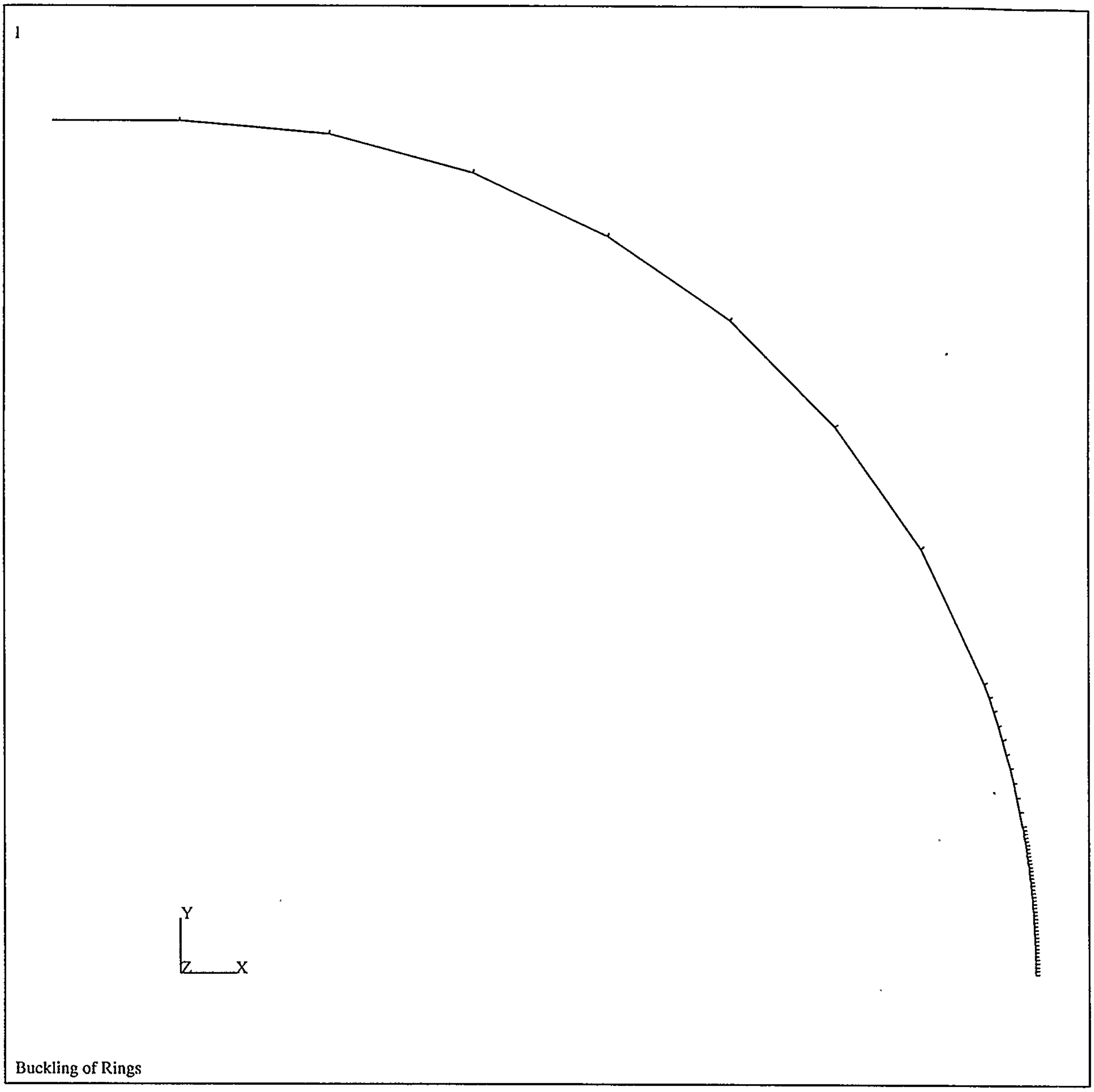

Figure 9.1 Half Ring Divided into Beam Elements

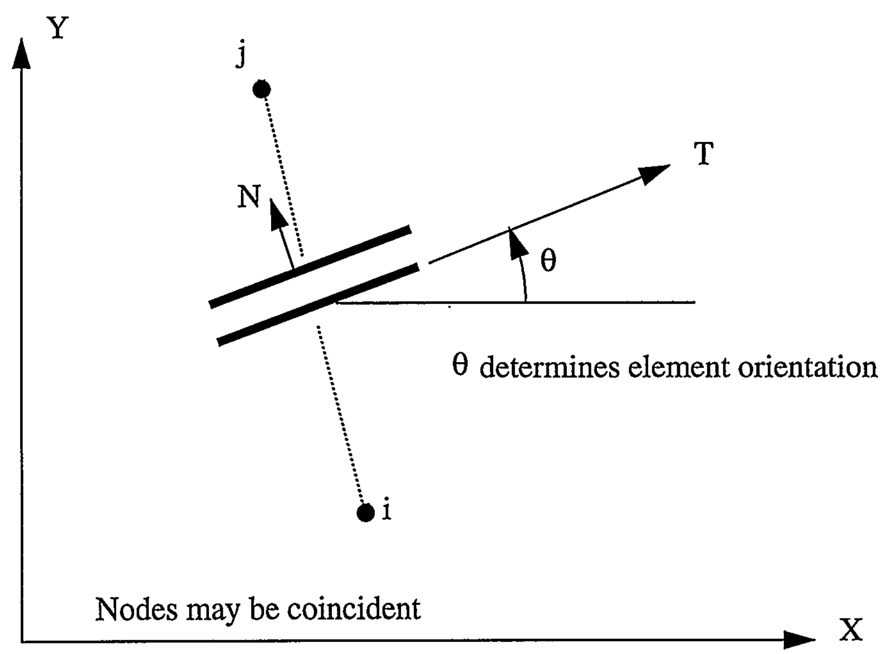

Figure 9.2 Two-Dimensional Interface Element

The interface between the ring and the rigid boundary was characterized by two-dimensional interface elements. The two-dimensional interface element represents two surfaces which may maintain or break physical contact and may slide relative to each other. The element is capable of supporting only compression in the direction normal to the surfaces and shear (Coulomb friction) in the tangential direction. The geometry, nodal point locations, and the coordinate system for the elements are shown in Figure 9.2. The element is defined by two nodal points, an angle to define the interface, a stiffness K, an initial displacement interference, and an initial element status. An element coordinate system (T-N) is defined on the interface. The orientation of the interface is defined by angle θ which is measured from the global X axis. The K value should be based upon the stiffness of the surfaces in contact. For this problem the local surface deformation is not important and K can be estimated as an order of magnitude of two greater than the adjacent element stiffness (AE/L). The stiffness K is associated with a zero or positive interference. For the negative interference which represents the gap size of interface, the stiffness K is zero. The only material property used is the interface coefficient of friction μ. A zero value represents frictionless surfaces.

The finite element model is shown in Figure 9.3 in which only a quarter of the assembly of a ring and a rigid boundary is presented because of the symmetry condition. The origin global coordinate system is located at the centre of the ring and the rigid boundary. A quarter of a ring was characterized by 59 elements having nodal points at the middle radius of the ring. The interface between the ring and the rigid boundary was characterized by 58 two-dimensional interface elements. ANSYS 4.4 preprocessing routine PREP7 [54, 55] was used to generate the model.

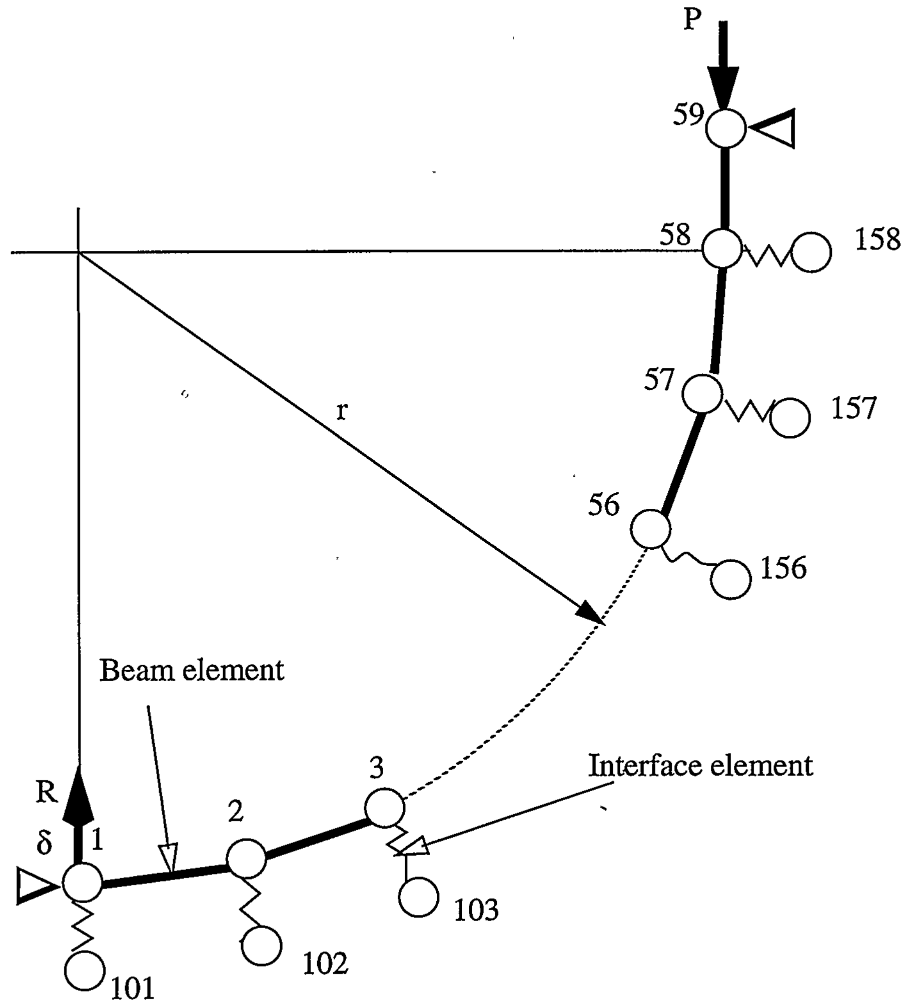

Figure 9.3 Half Ring Finite Element Model

The boundary conditions are that both the displacement in the tangential direction and the rotation at node 1 are zero. At node 59, both the displacement in the direction of the radius and the rotation are zero. All displacments for the interface element nodes at the boundary side are zero.

Two kinds of external conditions were applied. First at node 59 a vertical compression load P was applied. Then at node 1 a displacement δ in the radial direction was applied.

9.3 Calculation Steps

In the experimental process an initial deflection δ was given by inserting a wire with diameter δ in between the ring and the rigid support at the bottom. Then the critical end compression force P_{cr} can be obtained from the displacement-load diagram recorded in the experimental process. In the finite-element calculations the reverse was done. That is an end compression force P was applied first while the initial deflection is zero at the bottom of the ring. Then a small deflection δ_0 was introduced at the bottom of the ring, then the reaction force R at the bottom can be calculated. As shown in Figure 9.3, if the reaction force at the bottom is

$$R > 0$$

the ring is in a stable condition because a force is needed to push the ring in this position. If this force disappears, the ring will come back to the original position. After the initial deflection, the deflection will increase gradually until the reaction force R reaches zero.

$$R = 0$$

Then the deflection δ corresponding to the zero reaction force is the critical deflection δ_{cr} for the given end compression force P. That is if the inward displacement caused by the geometric imperfection, or the outside disturbance, or the combination of these two factors is smaller than δ_{cr}, the ring will not buckle but if the inward displacement is larger than δ_{cr}, the ring will buckle. When the initial deflection δ reaches beyond the value δ_{cr}, the reaction force R will change direction, i.e.

$$R < 0$$

Because this force at this stage is to hold the ring from jumping to the large deflection position, i.e. the buckled configuration.

The calculation steps can be summarized as follows:

Step 1 Apply load P at node 59.

Step 2 Apply inward displacement $\delta = \delta_0$ at node 1.

Step 3 Calculate the vertical reaction force R at node 1.

Step 4 If R=0, then δ_{cr}=δ, go to Step 6; else go to Step 5.

Step 5 If $R > 0$, $\delta = \delta + \Delta\delta$, go to Step 3; else $\delta = \delta - \Delta\delta$, go to Step 3.

Step 6 Stop.

Figure 9.4 is the calculation flow chart.

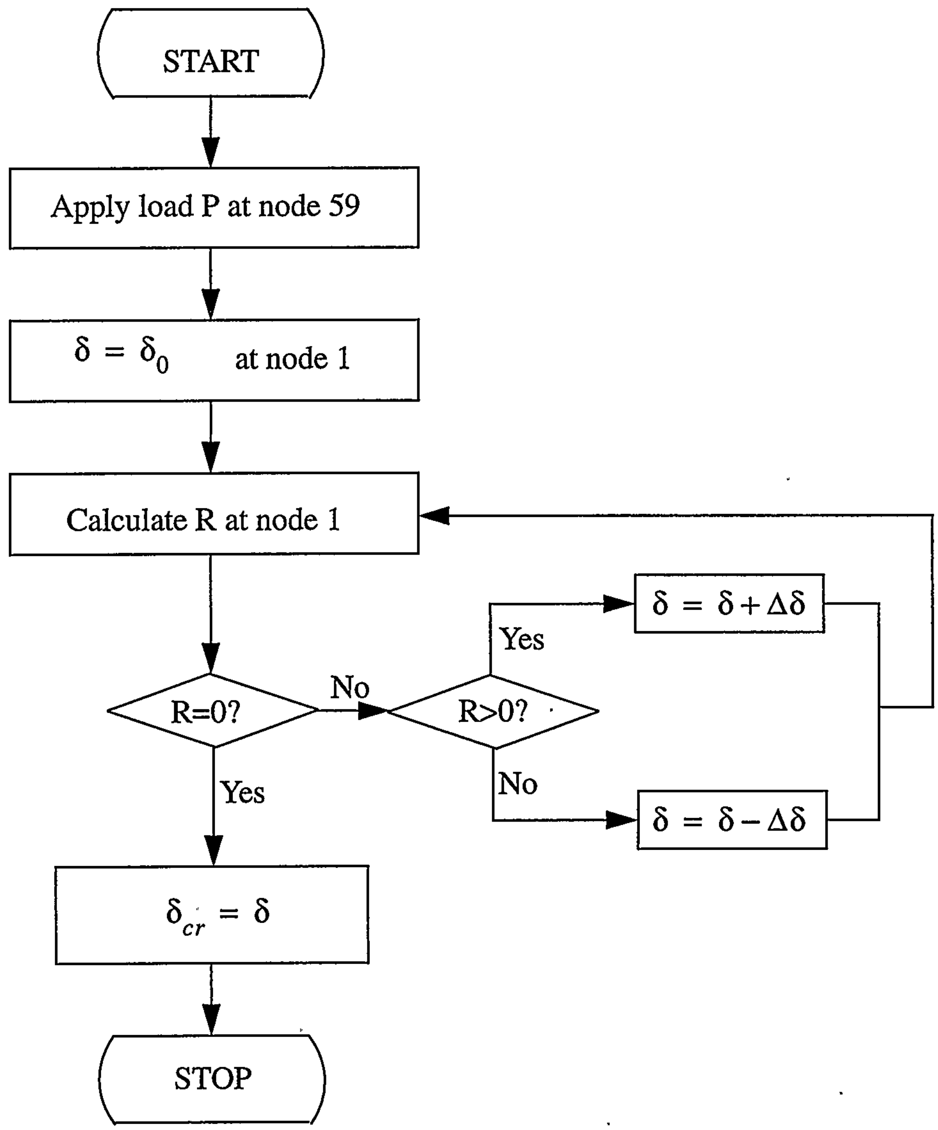

Figure 9.4 Calculation Flow Chart

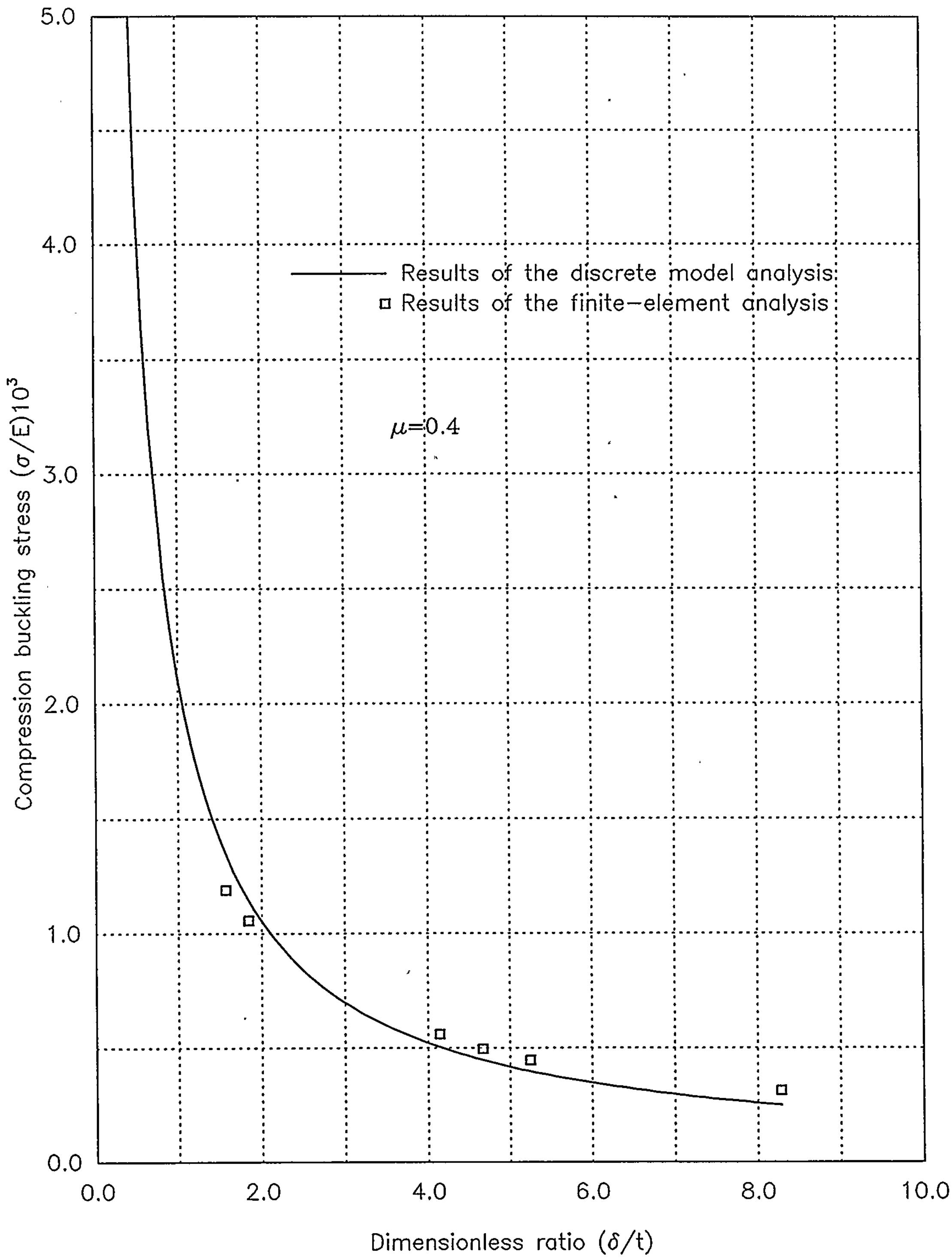

Figure 9.5 Comparison of Finite Element Results with Discrete Model Results

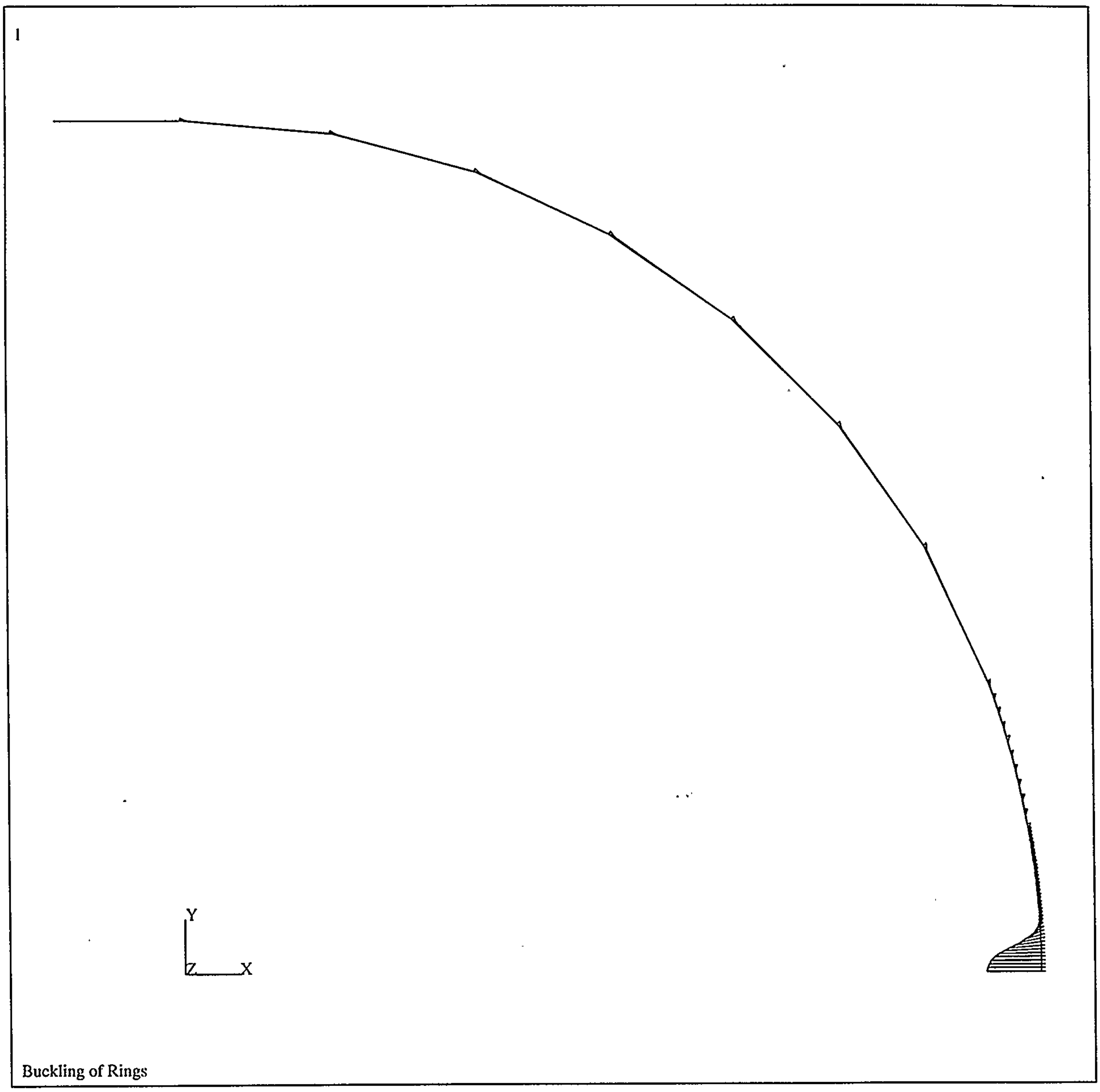

Figure 9.6 Buckled Configuration of the Ring

9.4 Results and Discussions

Figure 9.5 is the comparison of finite-element calculation results with the discrete element model described in Chapter 6 and Chapter 7. The friction coefficient, μ is 0.4 in Figure 9.5. It can be seen that the finite-element analysis results are in good agreement with the discrete element model analysis results. Figure 9.6 is the buckled configuration of the ring.

9.5 Summary

A half ring finite element model was developed by using the beam element and the interface element. ANSYS 4.4 was used to carry out the calculations. The results are in good agreement with the discrete element model results.

Chapter 10

CONCLUSIONS AND RECOMMENDATIONS

10.1 Introduction

From all theoretical analysis, experimental investigation and finite element calculation results presented from Chapter 1-Chapter 9, the buckling behaviour of a ring confined within a rigid boundary and the major factors which influence the critical buckling conditions were quite clear. In this chapter, the major results will be briefly summarized and conclusions and recommendations will be made. Finally, future work will be suggested.

10.2 Dimensional Analysis

A relationship of the critical buckling compression stress of a ring confined within a rigid boundary with the elastic modulus of the material, geometry and imperfections or external disturbances was developed by using the dimensional analysis method.

The critical buckling compression stress is proportional to the elastic modulus of materials. The buckling function $f\left[\left(\frac{r}{t}\right), \left(\frac{\delta}{t}\right)\right]$, only depends on two dimensionless variables $\left(\frac{r}{t}\right)$ and $\left(\frac{\delta}{t}\right)$. Thus the buckling function is determined by the geometry and the imperfections or the external disturbances.

The buckling function has one undetermined coefficient C and two undetermined exponents b and d. These undetermined coefficient and exponents can be determined from experimental results.

10.3 Discrete Element Model Analysis

The discrete element model can accurately describe the behaviour of the buckling of the ring confined in a rigid boundary and is a simple and good model for theoretical analysis. In addition the results from the dimensional analysis method and the discrete element method have the same pattern which demonstrates that these two methods are powerful tools for the structure stability analysis and helps to substantiate the methods.

The frictionless model results are on the safe side for a prediction of the critical buckling condition and are very conservative. The friction model results are closer to the real situation and are suitable for design purposes. The discrete element model is accurate for small α, and with α increasing, the error will increase.

Friction plays an important role in the buckling behaviour of a thin elastic ring confined in a rigid boundary. Friction resistance force at the interface has a positive effect on the critical buckling compression stress of the ring. The larger the friction resistance force, the larger the critical compression stress. The discrete element model when considering friction is closer to practice situation than the frictionless model. The frictionless model is just a special case of the friction model.

10.4 Experimental Results

From the experimental results, we find that the two exponents for dimensionless variables $(\frac{r}{t})$ and $(\frac{\delta}{t})$ are approximately -1 for total elastic materials, as displayed by the behaviour of the plastic materials. The experimental data are in good agreement with the discrete element model results for plastic materials. For other materials the experimental data are in good agreement with the discrete element model results in the large imperfection region when accounting for friction but are not in agreement with the discrete element model results in small imperfection region. Local plastic deformation is the main factor which causes these discrepancies between the experimental data and the discrete element model results. The friction coefficient has a strong effect on the critical buckling stress. But the friction resistance will only affect the coefficient of the buckling function. Local plastic deformation will affect both the coefficient and the exponents for the two dimensionless variables of the buckling function.

10.5 Finite Element Analysis

A half ring finite element model was developed by using the beam element and the interface element. ANSYS 4.4 was used to carry out the calculations. The results are in good agreement with the discrete element model results.

10.6 Conclusions

From the above brief summary, we conclude:

(1) It is confirmed that the critical buckling load is proportional to the elastic modulus of materials.

(2) It is also confirmed that the initial deflection δ, which may be caused by geomet-

ric imperfection of the boundary, or external disturbance, or combination of geometric imperfection and external disturbance, makes the ring buckle. When δ=0, there is no critical load in the elastic region.

(3) Friction at the interface has a positive effect on the critical load. The larger the friction is, the larger the critical load. The larger the friction is, the more difficult for the ring to slide along the boundary.

(4) Local plastic deformation which occurs in the lift out region of the ring has a negative effect on the critical buckling load. The larger the local plastic deformation is, the lower the critical buckling load becomes.

(5) In the elastic region, the critical load is proportional to the two dimensional variables $(\frac{t}{r})$ and $(\frac{t}{\delta})$.

10.7 Recommendations

From above conclusions, we have following recommendations:

(1) From the geometry view point, increasing the thickness, *t,* of the ring, reducing the radius, *r*, of the boundary can make the ring more stable.

(2) From the material view point, choosing high elastic modulus and high yield strength materials can improve the stability of the ring.

(3) From the boundary condition view point, increasing friction at the interface can increase the critical load.

(4) Last but the most important point, reducing geometric imperfections of the boundary and external disturbances in the manufacture and assembly process can prevent the ring from buckling.

10.8 Future Work

Local plastic deformation plays the important role in determine the critical buckling conditions for a ring confined within a rigid boundary. So far in the study, no quantitative relationship of plastic deformation and the critical buckling load has been derived. Further study should focus on this aspect.

REFERENCES

[1] Donnell, L.H. (1952). "Recent Developments in the Study of Buckling Problems," Applied Mechanics Reviews, Vol. 5, pp. 289-290.

[2] Langhaar, H.L. (1958). "General Theory of Buckling," Applied Mechanics Reviews, Vol. 11, pp. 585-588.

[3] Herrmann, G. (1967). "Stability of Equilibrium of Elastic Systems Subjected to Nonconservative forces," Applied Mechanics Reviews, Vol. 20, pp. 103-108.

[4] Lo, H., Bogdanoff,J.L., Golgberg, J.E., and Crawford,R.F.(1962). "A Buckling Problem of a Circular Ring," Proceedings of the Fourth U.S. National Congress of Applied Mechanics, ASME, pp. 691-695.

[5] Hsu,P.T., Elkon, J., and Pian,T.H.H.(1964). "Note on the Instability of Circular Rings Confined to a Rigid Boundary," Trans. ASME, Journal of Applied Mechanics, Vol. 31, No. 3, pp. 559-562.

[6] Chan, H.C.,and McMinn, S.J.(1966). "The Stability of Uniformly Compressed Ring Surrounded by a Rigid Circular Surface," International Journal of Mechanical Science, Pergamon Press Ltd., Great Britain Vol. 8, pp. 433-442.

[7] Chan, H.C.,and McMinn, S.J.(1966). "The Stability of the Steel Liner of a Pre-stressed Concrete Pressure Vessel," Nuclear Engineering and Design, Vol. 3, pp. 66-73.

[8] Bucciarelli, L.L., Jr.,and Pian,T.H.H.(1967). "Effect of Initial

Imperfections on the Instability of a Ring Confined in an Imperfect Rigid Boundary," Trans. ASME, Journal of Applied Mechanics, Vol. 34, No.4, pp. 979-984.

[9] Pian, T.H.H., and Bucciarelli,L.L., Jr.(1967). "Buckling of Radially Constrained Circular Ring Under Distributed Loading," Int. J. Solids Structures, Vol.3, pp. 715-730.

[10] Zagustin, E.A., and Herrmann, G.(1967). "Stability of an Elastic Ring in a Rigid Cavity," Trans. ASME, Journal of Applied Mechanics, pp. 263-270.

[11] Zagustin, E.A., and Herrmann, G.(1968). "Stability of an Elastic Arch in a Rigid Cavity," Experimental Mechanics, pp. 572-576.

[12] El-Bayoumy, L.(1972). "Buckling of a Circular Elastic Ring Confined to a Uniformly Contracting Circular Boundary," Trans. ASME, Journal of Applied Mechanics, Vol. 39, No. 3, pp. 758-766.

[13] Liszka, T. and Trojnacki, A. (1978). "The Stability of an Assembly of Two Interference-Fitting Thin Elastic Rings," Archiwum Budowy Maszyn, Zeszyt 3, pp. 535-548.

[14] Chicurel, R. (1968). "Shrink Buckling of Thin Circular Rings," Trans. ASME, Journal of Applied Mechanics, Vol. 35, Sept. 1968, pp. 608-610.

[15] Burgess, I.W. (1971). "On the Equilibrium and Stability of Discrete One-Way Structural Systems," Int. J. Solids Structures, Vol. 7, 667-683.

[16] Burgess, I.W. (1971). "The Buckling of a Radially Constrained Imperfect Circular Ring," Int. J. Mech. Sci., Pergamon Press, Vol. 13, pp. 741-753.

[17] Soong, T.C. and Choi, I. (1985). "Buckling of an Elastic Elliptical Ring

Inside a Rigid Boundary," Trans. ASME, Journal of Applied Mechanics, pp. 1-6

[18] Bottega, W.J. (1989). "On the Behavior of Elastic Ring Within a Contracting Cavity," Int. J. Mech. Sci., Vol.31, No.5, pp. 349-357

[19] Yamamoto, Y. and Matsubara, N. (1982). "Buckling of a Cylindrical Shell under External Pressure Restrained by an Outer Rigid Wall," Collapse and Buckling, Structural Theory and Practice, Symposium, London, Published by Cambridge University Press, Cambridge, 1983

[20] Pal'chevskii, A.S. "Stability of a Multilayer Cylindrical Shell in Interlayer Pressure," Translated from Prikladnaya Mekhanika, Vol. 24, No. 4, pp. 358-362

[21] Kyriakides, S. and Bobcock, C.D.(1980). "On the "Slip-On" Buckle Arrestor for Offshore Pipelines," Trans. ASME, Journal of Pressure Vessel Technology, Vol. 102, pp. 188-193

[22] Kyriakides, S. and Babcock, C.D.(1981). "Large Deflection Collapse Analysis of an Inelastic Inextensional Ring under External Pressure," Int. J. Solids Structures, Vol. 17, No. 10, pp. 981-993.

[23] Kyriakides, S. and Arikan, E.(1983). "Postbuckling Behavior of Inelastic Inextensional Rings Under External Pressure," Trans. ASME, Journal of Applied Mechanics, Vol. 50, pp. 537-543.

[24] Kyriakides,S. and Youn, S.-K. (1984). "On the Collapse of Circular Confined Rings Under External Pressure," Int. J. Solids Structures, Vol. 20, No. 7, pp. 669-713.

[25] Kyriakides, S., Yeh, M.-K. and Roach, D. (1984). "On the Determination of

the Propagation Pressure of Long Circular Tubes," Trans. ASME, Journal of Pressure Vessel Technology, Vol. 106, pp. 150-159.

[26] Kyriakides, S. (1986). "Propagating Buckles in Long Confined Cylindrical Shells," Int. J. Solids Structures, Vol. 22, No. 22, pp. 1579-1597.

[27] Li, F.-S. and Kyriakides, S.(1991). "On the Pressure and Stability of Two Concentric Contacting Rings Under External Pressure," Int. J. Solids Structures, Vol. 27, No. 1, pp. 1-14.

[28] Cheney, J. A. (1971). "Pressure Buckling of Ring Encased in Cavity," Journal of the Engineering Mechanics Division, Proceedings of the ASCE, pp. 333-343

[29] Cheney, J. A. (1971). "Buckling of Soil-Surrounded Tubes," Journal of the Engineering Mechanics Division, Proceedings of ASCE.

[30] Cheney, J. A. (1976). "Buckling of Thin-Walled Cylindrical Shells in Soil," TRRL Supplementary Report 204, Transport and Road Research Laboratory, Department of the Environment.

[31] Cheney, J. A. (1991). "Local Buckling of Tubes in Elastic Continuum," Journal of Engineering Mechanics, Vol. 117, No. 1, pp.205-216

[32] Forrestal, M.J. and Herrmann, G.(1965). "Buckling of a Long Cylindrical Shell Surrounded by an Elastic Medium," Int. J. Solids Structures, Vol. 1 pp. 297-309

[33] Sliter, G. E. and Boresi, A.P. (1967). "Buckling of Uniformly Compressed Ring with Radial Elastic Support," Developments in Mechanics, Vol. 3: Part 1, Solid Mechanics and Materials (Proceedings of the Ninth Midwestern Mechanics Conference held at the University of Wisconsin, Machson,

August 16-18, 1965), New York, John Wiley & Sons, pp. 443-450.

[34] Moore, I. D. (1989). "Elastic Buckling of Buried Flexible Tubes - A Review of Theory and Experiment," Journal of Geotechnical Engineering, Vol. 115, No. 3, pp. 340-358

[35] Allan, T.(1968). "One-Way Buckling of Compressed Strip Under Lateral Loading," Journal of Mechanical Engineering Science, Vol. 10, No. 2, pp. 175-181.

[36] El-Aini, Y.M. (1975). "A Nonlinear Analysis For One-Way Buckling of a Laterally Loaded Column," Journal of Mechanical Engineering Science, Vol. 17, No. 3, pp.150-154.

[37] El-Aini, Y.M. (1976). "Effect of Foundation Stiffness on Track Buckling," Journal of the Engineering Mechanics Division, Vol. 102, No. EM3, pp. 531-545.

[38] Kerr, A.D. (1973). "A Model Study for Vertical Track Buckling," High Speed Ground Transportation Journal, Vol. 7, No. 3, pp. 351-368.

[39] Kerr, A.D. (1973). "The Stress and Stability Analyses of Railroad Tracks," Trans. ASME, Journal of Applied Mechanics, pp.841-848.

[40] Wang, C.Y. (1984). "On Symmetric Buckling of a Finite Flat-Lying Heavy Sheet," Trans. ASME, Journal of Applied Mechanics, Vol. 51, pp. 278-282.

[41] Wang, C.Y. (1985). "Post-Buckling of Pressurized Elastic Sheet on a Rigid Surface," Int. J. Mech. Sci, Vol. 27, No. 11/12, pp. 703-709.

[42] Plaut, R.H. and Mroz, Z.(1992). "Uni-Directional Buckling of a Pinned Elastic with External Pressure," Int. J. Solids Structures, Vol. 29, No. 16, pp. 2091-2100.

[43] Shirima, L.M. and Giger, M.W. (1992). "Timoshenko Beam Element Resting on Two-Parameter Elastic Foundation," Journal of engineering Mechanics, Vol. 118, No. 2, pp. 280-295.

[44] Timoshenko, S.P. and Gere, J.M. (1961). "Theory of Elastic Stability," 2nd ed., McGraw-Hill, New York.

[45] Kachanov, L.M. (1988). "Delamination Buckling of Composite Materials," Kluwer Academic Publishers, The Netherlands.

[46] Yamaki, N. (1984). "Elastic Stability of Circular Cylindrical Shells," North Holland, Amsterdam, The Netherlands.

[47] Dally, W. and Riley, F. (1978). "Experimental Stress Analysis," McGraw-Hill, New York.

[48] Oberg, E., Jones, F.D. and Horton, H.L. (1980). "Machinery's Handbook," 21th edit., Industrial Press Inc., New York.

[49] Murphy, G. (1950). "Similitude in Engineering," The Ronald Press Company, New York.

[50] Douglas, J.F. (1969). "An Introduction to Dimensional Analysis for Engineers," Sir Isaac Pitman & Sons Ltd.

[51] El Nasohie, M.S. (1990). "Stress, Stability and Chaos in Structural Engineering: An Energy Approach," McGraw-Hill Book Co.

[52] Sarkar, A.D. (1980). "Friction and Wear," Academic Press INC., New York.

[53] Timoshenko, S.P. and Goodier, J.N. (1970). "Theory of Elasticity," Third Edition, McGraw-Hill, New York.

[54] Swanson Analysis Systems Inc. (1985). "ANSYS Engineering Analysis System User's Manual."

[55] Swanson Analysis Systems Inc. (1985). "ANSYS Engineering Analysis System Examples Manual."

[56] W.J.D. Shaw. Personal Information.

[57] Steel, R.G.D., and Torrie, J.H., (1960). "Principles and Procedures of Statistics," McGraw-Hill Book Company, Inc. New York.

[58] Walpole, R., and Myers, R.H., (1985). "Probability and Statistics for Engineers and Scientists," Third Edition, Macmillan Publishing Company, New York.

Appendix A

MEASUREMENT OF ELASTIC MODULUS

The elastic modulus of a material is a very important property for the buckling analysis of a ring confined within a rigid boundary. In the buckling experiment, four kinds of materials were used. These materials are steel, aluminium, plastic and cardboard. For steel and aluminium, the moduli can be obtained from the resource or material handbooks. For plastic and cardboard, these data are not available. Therefore the moduli of plastic and cardboard should be measured experimentally.

It is assumed that the relationship of stress and strain is linear in the small load region

$$\sigma = E\varepsilon \tag{A.1}$$

For cardboard, the tension modulus and the compression modulus are generally different. But for the small compression load which is the case in our experiment, it can be assumed that the tension and compression moduli are the same. Thus the tension modulus instead of compression modulus can be measured. Since plastic and cardboard are soft material, the method used to measure the modulus of metal is not suitable for this case. If the material is steel, strain gages can be placed on the specimen and the curve of stress versus strain is obtained directly. Then from Equation (A.1) the elastic modulus is easily deduced. But for the soft materials, strain gauges can not be placed on the specimen. The strain obtained this way would not be the real strain of the material because the material itself is much softer than the material of strain gauges. How to measure strains of soft materials such as tissues, papers and plastics is the technology challenge for the engineers and scientists. A new method was designed to measure the strains of the plastics and the cardboard, which is referred here as the relative method. Following is the detail description of the method.

For each test, two specimens should be prepared. The two specimens are identical in all sizes except the length of the gage as shown in Figure A.1. From Figure A.1 we have

$$\begin{aligned} L_1 &= 2a + l \\ L_2 &= 2a + 2l \end{aligned} \tag{A.2}$$

At the same load, the total elongations of specimens are

$$\begin{aligned} \Delta L_1 &= 2\Delta a + \Delta l \\ \Delta L_2 &= 2\Delta a + 2\Delta l \end{aligned} \tag{A.3}$$

If we can measure the elongation ΔL_1 and ΔL_2 of these two specimens, from Equations (A.3) we obtain:

$$\Delta L_2 - \Delta L_1 = \Delta l \tag{A.4}$$

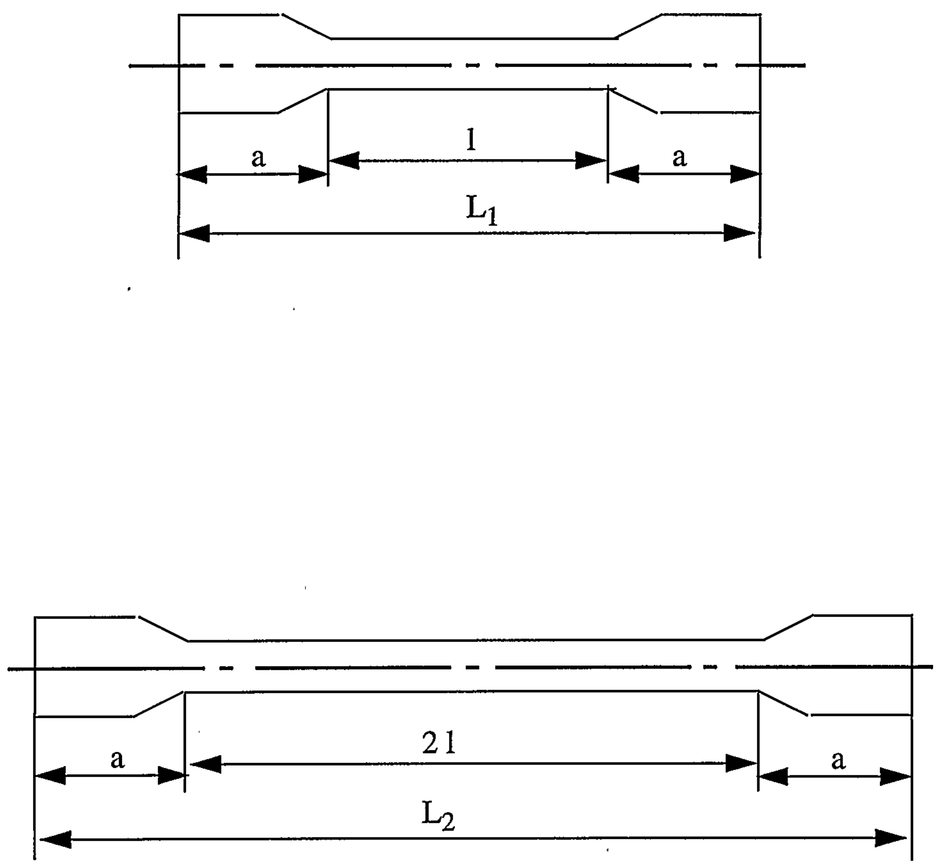

Figure A.1 Specimens for Measurement of Elastic Modulus

In this way all boundary effects are eliminated and the real gage elongation Δl is obtained. Then the strain of the specimen is calculated by

$$\varepsilon = \frac{\Delta l}{l} \tag{A.5}$$

As described above it can be sure that the relative method is a very effective and an easy method to measure the strains of soft material which can not be attached by strain gages or other gages.

The experiments were conducted on the MTS machine in the Laboratory, Department of Mechanical Engineering, The University of Calgary. The experimental setup is shown in Figure A.2.

The relationship of the load and the displacement between two grips is recorded automatically by the x-y record. The loading is displacement control and the rate of displacement is 0.00625 mm per second. For each material, at least three pairs of specimens were tested and an average of three data points were taken as the Young's modulus of the material.

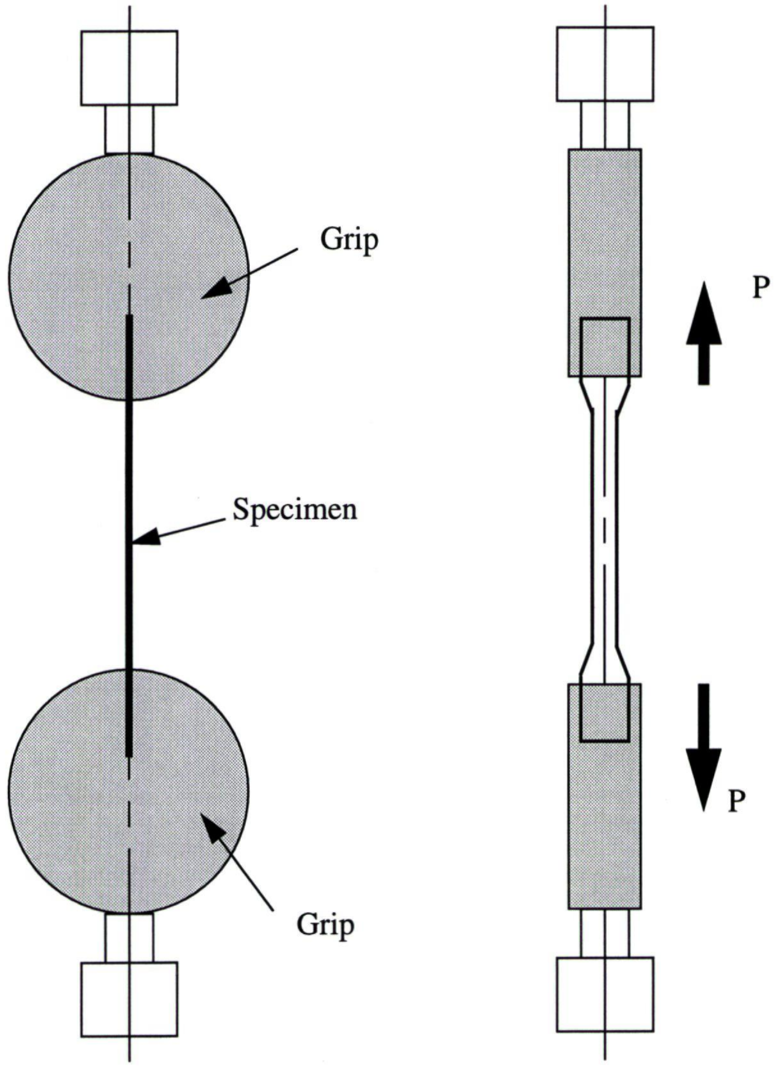

Figure 4.2 Experimental Setup for Measurement of Elastic Modulus

Table A.1 - A.4 are measured moduli of materials: cardboard and plastics.

Table A.1 Elastic Modulus of Cardboard

	P (N)	t (mm)	B (mm)	σ (MPa)	Δl (mm)	l (mm)	ε (10^{-3})	E (GPa)
Pair 1	222	0.60	20	18.53	0.44	100	4.45	4.17
Pair 2	222	0.60	20	18.53	0.45	100	4.54	4.08
Pair 3	222	0.53	20	20.98	0.50	100	5.00	4.20
Average Modulus								4.15

Table A.2 Elastic Modulus of Plastic Sample1

	P (N)	t (mm)	B (mm)	σ (MPa)	Δl (mm)	l (mm)	ε (10^{-3})	E (GPa)
Pair 1	222	0.508	20	21.89	1.07	100	10.70	2.05
Pair 2	222	0.508	20	21.89	1.12	100	11.17	1.96
Pair 3	222	0.508	20	21.89	0.95	100	9.53	2.29
Average Modulus								2.10

Table A.3 Elastic Modulus of Plastic Sample2

	P (N)	t (mm)	B (mm)	σ (MPa)	Δl (mm)	l (mm)	ε (10^{-3})	E (GPa)
Pair 1	178	0.381	20	23.41	0.98	100	9.78	2.39
Pair 2	178	0.381	20	23.41	0.97	100	9.65	2.43
Pair 3	111	0.381	20	14.83	0.64	100	6.35	2.34
Average Modulus								2.39

Table A.4 Elastic Modulus of Plastic Sample3

	P (N)	t (mm)	B (mm)	σ (MPa)	Δl (mm)	l (mm)	ε (10^{-3})	E (GPa)
Pair 1	111	0.254	20	22.24	0.97	100	9.66	2.30
Pair 2	111	0.254	20	22.24	0.99	100	9.91	2.25
Pair 3	89	0.254	20	17.79	0.69	100	6.99	2.55
Average Modulus								2.37

Appendix B

MEASUREMENT OF FRICTION COEFFICIENT

It is assumed that the friction between a ring and a rigid boundary obey Amonton and Coulomb's Law: (1) the friction resistance F_f is proportional to the weight of the object which is being moved as shown in Figure B.1, i.e.

$$F_f = \mu W \qquad \text{(B.1)}$$

where μ is the fiction coefficient; (2) the frictional force is independent of the apparent area of contact; (3) the interfacial resistance between two surfaces is independent of the velocity of sliding.

According to the definition of the friction coefficient μ, there are many ways to measure the fiction coefficient. The direct way is that of increasing the pull force F gradually until the object starts moving. Then from equilibrium condition, we have

$$F = F_f = \mu W \qquad \text{(B.2)}$$

Then

$$\mu = \frac{F}{W} \qquad \text{(B.3)}$$

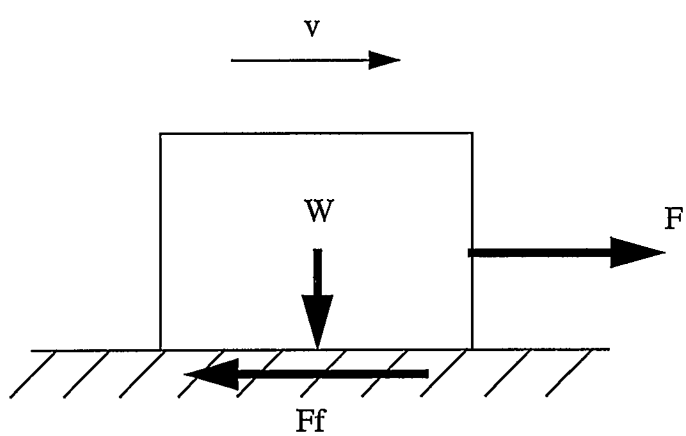

Figure B.1 Definition of the Friction Law

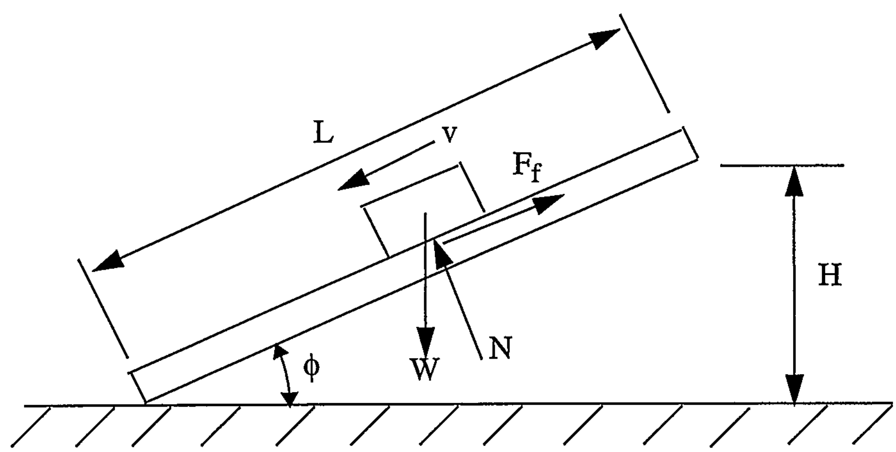

Figure B. 2   Setup for Measurement of Friction Coefficient

A different method was used to measure the friction coefficient. As shown in Figure B.2, we have

$$
\begin{aligned}
N &= W\cos\phi \\
F_f &= W\sin\phi
\end{aligned}
\qquad \text{(B.4)}
$$

According to Equation (B.1)

$$
F_f = \mu N \qquad \text{(B.5)}
$$

Bringing Equation (B.4) into Equation (B.5), we obtain

$$
\mu = \tan\phi = \frac{H}{\sqrt{L^2 - H^2}} \qquad \text{(B.6)}
$$

where ϕ is called friction angle. From Equation (B.6), it can be seen that the friction coefficient is independent of the weight of the object. The length of the base plate, L in Figure B.2 is known for the given setup. The only unknown is H. The base plate is made of the same material as the rigid support in the buckling experiment and was polished to be the same finish as the rigid support.

The procedure of measurement is very simple. First, put a piece of material of the ring on the base plate. Then gradually increase the angle ϕ until the material starts sliding along the plate. Measuring the height H and bringing it into Equation (B.6), we can calculate the friction coefficient. Ten measurements were made for each of materials. The results are listed in Table B.1-B.4.

Table B.1 Friction Coefficient for Steel

Lubricant: Three-in-one oil

No.	1	2	3	4	5	6	7	8	9	10	Average
H(mm)	59	77	73	63	73	73	70	66	69	81	70^{+11}_{-11}
μ	0.24	0.32	0.30	0.26	0.30	0.30	0.29	0.27	0.28	0.34	$0.29^{+0.05}_{-0.05}$

Table B.2 Friction Coefficient for Aluminium

Lubricant: Three-in-one oil

No.	1	2	3	4	5	6	7	8	9	10	Average
H(mm)	50	53	56	54	51	61	50	53	60	58	55^{+6}_{-5}
μ	0.20	0.21	0.23	0.22	0.21	0.25	0.20	0.21	0.24	0.23	$0.22^{+0.03}_{-0.02}$

Table B.3 Friction Coefficient for Cardboard

Lubricant: None

No.	1	2	3	4	5	6	7	8	9	10	Average
H(mm)	49	42	46	44	48	50	55	55	52	51	49^{+6}_{-7}
μ	0.20	0.17	0.18	0.18	0.19	0.20	0.22	0.22	0.21	0.20	$0.20^{+0.02}_{-0.03}$

Table B.4 Friction Coefficient for Plastic

Lubricant: Three-in-one oil

No.	1	2	3	4	5	6	7	8	9	10	Average
H(mm)	157	188	198	177	192	174	178	165	174	195	180^{+18}_{-23}
μ	0.79	1.10	1.24	0.97	1.15	0.94	0.98	0.85	0.94	1.20	$1.02^{+0.12}_{-0.23}$